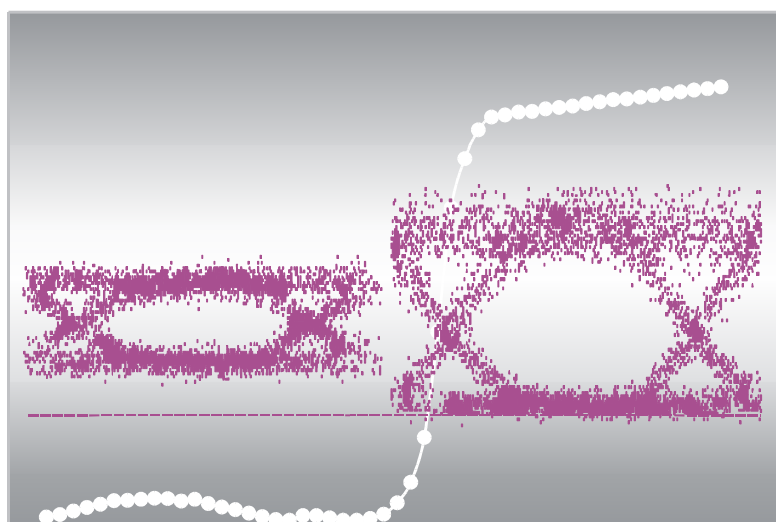


## All-Optical Signal Regeneration Based on Gain-Clamped Semiconductor Optical Amplifiers

---

Mingshan Zhao





Promoters: Prof. Geert Morthier  
Prof. Roel Baets

Ghent University  
Faculty of Engineering

Department of Information Technology

Sint-Pietersnieuwstraat 41  
B-9000 Gent, Belgium

Tel: +32 9 2643316  
Fax: +32 9 2643593



To Yaling, my wife



# ***Table of Contents***

|   |           |
|---|-----------|
| <b>Chapter 1 Introduction .....</b>   | <b>1</b>  |
| 1.1 Demand for optical regeneration in optical fiber telecommunications .....                                 | 1         |
| 1.2 Existing implementations of optical 2R regeneration ....  | 4         |
| 1.2.1 Generic operation principle of all-optical 2R regeneration based on a nonlinear transfer function ..... | 4         |
| 1.2.2 Qualification of optical 2R regeneration .....  | 5         |
| 1.2.3 State-of-the-art optical 2R regeneration techniques .....   | 6         |
| 1.3 Overview of the thesis, main achievements and publications .....  | 10        |
| <br>  |           |
| <b>Chapter 2 All-optical 2R regeneration based on gain-clamped SOAs .....</b>                                 | <b>17</b> |
| 2.1 The gain-clamped SOA (GCSOA) .....  | 17        |
| 2.1.1 Description of a GCSOA .....  | 17        |
| 2.1.2 Operation characteristics .....   | 18        |
| 2.2 All-optical 2R regenerator based on a MZI with GCSOAs .....   | 25        |
| 2.2.1 Structure and operation principle .....   | 25        |
| 2.2.2 Numerically simulated transfer characteristics .....  | 27        |
| 2.3 Experimental characterization .....   | 29        |
| 2.3.1 Static transfer characteristics .....   | 31        |
| 2.3.2 Decision threshold adjustment .....   | 32        |
| 2.3.3 Extinction ratio improvement .....  | 33        |
| 2.3.4 Discussions .....   | 35        |
| 2.4 Summary .....   | 37        |

---

|   |           |
|---|-----------|
| <b>Chapter 3 All-optical 2R regeneration based on an MZI with LOAs in both arms .....</b>                     | <b>41</b> |
| 3.1 LOA and its characteristics .....   | 41        |
| 3.1.1 Description of a LOA .....  | 41        |
| 3.1.2 Operating characteristics of the LOAs .....   | 42        |
| 3.2 2R regenerator based on an MZI with LOAs .....  | 48        |
| 3.2.1 Structure and operation principle .....   | 48        |
| 3.3 Experimental demonstration of the 2R regenerator .....  | 49        |
| 3.3.1 Static transfer characteristics .....   | 50        |
| 3.3.2 Dynamic performance .....   | 52        |
| 3.4 Discussion .....  | 55        |
| 3.5 Summary .....   | 55        |
| <br>  |           |
| <b>Chapter 4 All-optical 2R regeneration based on polarization rotation in a LOA .....</b>                    | <b>57</b> |
| 4.1 Polarization rotation in a LOA .....  | 58        |
| 4.1.1 Theoretical analysis .....  | 58        |
| 4.1.2 Experimental results .....  | 62        |
| 4.2 Operation principle of the polarization rotation-based all-optical 2R regenerator with a single LOA ..... | 64        |
| 4.3 Experimental demonstration of the regenerative capabilities .....   | 67        |
| 4.3.1 Static regeneration characteristics .....   | 68        |
| 4.3.2 Regenerative capabilities at 2.5 Gbit/s .....   | 70        |
| 4.3.3 Regenerative capabilities at 10 Gbit/s .....  | 72        |
| 4.4 Summary .....   | 76        |

---

|   |            |
|---|------------|
| <b>Chapter 5 Noise suppression in spectrum-sliced WDM systems .....</b>             | <b>79</b>  |
| 5.1 Intensity noise limits in spectrum-sliced WDM systems .....                     | 80         |
| 5.1.1 Spectrum-sliced WDM system .....  | 80         |
| 5.1.2 Limits on the transmission performance caused by excess intensity noise ..... | 82         |
| 5.1.3 Possible solutions of intensity noise suppression .....                       | 90         |
| 5.2 Intensity noise suppression using a saturated SOA .....                         | 92         |
| 5.2.1 Analytical analysis .....   | 92         |
| 5.2.2 Experimental demonstration .....  | 95         |
| 5.3 Summary .....   | 104        |
| <br>  |            |
| <b>Chapter 6 Conclusions .....</b>  | <b>109</b> |
| <br>  |            |
| <b>List of the acronyms .....</b>   | <b>113</b> |

# **Chapter 1**

## **Introduction**

### **1.1. Demand for optical regeneration in optical fiber telecommunications**

Telecommunication networks have been facing rapid increases in traffic demands due to the tremendous growth of the Internet, the World Wide Web and the telephone services. In order to fulfil these increasing demands, two generations of high-capacity optical networks have been developed. In the first generation networks, optical fiber is used to replace the copper cable to get higher capacities. All the switching and other intelligent network functions are handled by electronics. Examples of first-generation optical networks are SONET (synchronous optical network) and the essentially similar SDH (synchronous digital hierarchy) networks, which form the core of the telecommunications infrastructure in North America and in Europe and Asia, respectively, as well as a variety of enterprise networks such as ESCON (enterprise serial connection). In second-generation optical networks, some of the routing, switching, and intelligence are moved into the optical layer, and the techniques of wavelength division multiplexing (WDM) and electronic time division multiplexing (TDM) are employed to increase the capacity and make the network cost effective. The key network elements that enable optical networking are optical line terminals (OLTs), optical add/drop multiplexers (OADMs), and optical crossconnects (OXC). An OLT multiplexes multiple wavelengths into a single signal onto a single fiber and demultiplexes a multi wavelength signal into individual wavelength channels on separate fibers. OLTs are used at the ends of a point-to-point WDM link. An OADM takes in signals at multiple wavelengths and selectively drops some of these wavelengths locally while letting others pass through. It also selectively adds wavelengths to the composite outbound signal. An OADM has two line ports where the composite WDM signal is present, and a number of local ports where individual wavelengths are dropped and added. An OXC essentially performs a similar function but at much larger sizes. OXCs have a large number of ports (ranging from a few tens to thousands) and are able to switch wavelengths from one input port to several output ports. Both OADMs and OXCs may incorporate wavelength conversion capabilities. The second-generation optical networks are already being deployed. OLTs have been widely deployed for point-to-point applications. OADMs are now used in long-haul and metro networks. OXCs

are beginning to be deployed first in long-haul networks because of the higher capacities in those networks.

It is well known that signals propagating over optical fiber networks are significantly distorted due to a combined effect of amplifier noise accumulation, fiber dispersion, fiber nonlinearity, and inter/intrachannel interactions, which results in serious limits in both capacity and range of the system transmission. This is especially the case in advanced WDM-based optical networks, where many channels at different wavelengths and each carrying signals of up to 40 Gbit/s are sent through long stretches of fiber and are traversing a number of optical amplifiers and switches. Regardless of the transmission formats (RZ, NRZ, or Chirped RZ), the induced distortion is reflected in three main types of signal degradation: intensity noise, timing jitter, and pulse-envelope distortion [1]. Intensity noise might be more accurately referred to as the uncertainty in the energy content of a given bit slot. Fiber chromatic dispersion coherently mixes the contents of adjacent bits, optical amplification causes beat noise with spontaneous emission, fiber nonlinearities introduce information-dependent power transfer between WDM channels, all resulting in irreversible bit-energy fluctuations. Timing jitter is the uncertainty in the pulse-mark arrival time, or a synchronization default with respect to the bit stream. The main causes for timing jitter are nonlinearities of self-phase modulation (SPM), cross-phase modulation (XPM), polarization-mode dispersion (PMD), and for RZ formats, the Gordon-Haus and electrostriction effects [2]. Pulse distortion can be viewed as an irreversible change in the pulse envelope which increases the probability of symbol detection error. A most obvious pulse distortion effect is the fill-up of "0"-symbol spaces by amplified spontaneous emission (ASE), thus reducing the on/off extinction ratio. Fiber nonlinearities (SPM, XPM), four-wave mixing (FWM), stimulated Raman scattering (SRS), and PMD are the essential causes of pulse-envelope distortion.

In order to limit the above impairments, an efficient and powerful solution is that the signals are regenerated at intermediate nodes. This can be realized in two ways for given system impairments from amplifier noise and fiber nonlinearities after some transmission distance. The first, the electronic regeneration, consists in segmenting the system into independent trunks, with full electronic repeater/transceivers at interfaces. The second is inline optical regeneration, which performs the same signal-restoring functions as the electronic approach, but with reduced complexity and enhanced capabilities. Besides, several other methods have also been adopted so far: improving the transmission format (e. g. , Chirped RZ vs. NRZ in submarine systems) or reducing power levels [3]. At the terminal side, the introduction of error-correcting codes (ECCs) has made possible high levels of received signal quality ( $\text{BER} < 10^{-7}$ ), while allowing relatively substantial signal degradation through the transmission line [4].

The electronic regeneration has been widely used in the networks being deployed today. In the electronic regenerators (as seen in Fig. 1-1), the incoming optical signal is converted to the electrical domain by means of a high-speed photodiode. Signal regeneration/processing is then achieved using broadband RF circuitry, after which the regenerated electrical signal is converted back in the optical domain using an electrooptical modulator coupled with a laser diode. As seen, complete integration of such an architecture is rather complex. As the bitrate increases, electronic

regenerators become very expensive and physically more difficult to realize due to the electronic bandwidth bottleneck. To our knowledge, no electro-optical regenerator has been experimentally tested yet at 40 Gbit/s line rate.

All-optical regeneration is a very promising technique in the evolution of high bitrate systems, thanks to its strong potential for compact integration and very high bandwidth. All-optical regeneration has been one of the most attractive fields of optical fiber communications research. It is now generally accepted that all-optical regeneration will be the key technique in the next generation all-optical high bitrate networks.

In optical regeneration, there are three basic signal-processing functions: reamplifying, reshaping and retiming, as seen in Fig. 1-2, hence the generic acronym 3R. Thus, optical amplification (such as with erbium-doped fiber amplifier-EDFAs) provides a mere 1R signal-processing function. When retiming is absent, one usually refers to the regenerator as a 2R device, with only reamplifying and reshaping capabilities. A device with the full 3R capabilities is called a 3R regenerator and requires clock extraction. This PhD research focuses on all-optical 2R regeneration.

There are various ways of defining optical regeneration. It can refer to pure optical/optical signal processing. The all-optical label usually refers to the case where the regenerator subcomponents are optically controlled.

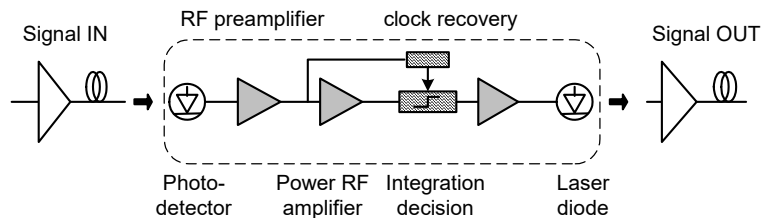


Fig. 1-1 Basic setup of electrooptical regenerator.

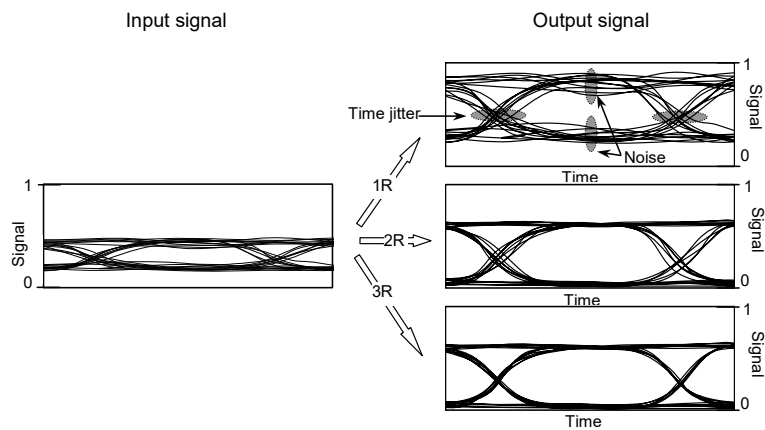


Fig. 1-2 Illustration of 3R regeneration: reamplification, reshaping, and retiming.

## 1.2. Existing implementations of optical 2R regeneration

### 1.2.1 Generic operation principle of all-optical 2R regeneration based on a nonlinear transfer function

The generic principle of the all-optical 2R regeneration based on a nonlinear transfer function is shown in Fig. 1-3. The device is assumed to exhibit a nonlinear transfer function. At the low input powers, the output of the device remains at a low and steady level. Once the input power exceeds a certain power level, i. e. the decision threshold, the output rises rapidly up to a steady high level. When the noisy signals to be regenerated are launched into the device, the intensity noise at both "0" and "1" symbols is thus suppressed (i. e. the noise is redistributed) and the extinction ratio (ER, definition seen in the following section) is simultaneously improved. The input noisy signals are regenerated. In the 2R regeneration above, the regenerated signals have the same polarity as the input signal, which is referred to as non-inverted regeneration. If the nonlinear transfer function converts logical ones to zeroes and vice versa, the regenerated signal will be of opposite polarity. The regeneration is referred to as inverted regeneration.

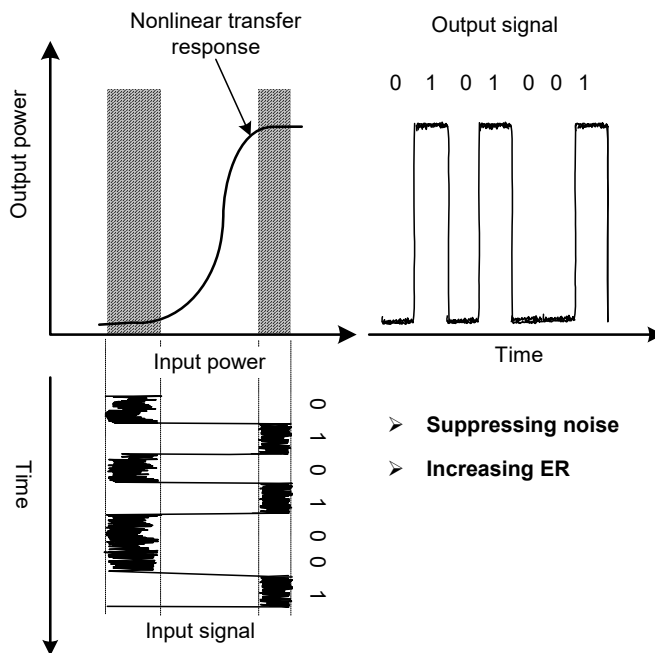


Fig. 1-3 Generic principle of 2R regeneration based on nonlinear transfer function.

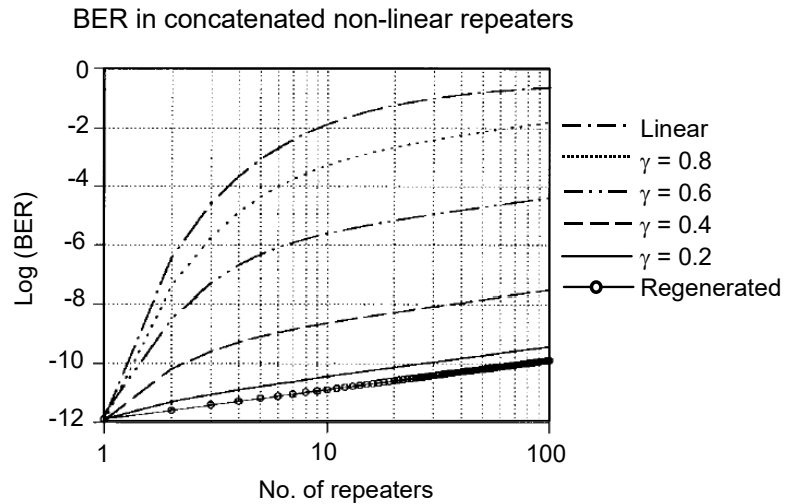


Fig. 1-4 Evolution of the BER with concatenated regenerators for different nonlinear transfer function (i. e.  $\gamma$  parameter). (Ref. P. Öhlén and E. Berglind, *IEEE Photon. Technol. Lett.*, Vol. 9, No. 7, pp. 1011-1013, 1997).

Clearly, the nonlinear transfer function of the device is the key parameter that governs regenerative properties. It has been shown theoretically that the highest regeneration efficiency (as obtained when considering the less-penalizing concatenation of regenerators) is achieved with an ideal step function [5]. Fig. 1-4 shows the theoretical evolution of bit-error-rate (BER) with the number of concatenated regenerators for regenerators having different nonlinear transfer functions. The calculation however does not account for dynamic effects or jitter impact in the regenerator cascade. The degree of nonlinear function is characterized through the factor  $\gamma$ , which changes the shape of the nonlinearity from a step function ( $\gamma = 0$ ) to a linear function ( $\gamma = 1$ ). The noise level is adjusted so that the output BER is fixed to  $10^{-12}$  after a single regenerator. As seen in the figure, the smaller the  $\gamma$ , the lower the BER and the larger the cascade can be. The optical 2R regenerator with quasi-ideal nonlinear function is therefore of great importance.

### 1.2.2 Qualification of optical 2R regeneration

The qualification of the regenerative capabilities of a 2R device basically consists of the evaluation of a limited number of key-parameters such as ER, input power fluctuations, polarization sensitivity. This is practically accomplished by measuring the eye-diagrams and BER. The ER is here defined as  $P_s(1)/P_s(0)$ , the ratio of the powers (electrical) for "1"-symbols and "0"-symbols. As mentioned in the previous section, the fill-up of "0"-symbol spaces by the ASE degrades the ER. ER improvement achieved with a 2R device proves its regenerative capability. (Note that a mere optical amplification can not result in any ER improvement). The BER is defined as the probability of incorrect identification of a bit by the decision circuit of

the receiver, i. e. the sum of the probabilities of a "1" bit being read as "0" and vice versa. The BER is the ultimate test for a digital transmission link. A transmission link is typically characterized by BER as a function of received power. The minimum average power required at the receiver to get a given BER (typically  $10^{-9}$ , or  $10^{-10}$ ) is referred to as receiver sensitivity. If, for a given BER and due to transmission impairments, more power is required at the receiver, the additional power is called power penalty. Improvement of receiver sensitivity (negative power penalty) for degraded input signals or lower power penalty for "perfect" input signals, due to the insertion of the 2R device, also proves the regenerative capability of the 2R regenerator.

Certainly, validation of the structure and operation margins, the high bitrate potential, and cascadability issues are also important aspects of the qualification of the 2R regenerators.

It should be pointed out that optical regenerators can not "correct" errors but can only avoid for noise and other impairments to accumulate. This is because a 2R regenerator is essentially a decision circuit. Ideally, the optical regenerator should be tested also in a recirculating loop [6], especially for 3R regenerators. In that measurement, one might qualify regeneration performance through the evolution of the receiver sensitivity penalty at fixed BER with respect to key relevant parameters, such as optical signal-to-noise ratio (OSNR). Evaluation and comparison of regenerative properties then amounts to measuring the minimum OSNR, corresponding for example to 1 dB penalty on the receiver sensitivity with respect to the first lap, which is tolerated by the regenerative apparatus throughout the cascade. This measurement then reflects the accumulated effects of all degrading factors occurring in the transmission, such as chromatic dispersion, timing jitter accumulation, and amplifier noise, and hence enables the extraction of the actual regenerative performance of the tested device.

Considering the 2R regenerators in this PhD research, however, we focus on the qualification of regenerative capabilities by measuring the ER improvement, the BER reduction or the receiver sensitivity improvement; quantities which are often used in recent research on optical regeneration. Actually, it will be explained in the following chapters that due to the fact that a pass-through scheme works inherently in the non-inverted scheme and the component is based on self-gain-modulation, a red shift will occur at the leading edge and a blue shift at the trailing edge. This is the desired chirp behaviour for a propagating pulse. With improvements in both ER and receiver sensitivity, we can state that the tested device should be able to work in a cascade in order to have the signal propagated over large distances, which means the device could deliver an efficient regeneration.

### 1.2.3 State-of-the-art optical 2R regeneration techniques

In recent years, several techniques for optical 2R regeneration have been proposed and experimentally demonstrated. These techniques make use of SOA-based interferometers (e. g. , SOA-based Mach-Zehnder or Michelson interferometer, SOA-based ultra-fast nonlinear interferometer-UNI), multi-section lasers (e. g. , multi-section Q-switched laser or DFB laser), and saturable absorbers, respectively.

### Optical 2R regeneration using SOA-based interferometers

The 2R regeneration using SOA-based interferometers is based on a phase shift resulting from photo-induced carrier depletion in the gain saturation regime. Two basic structures have been explored to realize optical 2R regeneration with monolithic SOA-based interferometers, namely Mach-Zehnder interferometer (MZI) and Michelson interferometer (MI) as shown in Fig. 1-5 and Fig. 1-6, respectively [1]. In these structures, both an input signal carried by wavelength  $\lambda_1$  and acting as a pump signal and a local CW signal carried by wavelength  $\lambda_2$  and acting as a probe signal are used. In the Mach-Zehnder interferometer, injection of the signal at  $\lambda_1$  induces a phase shift through XPM in SOA2, the amount of which depends upon the power level  $P_{in}(\lambda_1)$ . The probe signal at  $\lambda_2$  is injected into the interferometer, where it splits equally in the two interferometer arms, and then recombines at the output, either constructively or destructively depending on the phase difference between the interferometer arms. The phase difference is determined by both a XPM-induced phase shift in SOA2 and a static phase shift in SOA1 and SOA2, and changes with  $P_{in}(\lambda_1)$ . Therefore, the output of the interferometer changes nonlinearly with increasing input signal power, as seen in Fig. 1-5b. As explained previously, the nonlinearity of the transfer function induces noise redistribution, resulting in a narrower distribution for marks and spaces and in an improvement of the data ER. The interferometer operates as an all-optical 2R regenerator. In the MI, the probe signal is coupled to the interferometer via a circulator and is back-reflected in two SOAs. As in the previous case, only SOA2 induces XPM. The MI type has higher speed potential compared to the MZI type, mainly due to the fact that back reflection doubles the interaction length. The optical bandpass filters in these structures are used for removing the pump signal (wavelength  $\lambda_1$ ).

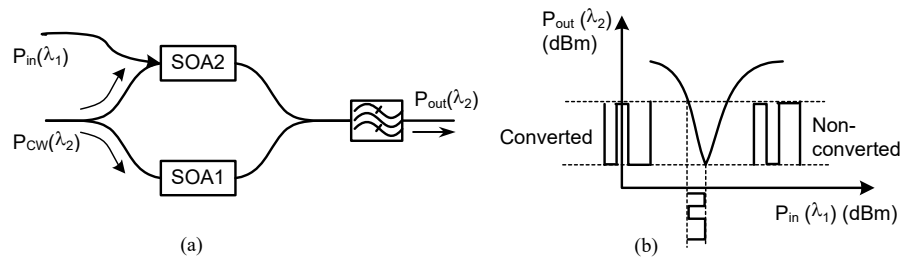


Fig. 1-5 Principle structure of the 2R regenerator based on a Mach-Zehnder interferometer with SOAs in both arms.

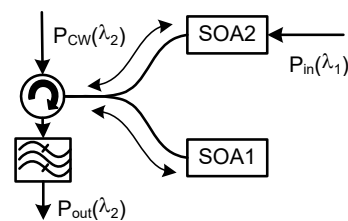


Fig. 1-6 SOA-based Michelson interferometer for 2R regeneration.

An alternative implementation of the 2R regenerator using an SOA-based interferometer is similar to the previous one but no local CW signal needed [7-8]. In this 2R regenerator, a nonlinear phase difference between the two interferometer arms is the result of a self-phase modulation (SPM, i. e. , the phase shift induced by the input signal itself) in both SOAs that are now asymmetrically biased.

All of the 2R regenerators using SOA-based interferometers have a high integration potential and open the possibility to integrate complex optical functions for optical signal processing. The implementations using SPM are simple and cost effective. The 2R regenerators based on wavelength conversion are more complex due to the probe laser, but they can be easily upgraded to full 3R regeneration if the CW-signal at  $\lambda_2$  is substituted by an optical clock signal. Reshaping and retiming can then be simultaneously obtained using sampling [9]. Optical regeneration (2R or 3R) based on MIs or MZIs has been demonstrated at 10 Gbit/s (MZI) [9, 10] and at 20 Gbit/s (MI) [11]. With a differential mode of the SOA-based MZI, the bitrate can be improved up to 40 Gbit/s or beyond [12, 13].

Very recently, an asymmetric MZI with an MMI-SOA was proposed [14], in which the SOA in one arm is replaced by a one-by-one multi-mode interference semiconductor optical amplifier (MMI-SOA). This device has advantages of being small and easy to fabricate, and also gives a better regeneration characteristic than the above mentioned interferometers. Regeneration at 2.5 Gbit/s has been experimentally demonstrated.

In addition, the SOA-based ultra-fast nonlinear interferometer (UNI) is an attractive approach for very high-speed optical regeneration [15,16].

### Optical 2R regeneration using multi-section lasers

Recently, two approaches using multi-section lasers, namely the Q-switched laser-based 2R regenerator and the distributed feedback (DFB) laser-based 2R regenerator, have been investigated. The Q-switched laser-based device consists of three sections: a lasing DFB section, a passive phase tuning, and a second lasing section pumped at transparency and used as a reflector section, as seen in Fig. 1-7 [17,18]. The combination of passive phase tuning and reflector sections allows the control of the back reflected signal in amplitude and phase.

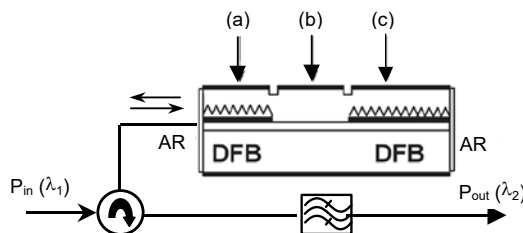


Fig. 1-7 Q-switched laser-based optical regenerator: (a) laser section, (b) phase tuning section, (c) reflector section.

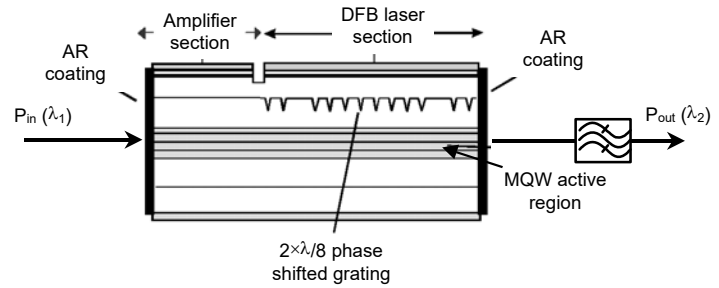


Fig. 1-8 Optical regenerator using a DFB laser integrated with an SOA

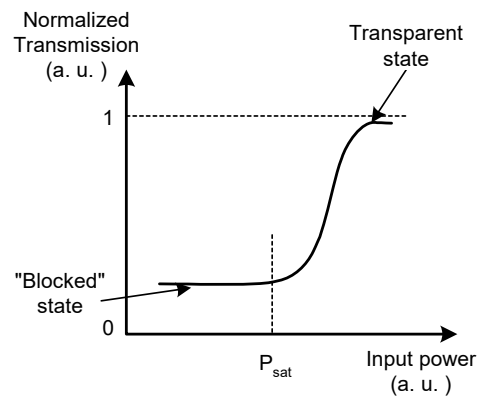


Fig. 1-9 Transfer function of a saturable absorber.

The DFB laser integrated with an SOA is shown in Fig. 1-8. In this device, lasing is turned off due to the gain saturation induced by the injection of a high-power signal [19]. Both of the two structures deliver optical 2R regeneration through wavelength conversion. The output laser power exhibits a very sharp nonlinear response, which thus results in an efficient optical regeneration.

### Saturable absorber-based optical 2R regeneration

A saturable absorber (SA) has a highly nonlinear transfer function, as shown in Fig. 1-9 (Note that the  $y$ -axis does not refer to the output power there). When illuminated with an optical signal with instantaneous peak power below some threshold  $P_{sat}$ , the photon absorption of the SA is high and the device is opaque to the signal. Above  $P_{sat}$ , the SA transmission rapidly increases and saturates to an asymptotic value near unity (passive loss neglected). Obviously, such a nonlinear transfer function of the SA makes it possible to use it for 2R optical regeneration (when used together with an optical amplifier).

The SA-based 2R regenerator can reduce the ASE noise level in the “0” symbols, resulting in a higher signal ER and hence improving the system performance. However, since SAs do not provide effective control of amplitude fluctuations, it is mandatory to associate them with a means of control for marks (“1” symbols). This can be accomplished by using a cascaded SOA [20] or a narrow-band optical filter with nonlinear (soliton) propagation [21]. The SA-based device is simple and has the capability of operating at high bitrate. A 2R regenerator operating together with both an optical filter and nonlinear propagation has been demonstrated at 20 Gbit/s with a specially designed fast SA device (the multi-quantum-well microcavity SA) [22]. The disadvantages of the SA-based devices are the high input power level requirements (typically 7~10 dBm) and high insertion loss. Further research on SA-based regenerators should address the reduction of saturation energy, the recovery time, and the insertion loss, and an increase in the dynamic extinction ratio.

### 1.3. Overview of the thesis, main achievements and publications

As seen earlier in the previous sections, all-optical regeneration can be accomplished in many different ways, focusing on either high bitrate or good regeneration performance, or on both, and the nonlinear response of the devices is the key parameter that governs regeneration efficiency. The SOA-based devices have high integration potential and are thus very promising for all-optical regeneration in high-bitrate optical networks. However, these devices suffer from a rather slow nonlinear transfer function. To get a steeper nonlinear response, cascaded MZIs are needed [23], as seen in Fig. 1-10. Furthermore, in most cases the 2R optical regeneration is realized through wavelength conversion and an extra CW laser signal is needed. All of this results in increased cost and complexity.

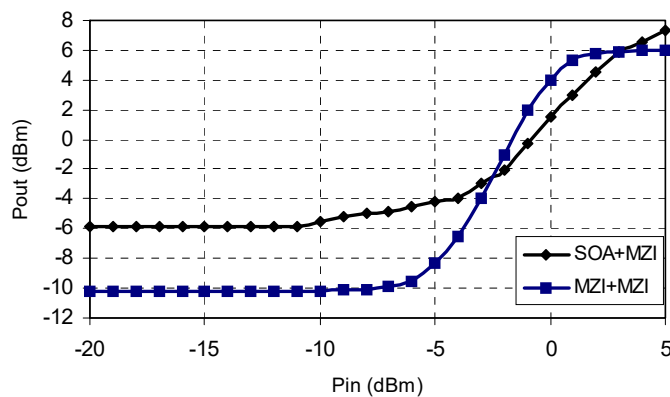


Fig. 1-10 Comparison between the transfer functions of the cascades SOA+MZI and MZI+MZI (B. Lavigne, et al., *Techn. Dig. Conference on Optical fiber communication OFC 1999*, Paper-TuJ3, pp. 128-130, San Diego, USA, February 21-26, 1999)

The main goal of this PhD research was to develop new all-optical 2R regenerators that have a steep nonlinear transfer function, operate on the signal itself instead of on a pump or external pulse sequence, and give the same benefits as SOA-based devices. To this end, two new concepts of all-optical 2R regeneration, based on gain-clamped SOAs (GCSOA) and linear optical amplifiers (LOA), respectively, have been proposed and experimentally investigated. In addition, reduction of the intensity noise in spectrum-sliced WDM systems has also been investigated.

In chapter 2, an all-optical 2R regenerator using an MZI with GCSOAs in both arms is described. The operation of this regenerator is based on the specific property of a GCSOA that its amplification in the linear regime is independent of the injected current, whereas the saturation power increases linearly with the injected current. A digital-like nonlinear transfer function and a flexible adjustment of decision threshold are demonstrated. Dynamic measurements at 2.5 Gbit/s show a tremendous intensity noise suppression at the logic "0" and a large improvement in the extinction ratio even for a very deteriorated input signal with small extinction ratio: e.g. 8 dB improvement in extinction ratio has been obtained for an input extinction ratio of 5 dB, and 7 dB improvement for an input extinction ratio of 2 dB.

Chapter 3 gives an alternative implementation of the above GCSOA-based 2R regeneration, which has higher speed potential. In this 2R regenerator, two very recently introduced devices, LOAs, are used in the two arms of the MZI, instead of the GCSOAs. A significant improvement in extinction ratio and operation at 10 Gbit/s are demonstrated.

In addition to nonlinearities of gain and phase in the SOAs, nonlinear birefringence is also an interesting behaviour. In chapter 4, we demonstrate all-optical 2R-regeneration based on such nonlinearity in a single LOA. First, polarization rotation induced by nonlinear birefringence in LOAs is analysed theoretically and experimentally. Secondly, the operation principle of the polarization rotation based-2R regeneration is described in §4.2. In §4.3, experimental demonstration of the regenerative capabilities is given. An ER improvement of 15 dB has been obtained with an input extinction ratio of 5 dB for static operation. Experimental results for bit-rates of both 2.5 Gbit/s (NRZ,  $2^9-1$  PRBS) and 10Gbit/s (NRZ,  $2^{31}-1$  PRBS) are presented, respectively. With a degraded input signal, a receiver sensitivity improvement of over 3 dB at a bit-error-rate (BER) of  $10^{-9}$  is found for 2.5 Gbit/s. For 10 Gbit/s, zero power penalty is observed. Significant improvements of ER are obtained for both 2.5 Gbit/s and 10 Gbit/s. The features of simple configuration, stable operation and high regenerative capabilities make this new scheme a promising technique for all-optical regeneration in future optical networks.

In addition to the high bitrate, long-haul point-to-point transmission and large scale networks, there are short distance and low bitrate (e. g. , 2.5 Gbit/s) networks, such as campus or metropolitan networks and fiber-to-the-home (FTTH) access networks. The spectrum-sliced WDM technique, in which optical filters are used to obtain a spectral slice of light from a broadband source (e. g., LEDs, superluminescent LEDs) and modulators encode data onto the slice, is a strong candidate for these cost-sensitive local area networks due to its advantages of low cost, high wavelength selectivity and temperature stability as compared to conventional DWDM systems. Spectrum-sliced incoherent light, however, exhibits a large intensity noise that places limits on the achievable system performances. An efficient method to reduce

this noise is using a saturated SOA. In chapter 5, a theoretical analysis and an experimental demonstration of the noise reduction in spectrum-sliced WDM systems is presented. The influence of the injected current and the input power level of the SOA on the noise reduction and its bandwidth is studied theoretically in §5.2.1. Measurement results of the RIN, the SNR, and the BER with and without noise reduction are given in §5.2.2. Experimental results of SNR show an increase of 13.5 dB in the intensity-noise-limited signal-to-noise ratio (SNR) for a bitrate of 2.5 Gbit/s and of 17.5 dB for a bitrate of 622 Mbit/s. The measured BER results show that for an optical slice with 0.3 nm bandwidth, the error floor level is at  $2 \times 10^{-4}$  without the noise reduction at the back-to-back operation, while with the noise reduction using the saturated SOA, the error floor is removed and error free operation is obtained. The BER measurement results for different injection currents and different input power to the SOA for 2.5 Gbit/s show that increasing both injection current and input power to the SOA improves the BER, which is agree with the theoretical prediction. Experimental results of the optical spectra of the slice before and after the SOA has shown that in addition to the gain-saturation characteristics of the SOA, the intrachannel four-wave-mixing (IC-FWM) within the SOA is also an important mechanism of the intensity noise reduction. In a sense of noise suppression (redistribution), this approach could be thought also as an optical regeneration.

Finally, chapter 6 covers some conclusions, and several ideas for future works.

## Publications in the context of this work

1. Mingshan Zhao, Geert Morthier, and Roel Baets, "Demonstration of Extinction Ratio Improvement from 2 to 9 dB and Intensity Noise Reduction with the MZI-GCSOA All-Optical 2R Regenerator," *IEEE Photonics Technology Letters*, Vol. 14, No. 7, pp. 992-994, 2002.
2. Mingshan Zhao, Geert Morthier, and Roel Baets, "Analysis and Optimization of Intensity Noise Reduction in Spectrum-Sliced WDM Systems Using a Saturated Semiconductor Optical Amplifier," *IEEE Photonics Technology Letters*, Vol. 14, No.3, pp. 390-392, 2002.
3. Geert Morthier, Mingshan Zhao, Bart Vanderhaegen, and Roel Baets, "Experimental demonstration of an all-optical 2R regenerator with adjustable decision threshold and true regeneration characteristics," *IEEE Photonics Technology Letters*, Vol. 12, No. 11, pp. 1516-1518, 2000.
4. Mingshan Zhao, Jan De Merlier, Geert Morthier, Roel Baets, "Dynamic birefringence of the linear optical amplifier (LOA) and application in optical regeneration," *IEEE Journal of Selected Topics in Quantum Electronics*, the Integrated Optics & Optoelectronics issue (November/December), Vol. 8, No. 6, 2002.
5. Mingshan Zhao, Jan De Merlier, Geert Morthier, and Roel Baets, "All-optical 2R regeneration based on polarization rotation in a linear optical amplifier," *IEEE Photonics Technology Letters*, Vol. 15, No. 2, 2003 (accepted).
6. Mingshan Zhao, Geert Morthier, and Roel Baets, "Quasi-ideal optical decision characteristic from a Mach-Zehnder interferometer with gain-clamped semiconductor optical amplifiers," *OFC 2002 (Optical Fiber Communication Conference)*, p. ThGG94, Anaheim, California, USA, March 17-22, 2002.
7. Mingshan Zhao, Jan De Merlier, Geert Morthier, Roel Baets, "Experimental demonstration at 10 Gbps of 2R optical regeneration in a fiber-based MZI with LOAs," *ECOC 2002 (European Conference on Optical Communication)*, p. 7.3.6, Copenhagen, Denmark, September 8-12, 2002.
8. Mingshan Zhao, Jan De Merlier, Geert Morthier, Roel Baets, "Experimental demonstration of all-optical 2R regeneration based on non-linear birefringence in a LOA," *LEOS 2002 (Annual Lasers and Electro Optics Meeting)*, p. MM2, Glasgow, Scotland, November 10-14, 2002.
9. Mingshan Zhao, Geert Morthier, Roel Baets, and Johan Dekoster, "Investigation of the intensity noise reduction using a saturated semiconductor optical amplifier in spectrum sliced WDM systems," *CLEO 2001, (Conference on Lasers and Electro-Optics)*, p. CThB3, Baltimore, Maryland, USA, May 8-10, 2001.
10. Mingshan Zhao, Geert Morthier, and Roel Baets, "Experimental demonstration of an all-optical 2R regenerator with a quasi-ideal optical decision characteristic," *International workshop on Optical Signal Processing*, Copenhagen, Denmark, November 29-30, 2001.
11. Geert Morthier, Mingshan Zhao, Jan De Merlier, Roel Baets, "All-Optical Regeneration Using InP-Based Photonic Integrated Circuits," *IEEE/LEOS-Benelux*, Brussels, Belgium, December, 2001.

12. Mingshan Zhao, Geert Morthier, Bart Moeyersoon, and Roel Baets, "Influence of intensity noise on link transmission performance of spectrum-sliced WDM systems," *Towards an Optical Internet (New Visions in Optical Network Design and Modeling)*, pp. 253-261, Edited by Admela Jukan, Kluwer Academic publishers, 2001.
13. Jan De Merlier, Mingshan Zhao, Geert Morthier, and Roel Baets, "Some new concepts for all-optical 2R regeneration using InP-based Photonic Integrated Circuits," *IFIP TC6 Sixth working Conference on optical Network Design and Modeling (ONDM2002)*, Torino, Italy, February 2002.
14. Mingshan Zhao, Geert Morthier, Bart Moeyersoon, and Roel Baets, "Optimization of SOA-based transmitters in spectrum-sliced WDM systems," *IEEE/LEOS-Benelux*, Mons, Belgium, March 2000.

## References

- [1] O. Leclerc, B. Lavigne, and D. Chiaroni, "All-optical regeneration: Principles and WDM implementation," in *Optical Fiber Telecommunications IVA (Components)*, I. P. Kaminow and T. Li, Ed. San Diego: Academic Press, 2002, pp. 732-783.
- [2] C. J. McKinstry, J. Santhanam, G. P. Agrawal, "Gordon-Haus timing jitter in dispersion-managed systems with lumped amplification: analytical approach," *J. Opt. Soc. Am.*, B/Vol. 19, No. 4, pp. 640-649, 2002.
- [3] R. M. Mu, T. Yu, V. S. Grigoryan, and C. R. Menyuk, "Dynamics of the chirped return-to-zero modulation format," *J. Lightwave Technol.*, Vol. 20, No. 1, pp. 47-57, 2002.
- [4] S. Lin and D. J. Costello, Jr., *Error Control Coding: Fundamentals and applications*, Prentice Hall: Englewood Cliffs, NJ, 1983. (Or, <http://www-theory.dcs.st-and.ac.uk/~sal/school/CS3010/Lectures/forhtml/node3.html>).
- [5] P. Öhlén and E. Berglind, "Noise accumulation and BER estimates in concatenated nonlinear optoelectronic repeaters," *IEEE Photon. Technol. Lett.*, Vol. 9, No. 7, pp. 1011-1013, 1997.
- [6] B. Lavigne, P. Guerber, C. Janz, A. Jourdan, and M. Renaud, "Full validation of an optical 3R regenerator at 20 Gbit/s," *Tech. Dig. Optical fiber communication Conference OFC 2002*, Vol. 3, pp. 93-95, 2002.
- [7] D. Wolfson, P. B. Hansen, A. Kioch, and K. E. Stubkjaer, "All-optical 2R regeneration based on interferometric structure incorporating semiconductor optical amplifiers," *Electron. Lett.*, Vol. 35, No. 1, pp. 59-60, 1999.
- [8] D. Wolfson, T. Fjelde, A. Kloch, C. Janz, A. Coquelin, I. Guillemot, F. Gaborit, F. Poingt, and M. Renaud, "Experimental investigation at 10 Gbit/s of the noise suppression capabilities in a pass-through configuration in SOA-based interferometric structures," *IEEE Photon. Technol. Lett.*, Vol. 12, No. 7, pp. 837-839, 2000.
- [9] D. Chiaroni, B. Lavigne, A. Jourdan, L. Hamon, C. Janz, and M. Renaud, "10 Gbit/s 3R NRZ optical regenerative interface based on semiconductor optical amplifiers for all-optical networks," *Proc. of European Conference on Optical communications, ECOC'97*, Post-Deadline paper PD 41, Edinburgh, UK, 22-25 Sept. 1997.
- [10] B. Lavigne, D. Chiaroni, L. Hamon, C. Janz, and A. Jourdan, "Performance and system margins at 10 Gbit/s of an optical repeater for long-haul NRZ transmission," *Proc. European Conference on Optical communications, ECOC'98*, Vol. 1, pp. 559-560, Madrid, Spain, 20-24 Sept. 1998.
- [11] K. S. Jepsen, A. Buxens, A. T. Clausen, H. N. Poulsen, B. Mikkelsen, and K. E. Stubkjaer, "20 Gbit/s optical 3R regeneration using polarization-independent monolithically integrated Michelson interferometer," *Electron. Lett.*, Vol. 34, No. 5, pp. 472-474, 1998.
- [12] D. Wolfson, A. Kloch, T. Fjelde, C. Janz, B. Dagens, and M. Renaud, "40 Gbit/s all-optical wavelength conversion, regeneration, and demultiplexing in an SOA-based all-active Mach-Zehnder interferometer," *IEEE Photon. Technol. Lett.*, Vol. 12, No. 3, pp. 332-334, 2000.
- [13] Y. Ueno, S. Nakamura, and K. Tajima, "Penalty-free error-free all-optical data pulse regeneration at 84 Gbit/s by using a symmetric-mach-Zehnder-type semiconductor regenerator," *IEEE Photon. Technol. Lett.*, Vol. 13, No. 5, pp. 469-471, 2001.

- [14] J. De Merlier, G. Morthier, P. Van Daele, I. Moerman, R. Baets, "All-optical 2R regeneration based on integrated asymmetric Mach-Zehnder interferometer incorporating MMI-SOA", *Electron. Lett.*, Vol. 38, pp. 238 -239, 2002.
- [15] A. E. Kelly, I. D. Phillips, R. J. Manning, A. D. Ellis, D. Nasset, D. G. Moodie, and R. Kashyap, "80 Gbit/s all-optical regenerative wavelength conversion using semiconductor optical amplifier based interferometer," *Electron. Lett.*, Vol. 35, No. 17, pp. 1477-1478, 1999.
- [16] H. J. Thiele, A. D. Ellis, and I. D. Phillips, "Recirculating loop demonstration all-optical 3R data regeneration using a semiconductor nonlinear interferometer," *Electron. Lett.*, Vol. 35, No. 3, pp. 230-231, 1999.
- [17] O. Brox, S. Bauer, C. Bornholdt, D. Hoffmann, M. Möhrle, G. Sahin, and B. Sartorius, "Optical 3R regenerator based on Q-switched laser," *Techn. Dig. Conference on Optical fiber communication OFC 2001*, Paper-MG6, Anaheim, CA, USA, March 19-22, 2001.
- [18] M. Möhrle, C. Bornholdt, O. Brox, S. Bauer, and B. Sartorius, "Multi-section DFB lasers for high speed signal processing/regeneration," *Techn. Dig. Conference on Optical fiber communication OFC 2002*, Vol.2 pp. 136-138, Anaheim, CA, USA, March 17-22, 2002.
- [19] M. Owen, M. F. C. Stephens, R. V. Penty, and I. H. White, "All-optical 3R regeneration and format conversion in an integrated SOA/DFB laser," *Techn. Dig. Conference on Optical fiber communication OFC 2000*, Paper-ThF1, Baltimore, USA, March 5-10, 2000.
- [20] Z. Bakonyi, G. Onishchukov, C. Knoll, M. Golles, F. Lederer, and R. Ludwig, "In-line saturable absorber in transmission systems with cascaded semiconductor optical amplifiers," *IEEE Photon. Technol. Lett.*, Vol. 12, No. 5, pp. 570-572, 2000.
- [21] D. Atkinson, W. H. Loh, V. V. Afanasjev, A. B. Grudinin, A. J. Seeds, and D. N. Payne, "Increased amplifier spacing in soliton system with quantum-well saturable absorber and spectral filtering," *Opt. Lett.*, Vol. 19, No. 19, pp. 1514-1516, 1994.
- [22] O. Leclerc, G. Aubin, P. Brindel, J. Mangeney, H. Choumans, S. Barre, and J. L. Oudar, "Demonstration of high robustness to SNR impairment in 20 Gbit/s long-haul transmission using 1.5  $\mu\text{m}$  saturable absorber," *Electron. Lett.*, Vol. 36, No. 23, pp. 1944-1945, 2000.
- [23] B. Lavigne, D. Chiaroni, P. Guerber, L. Hamon, and A. Jourdan, "Improvement of regeneration capabilities in semiconductor optical amplifier based 3R regenerator," *Techn. Dig. Conference on Optical fiber communication OFC 1999*, Paper-TuJ3, pp. 128-130, San Diego, USA, February 21-26, 1999.

## **Chapter 2**

# **All-optical 2R regeneration based on gain-clamped SOAs**

As seen earlier in the previous chapter, the SOA-based MZI is one of the most attractive implementations of all-optical 2R regeneration due to its high integration potential. This device, however, suffers from a rather slow nonlinear transfer function, which results in a limit to the regeneration efficiency. An all-optical 2R regenerator that has a steep nonlinear transfer function and gives the same benefits as SOA-based devices would be a very promising component for the all-optical networks. In this chapter, we present an all-optical 2R regenerator using an MZI with GCSOAs in both arms, which does possess all these features. The operation of this regenerator is based on the specific property of a GCSOA that its amplification in the linear regime is independent of the injected current, whereas the saturation power increases linearly with the injected current.

In §2.1, the description of the GCSOA and its operation characteristics are given. §2.2 describes the structure and the operation principle of the 2R regenerator. Some simulation results are also shown in this section. In §2.3, the experimental demonstration of the regenerative capabilities is given. A digital-like nonlinear transfer response and a flexible adjustment of the decision threshold are presented. Dynamic measurements at 2.488 Gbit/s show a significant intensity noise suppression at the logic “0” and a large improvement in the extinction ratio even for a very deteriorated input signal with small extinction ratio. 8 dB improvement in extinction ratio has been obtained for an input extinction ratio of 5 dB, and 7 dB improvement for an input extinction ratio of 2 dB. Some discussions of the bitrate limitation due to relaxation oscillations are made in §2.4. At the end, a summary is drawn in §2.5.

## **2.1 The gain-clamped SOA**

### **2.1.1 Description of a GCSOA**

The GCSOA was first introduced for suppressing signal induced gain fluctuations of SOAs in WDM systems with an intensity modulation scheme in the middle of the 1990s [1-5]. It has been intensively investigated and used for linear optical

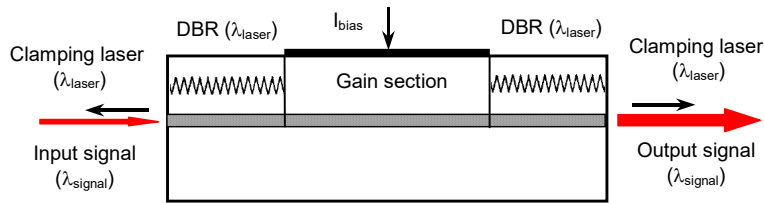


Fig. 2-1 Schematic structure of a GCSOA.

amplification, intensity noise suppression and switching applications in optical fiber telecommunications [6-12]. The GCSOA operates based on gain clamping by laser oscillation and provides a constant gain characteristic independent of injected current and optical input power, as opposed to a conventional SOA in which the gain changes with both the injected current and input power.

The basic structure of the GCSOA consist of three sections: a central gain section and two passive sections at input and output with distributed feedback (DFB) or distributed Bragg reflector (DBR) structures for wavelength selective feedback, as shown in Fig. 2-1. The physical principle of the GCSOA relies on the fact that in a laser operating above oscillation threshold, the gain at the lasing wavelength is clamped at a value equal to the cavity power losses. If the cavity losses are wavelength selective, as in for example a DBR structure, and if the facets are AR-coated, the device will behave like a gain-clamped travelling wave SOA for signal wavelengths far away from the lasing wavelength, provided the gain lineshape is homogeneously broadened. Owing to the gain-clamping effect, the signal gain is independent of signal intensity variations as long as the lasing oscillation is not switched off through a carrier depletion effect. The optical power is, in fact, stored in the lasing wavelength and converted into the amplified signal following intensity modulations with a time response limited by the relaxation oscillation frequency. A different value of the constant gain of the GCSOA may be obtained by changing the design of the feedback gratings.

### 2.1.2 Operation characteristics

Due to the gain-clamping effect, the GCSOA has specific properties in signal amplification, phase shift, and polarization. As expected from the physical principle of the GCSOA, the signal gain is independent of signal intensity variations as long as the signal power is not too high to switch off the lasing oscillation, and thus the signal is linearly amplified for low input powers. As the input power increases, the lasing oscillation will be switched off by the injected signal at a certain input power (i. e. saturation input power), and the signal gain drops suddenly due to the saturation of the GCSOA. The saturation input power increases with increasing injected current, while the unsaturated gain remains constant. Furthermore, the phase shift and the state of polarization at the output of the GCSOA also exhibit specific properties. It will be seen in §2.2 that it is these specific properties that

result in a "true" step-like regenerative response in a GCSOA-based MZI. In this section, we will demonstrate these properties.

### Amplification properties

Fig. 2-2 shows a typical simulation result of the amplification characteristics of a GCSOA [13]. As a comparison, the gain curve of a conventional SOA is also given in the figure. One can see clearly that the gain of the conventional SOA decreases as the input power increases, whereas, the gain of the GCSOA remains constant, as expected, until it is suddenly saturated. Furthermore, the gain in the linear regime is independent of the injected current.

Fig. 2-3 gives the measured output power and gain of a practical GCSOA as a function of input power for different injected currents. The GCSOA used in our measurements is commercially supplied by Alcatel Optronics, France [14]. The chip length is approximately 1000  $\mu\text{m}$ . The results show clearly the gain-clamping effect. In the lower input power region, the signal is linearly amplified, and the gain remains at a value of around 14.5 dB and is independent of injected current. The saturation input power and output power increase when the injected current changes from 120 mA to 160 mA. For input powers exceeding the saturation power, the gain drops quickly.

The polarization dependence of the gain (PDG) of the GCSOA is smaller than 0.5 dB for the injected current between 100 mA and 200 mA at a signal wavelength of 1550 nm, a number which was given in the data sheet of the device.

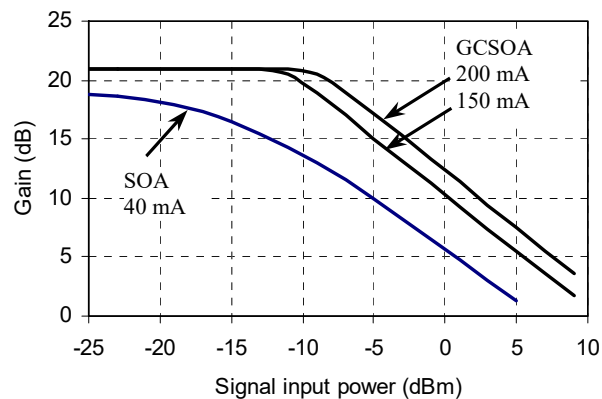
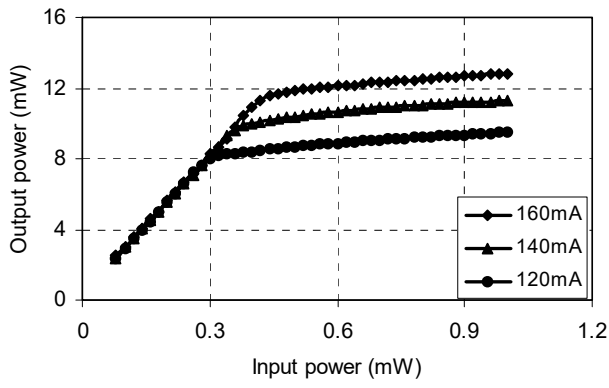
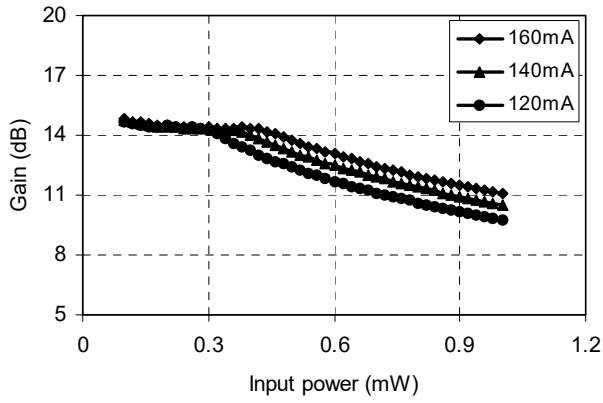


Fig. 2-2 Calculated gain as a function of the input power for a 1000- $\mu\text{m}$ -long GCSOA operated at 150 mA and 200 mA and a 450- $\mu\text{m}$ -long SOA operated at 40 mA. Signal wavelength: 1550 nm. [Ref. 13, D. Wolfson, *IEEE Photon. Technol. Lett.*, Vol. 11, No. 11, pp. 1494-1496, 1999].



(a)



(b)

Fig. 2-3 Measured output power and gain of the GCSOA as a function of input power for different injected currents. Signal wavelength: 1550 nm.

### Phase shift

The phase shift,  $\delta\varphi$ , experienced by the optical signal while travelling through the device is determined by the effective index,  $n^{eff}$ , as seen in Eq. 2-1.

$$\delta\varphi = k \int_0^l n(z)_{TE/TM}^{eff} dz + \delta\varphi_{DBR} \quad (2.1)$$

$$n(z)_{TE/TM}^{eff} = n_{0TE/TM} + \Gamma_{TE/TM} N(z) \left( \frac{\partial n}{\partial N} \right) \quad (2.2)$$

$$\delta\varphi_{DBR} = 2kl_{Bragg} \cdot n_{eff/B}^{TE/TM} \quad (2.3)$$

where  $n_0$  is the effective refractive index of the waveguide for zero free carrier density,  $\Gamma$  is the confinement factor, and  $(\partial n/\partial N)$  is the rate of change of the refractive index of the active region with the local carrier density  $N(z)$ .  $l$  is the length of the active layer of the device.  $l_{Bragg}$  is the length of the DBR section.  $n_{eff/B}$  is the effective refractive index of the DBR section. The subscripts *TE/TM* refer to the TE and TM mode.

In a GCSOA, the carrier density is pinned due to gain clamping, and thus the effective index of the devices does not change with input power in the linear regime. Consequently the phase shift stays constant in the linear regime. Once the linear power range is exceeded, the carrier density will drop rapidly, and thus a significant change in the phase shift will result from an induced change of the effective index. Simulation results given in Fig. 2-11 in the next section clearly show this specific property.

### State of Polarization

The TE and TM effective indices in an SOA exhibit different values owing to the guiding properties of the amplifier waveguides, which results in an effective birefringence [15,16]. Even though this effective birefringence is usually very small, and does not affect the polarization independent gain, a significant change in the state of polarization at the output of the SOA can be induced. In addition, for a given device the effective birefringence depends on the carrier density. The state of polarization at the output of the SOA depends on the input polarization state and the effective birefringence of the device. Therefore, the state of polarization at the output is generally different from the input polarization state as long as the input light is not exactly TE or TM polarized, and changes with the input power owing to the induced change in the carrier density and thus in the effective birefringence.

For a GCSOA, the gain is clamped and both the free carrier density and the total photon density (photon density of both laser and optical signal) are constant when the input power level varies in the linear regime. The effective birefringence, therefore, remains a constant, and thus the state of polarization at the output does not change. Once the linear power range is exceeded, the gain and thus the carrier density will drop rapidly. The effective birefringence and thus the polarization state of the output will significantly vary with the input power. Figs. 2-4 and 2-5 show the experimental setup and the measured evolutions of the state of polarization at the output of the GCSOA with the input power variation, respectively. In the experimental setup, a CW light beam from a tunable laser (Model Tunics-plus, Photonics) at 1550 nm is amplified and then coupled into the GCSOA with its input polarization set to be at some angle to the TE axis. The exact coupled input signal polarization is difficult to measure since the GCSOA has a pigtail of standard SM-fiber. However, there is a certain polarization for which the polarization effect is maximized, and it is this condition that is used in the measurements. The variable

attenuator is used to change the input power to the GCSOA. The polarization controller after the GCSOA linearises the polarization of the output, elliptically polarized, when the GCSOA operates with a low input power in the linear regime. The polarizer before the power meter is used as an analyzer to check the evolution of the state of polarization of the output light from the GCSOA. By rotating the analyzer around the light beam axis, a minimum and a maximum detected power,  $P_{\min}$  and  $P_{\max}$ , can be found. The elliptical polarization parameters, *azimuth*  $\theta$ , *ellipticity*  $e$  and amplitude  $A$  can be determined from the azimuth angle of the analyzer and the measured optical power  $P_{\min}$  and  $P_{\max}$ . Here, the *azimuth*  $\theta$  is the angle between the major axis of the ellipse and the positive direction of the  $x$ -axis and defines the orientation of the ellipse in its plane, and the *ellipticity*  $e$  is the ratio of the length of the semi-minor axis of the ellipse  $b$  to the length of the semi-major axis  $a$ . The detailed description of the method of measuring the state of polarization can be seen in §4.1.1.

In Fig. 2-5 (b), the variation of the polarization direction, azimuth  $\theta$ , versus the input power is illustrated for two different injected currents: 145 mA and 176 mA, while in Fig. 2-5 (c) the ellipticity of the output light as a function of input power is shown. As a comparison, the saturation characteristic of the GCSOA is also given in Fig. 2-5 (a). One can see that, as expected, both the polarization direction and the ellipticity remain constants in the linear regime, i. e., the state of polarization at the output does not change with input power, but change rapidly with increasing input power above the saturation input power. Changing injected current from 145 mA to 176 mA, the polarization direction rotates over 1 degree and the ellipticity changes very little in the linear regime. This small change of the state of polarization can be explained as follows. For a given input power in the linear regime, the gain remains constant but, due to gain suppression, the carrier density also increases a little with increasing injected current to the GCSOA. Therefore, the effective birefringence changes with the injected current, and thus the state of polarization at the output of the GCSOA changes when changing the injected current. In Fig. 2-5, an abnormal variation of the polarization can also be seen. The explanation of this behavior is not clear yet.

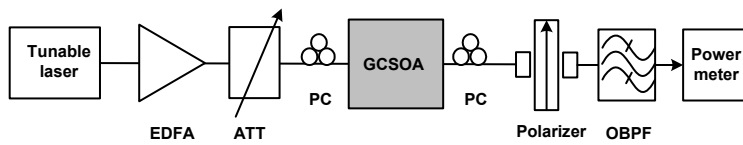


Fig. 2-4 Experimental set-up for measuring the polarization properties of the GCSOA. ATT: Tunable attenuator; PC: Polarization controller; OBPF: optical band pass filter. The polarizer is rotatable around the light beam axis. Two collimators are used for the in- and out-of-fiber coupling of the polarizer.

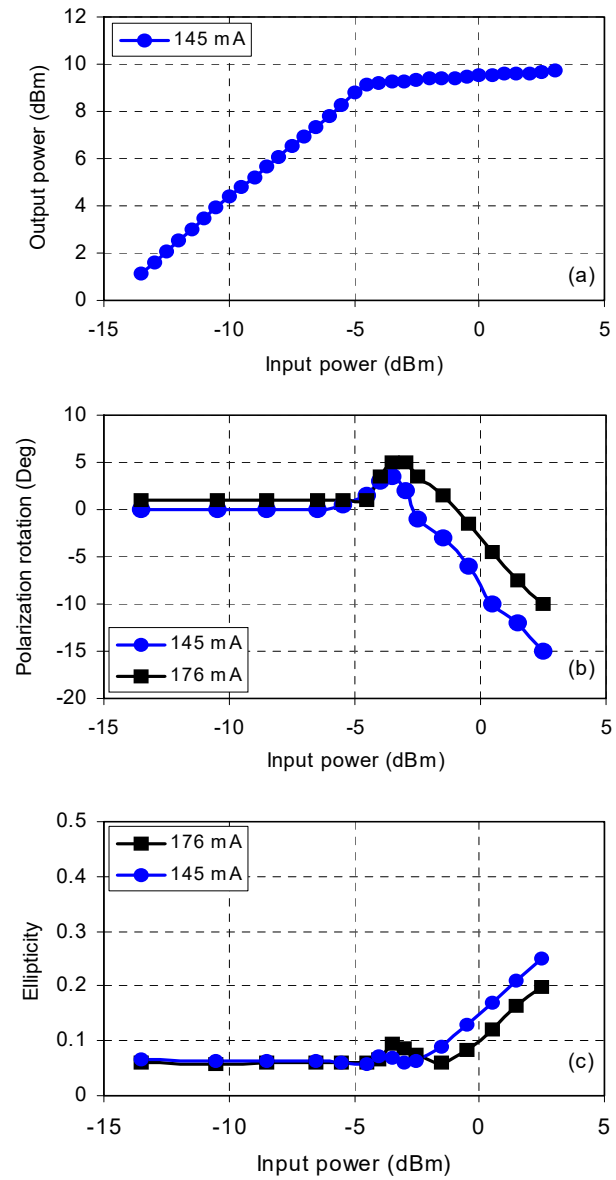


Fig. 2-5 Measured evolutions of the state of polarization at the output of the GCSOA with the input power variation for different injected currents, (a) the output power versus input power, (b) the variation of the polarization direction (azimuth  $\theta$ ), (c) the ellipticity of the output light. Signal wavelength: 1550 nm.

### Optical spectrum

The measured optical spectra of the output of the GCSOA are shown in Fig. 2-6 for different input power levels. One can see the lasing wavelength at 1508 nm, at the short wavelength side of the amplified spontaneous emission (ASE) spectrum. For the low input power, the lasing oscillation occurs simultaneously with the signal amplification and the gain is clamped. When the input signal power exceeds the saturation input power, the lasing oscillation is switched off and the GCSOA is saturated. The ASE peak is at 1538 nm for an injected current of 120 mA when the GCSOA is unsaturated. 3 dB optical bandwidth given from the data sheet is 30 nm.

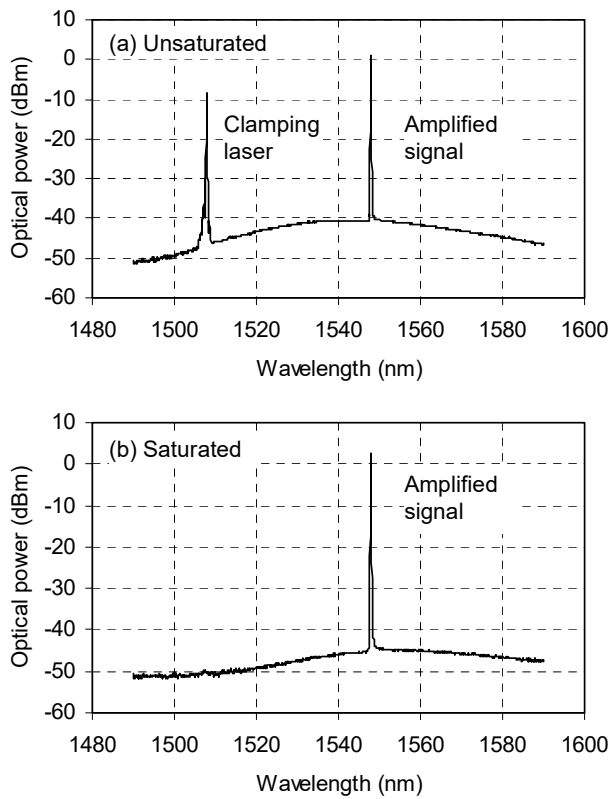


Fig. 2-6 Measured optical spectra of the output of the GCSOA for different input power levels, (a) low input power (unsaturated), (b) high input power (saturated). The injected current to the GCSOA is 120 mA.

## 2.2 All-optical 2R regenerator based on a MZI with GCSOAs

### 2.2.1 Structure and operation principle

The structure of an all-optical 2R regenerator based on a MZI with GCSOAs in both arms is shown in Fig. 2-7. The splitters are symmetric (3 dB splitter and coupler), and the two GCSOAs are assumed to be identical but biased with a different injected current. The static phase difference between the two arms is  $\pi$  in the linear regime, which can be implemented as a phase modulator or as an optical path length difference.

The operation of this regenerator is based on Mach-Zehnder interference and the specific property of a GCSOA that its amplification in the linear regime is independent of the injected current, whereas the saturation power increases linearly with the injected current, which has been described in the previous section. The output power of a MZI for linearly polarized input light is given by

$$P_{out} \propto P_{in} \left( A_1 + A_2 + 2\sqrt{A_1 A_2} \cos(\Delta\varphi) \right) \quad (2.3)$$

where  $A_1$  and  $A_2$  are the amplification of GCSOA1 and GCSOA2, respectively, and  $\Delta\varphi$  the phase difference between the two arms. In the linear regime, both arms of the MZI give the same signal gain, and the light waves travelling through the two arms have the same amplitude and same state of polarization. Hence, the phase shift of  $\pi$  in one of the arms causes total destructive interference below the input saturation powers of both GCSOAs at the output of the MZI, as seen in Fig. 2-8. Beyond the saturation power of both GCSOAs, the output powers from both GCSOAs are saturated. Furthermore, due to additional phase shifts accompanying the saturation in each GCSOA, the phase difference between both interference arms becomes different from  $\pi$ , and, in addition, the state of polarization of the two arms becomes different from each other. Therefore, there is no longer total destructive interference. However, the fact that the amplifier output powers in both arms and the phase difference between both arms remain constant as the input power varies above the saturation powers causes the output power of the MZI to be constant as well. In between the saturation power of the first amplifier and the saturation power of the second amplifier, there is a gradual increase in the output power of the MZI. Since the saturation of the GCSOAs happens suddenly due to switching off of the clamping lasing oscillations and the gain drops very fast once the GCSOA is saturated, the output power shifts quickly from the low to the high level. Consequently, the output power versus input power of the MZI behaves like a step function, as shown in Fig. 2-8. The decision threshold of the step-like transfer function is determined by the saturation input powers of the GCSOAs. Obviously, the decision threshold changes with changing injected currents to the GCSOAs. This is due to the fact that the saturation input power of the GCSOAs increases with increasing injected current, while the unsaturated gain remains constant in the linear regime. It is emphasized that an identical amplification for different saturation

powers can only be obtained with GCSOAs and not with conventional traveling wave SOAs.

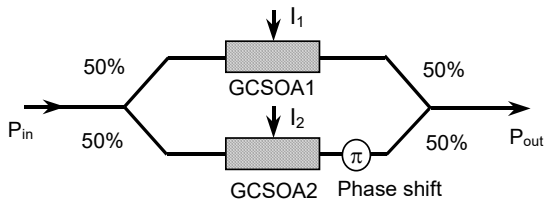


Fig. 2-7 Schematic structure of all-optical 2R regenerator based on MZI with GCSOAs.

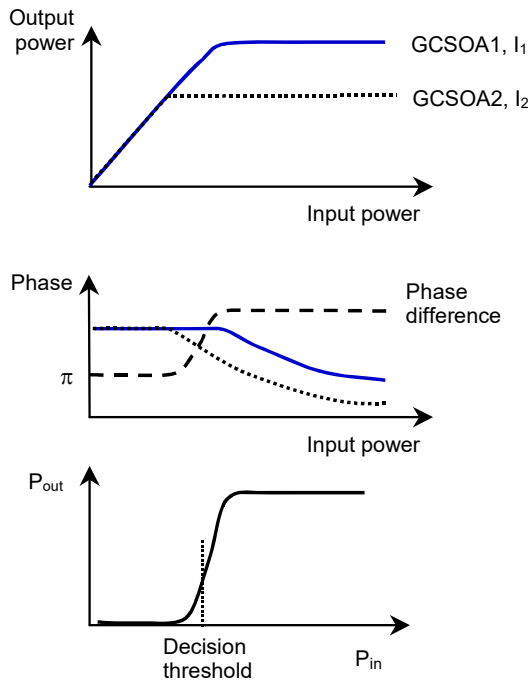


Fig. 2-8 Operation principle of the all-optical 2R regeneration based on an MZI with GCSOAs in both arms. The two GCSOAs are assumed to be identical, and the two arms of the MZI have same amplification in the linear regime.

More generally, one could also design the regenerator with non-identical GCSOAs and asymmetric splitters and couplers. In addition, an alternative for the MZI-based 2R regenerator is the Michelson interferometer (MI) version. In this configuration, the amplifiers must be reflecting. They can, therefore, be implemented as DFB lasers with one AR-coated facet and one cleaved or HR-coated facet. As in the MZI-based structure, both amplifiers are assumed to have a different injected current such that they exhibit equal amplification and phase shift below the saturation power and a different saturation power. The operation principle of this MI-based 2R regenerator is then identical to that of the MZI-based 2R regenerator.

### 2.2.2 Numerically simulated transfer characteristics

A good agreement between simulation and experimental results needs all the parameters that are not, however, available for commercial devices. The simulations were, therefore, just done (before the experiments) to show that the principle works, not to get good agreement with the experiments, and to show how good the characteristic can be in theory. Typical parameters representative for this type of device but not necessarily accurate for the specific component were used in the simulations, which are summarized in Table 2-1. The material parameters (i. e.,  $C_1$ - $C_6$ ) are based on the values used in [17], the other parameters in Table 2-1 were chosen with the intent of obtaining about 20-dB amplifier gain. No gain suppression (or explicit power dependence of the gain  $g$ ) has been taken into account. The simulations have been performed using the longitudinal computer model CLADISS [17]. The GCSOAs exhibit lasing with a threshold current of 24.8 mA and at an emission wavelength of 1.5298  $\mu\text{m}$ . The wavelength of the injected signal was chosen to be 1.55  $\mu\text{m}$ , i. e., sufficiently far from the lasing wavelength and the Bragg wavelength of the Bragg sections. It can further be noticed that the (monomolecular, bimolecular and Auger) recombination parameters mainly affect the threshold current of the GCSOAs, and hence also the currents corresponding with a certain saturation power, and the damping of the relaxation oscillations during the switching. In the simulations, a symmetric MZI with traveling-wave GCSOAs, consisting of an amplifying section surrounded by passive DBR sections on either sides (as seen in Fig. 2-1) was considered. Fig. 2-9(a) and Fig. 2-9(b) show the simulation results of the amplification and phase shift characteristics of the GCSOAs under different bias currents (86 and 117 mA) and the output power versus input power characteristics of the 2R regenerator, respectively [18]. One can see that the amplification and phase shift of the GCSOAs are independent of the injected current and remain constant when the input power varies in the linear regime, which agrees with the experimental results demonstrated in the previous section. The output power of the MZI is fairly constant below 2 mW and above 3 mW, showing a step-like transfer response of the 2R regenerator.

It should be noted that from the simulation the additional phase shift due to saturation of the GCSOA with lowest injected current is only 0.5 rad. Ideally, this phase shift should be  $\pi$ , but this value is not easily obtained with realistic values for material and device parameters [18].

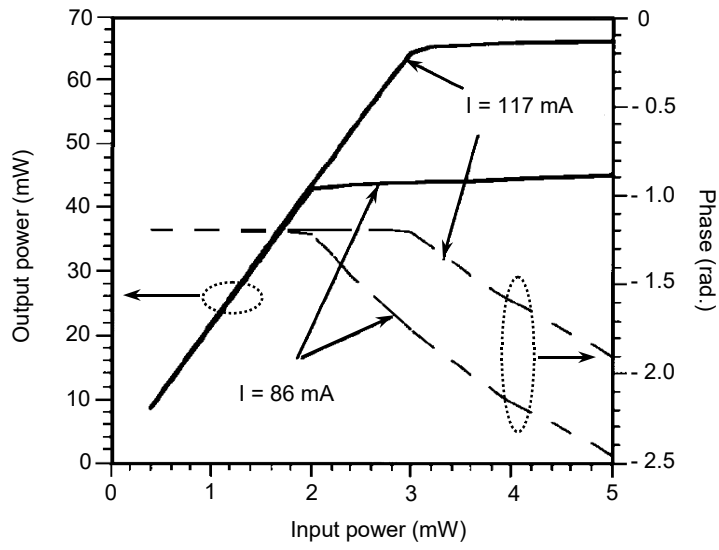


Fig. 2-9 (a) Amplitude (—) and phase (---) characteristics of two GCSOAs with different injected currents (86 and 117 mA).

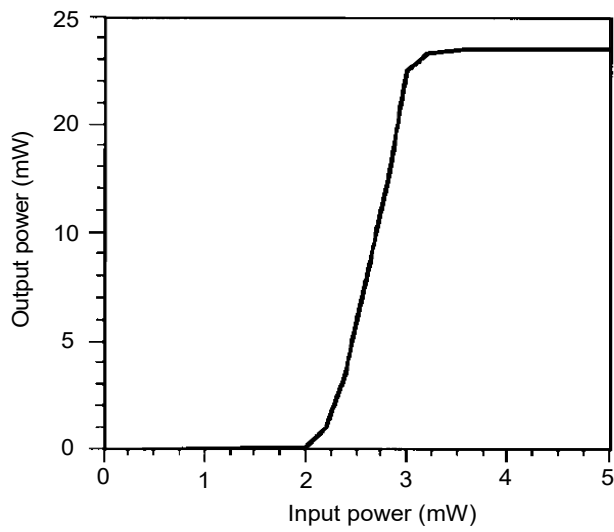


Fig 2-9 (b) Output power versus input power of a symmetric MZI with GCSOAs in both arms.

Table 2-1 GCSOA parameters used in the numerical simulation [18]

| Parameters                                      | Value                   | Unit                   |
|---|-------------------------|------------------------|
| Length of the Bragg sections                    | 400                     | $\mu\text{m}$          |
| Period of the Bragg gratings                    | 233                     | nm                     |
| Coupling coefficient of the Bragg gratings      | 7.5                     | $\text{cm}^{-1}$       |
| Effective index of the Bragg sections           | 3.283                   |                        |
| Length of the active section                    | 1000                    | $\mu\text{m}$          |
| Cross section of the waveguide                  | 0.3                     | $\mu\text{m}^2$        |
| Confinement factor                              | 0.4                     |                        |
| Internal loss                                   | 25                      | $\text{cm}^{-1}$       |
| Monomolecular recombination coefficient         | $0.167 \times 10^9$     | $\text{s}^{-1}$        |
| Bimolecular recombination coefficient           | $10^{-10}$              | $\text{cm}^3/\text{s}$ |
| Auger recombination coefficient                 | $3 \times 10^{-29}$     | $\text{cm}^6/\text{s}$ |
| Effective index without injection               | 3.283                   |                        |
| Change of $n_{\text{eff}}$ with carrier density | $-1.69 \times 10^{-20}$ | $\text{cm}^3$          |
| Gain $g = C_1(E-C_2)^{C_3}N-C_4(E-C_5)^{C_6}$   |                         |                        |
| $C_1$   | $4.68 \times 10^{-15}$  | $\text{cm}^2$          |
| $C_2$   | 0.7477                  | eV                     |
| $C_3$   | 0.7743                  |                        |
| $C_4$   | $77.16 \times 10^4$     | $\text{cm}^{-1}$       |
| $C_5$   | 0.6237                  | eV                     |
| $C_6$   | 4.1727                  |                        |

### 2.3 Experimental characterization

The MZI 2R regenerator proposed above can in principle be integrated. For our experiments, however, the MZI was built using fiber-optic 3dB splitters and two commercial, packaged GCSOAs. The two GCSOAs happen to exhibit considerably different amplification and equal gain in both interferometer arms is achieved using an extra variable attenuator in one arm. The temperature control of one of the packaged GCSOAs was used to obtain a phase difference of  $\pi$  between the two arms and thus destructive interference at a low input power level. To avoid instabilities due to airflow, the fiber-optic interferometer is concealed in a plastic box. At the output, an optical filter with a 3 dB bandwidth of 0.3 nm is used to suppress the laser mode and the amplified spontaneous emission from the GCSOAs. Fig. 2-10 shows a photograph of the MZI-based 2R regenerator built using fiber-optical 3 dB splitters and the GCSOAs with single mode fiber pigtails.

The schematic experimental setup for measuring the static and dynamic characteristics of the 2R regenerator is shown in Fig. 2-11. A tunable laser source (Model Tunics-plus, Photonics), an external modulator, and a pulse generator are combined and used as a transmitter. The optical data signal at 2.5 Gbit/s (PRBS= $2^{23}-1$ , RZ format) is first transmitted through an EDFA, and then coupled into the MZI. The extinction ratio of the data signal can be controlled by changing the driving pulse amplitude (i. e., electrical pulse signal amplitude) of the external modulator. The optical band pass filter (OBPF) behind the EDFA has a 3-dB bandwidth of 0.2 nm and the same central wavelength as the filter at the output of the MZI. In the following sections, we present the detailed experimental results of the static and dynamic characteristics of the 2R regenerator, which clearly demonstrate a quasi-ideal optical transfer function and excellent regeneration capabilities.

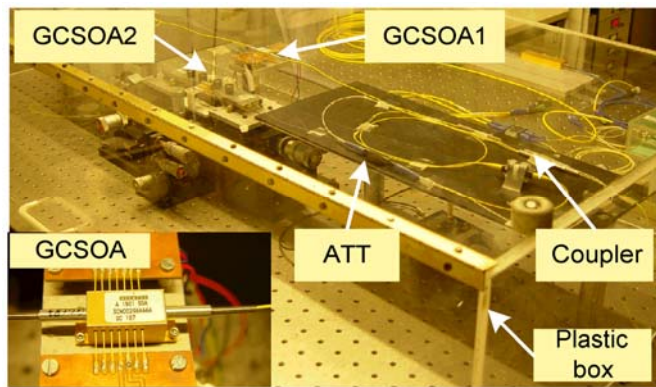


Fig. 2-10 Photograph of the fiber-based 2R regenerator using MZI with GCSOAs in both arms.

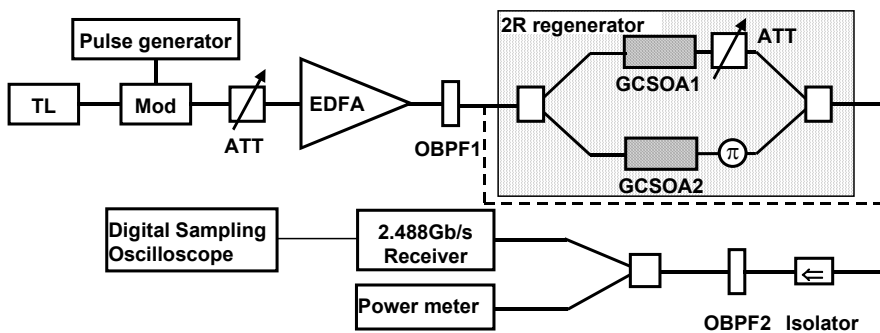


Fig. 2-11 Experimental setup for 2R regenerator based on a MZI with equal GCSOAs in both arms. TL: tunable laser, ATT: Attenuator, Mod: Mach-Zehnder modulator, The dashed line indicates the setup without the 2R regenerator.

### 2.3.1 Static transfer characteristics

The measured static transfer characteristic of the MZI is shown in Fig. 2-12. The bias currents applied to the two GCSOAs are 140mA and 145mA, respectively, and the signal wavelength is 1553.3 nm. As can be seen, the optical transfer characteristic has a true digital-like shape. For both a logical “1” (high power level) and a logical “0” (low power level) quasi-perfect regeneration is achieved, which is consistent with the simulation result described in the previous section. The output power shifts from the low to the high level over an input power range of about 0.2 mW at a threshold power of 1.0 mW. This means that under static conditions an output extinction ratio of 15 dB can be obtained for an input extinction ratio of less than 1 dB. We note that this is in sharp contrast with the sinusoidal-like regeneration obtained from most other regenerators that have been proposed so far [19-22].

The small power fluctuation of the logical “0” in Fig. 2-12 is due to the fact that the two GCSOAs are not exactly identical and also their gains are not constant but change a little when input power varies, as seen in Fig. 2-3. For a given input power ( $\sim 0.75$  mW in our experiments), a same amplification of the two arms of the MZI can be obtained by adjusting the attenuation of the attenuator in one arm and a completely destructive interference can be achieved. But for other input powers below the input saturation power, there could be a small amplification difference between the two arms due to the small change of the gain of the GCSOAs. Consequently, the interference could not be completely destructive and it causes a non-zero output of the MZI in the low power region. This power fluctuation could be reduced using two selected identical devices.

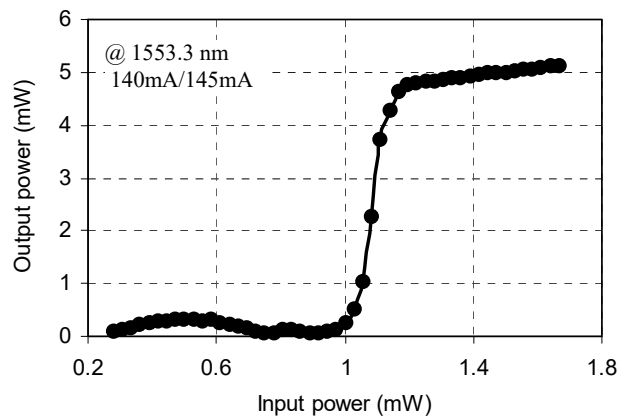


Fig. 2-12 Measured static transfer characteristic of the all-optical 2R regenerator. Injected current to the two GCSOAs: 140 mA/145 mA; signal wavelength: 1553.3 nm.

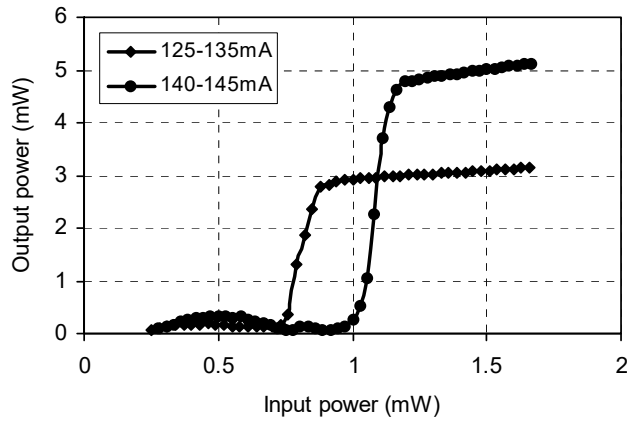


Fig. 2-13 Change of the static transfer characteristics with changing injected current to the GCSOAs. Signal wavelength: 1553.3 nm.

### 2.3.2 Decision threshold adjustment

Optical decision threshold is one of the key parameters of an optical 2R regenerator. The flexible adjustment of the decision threshold of the 2R regenerator will give certain benefits to the design of optical networks. The 2R regenerator based on the GCSOAs has the advantage of adjustable decision threshold, thanks to the adjustable saturation power of the GCSOAs.

Fig. 2-13 gives the measured static transfer function for different injected currents to the GCSOAs. The results demonstrate very clearly a significant shift of the decision threshold when the injected currents change from 125/135 mA to 140/145 mA. Therefore, a very flexible adjustment of the decision threshold can be achieved easily by altering the injected currents to the GCSOAs. Note that the lower output power for logical "1" at the lower injected currents is due to the lower saturation output powers of the GCSOAs.

An important feature for practical use of all-optical regeneration is wavelength insensitivity. Fig. 2-14 shows the measured static transfer characteristics for different signal wavelengths, with the same bias currents being applied to the GCSOAs. Clearly, good regeneration has been obtained over a broad wavelength range from 1540 to 1560 nm. There is a small shift of the decision threshold ( $\sim 1$  dB) for a wavelength range of 20 nm. This could be due to the fact that the saturation input power of the GCSOAs changes a little with the signal wavelength.

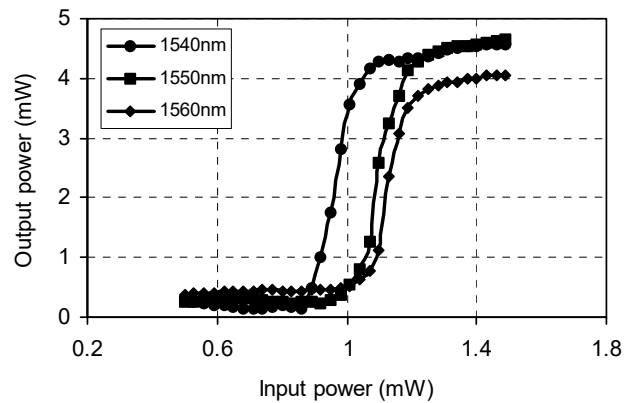


Fig. 2-14 Static transfer characteristics for different wavelengths. Injected currents to the two GCSOAs: 135 and 147 mA, respectively.

### 2.3.3 Extinction ratio improvement

The regenerative capabilities of the 2R regenerator under dynamic operation are demonstrated in Figs. 2-15 and 2-16. Fig. 2-15 shows the eye diagrams with and without the 2R regenerator for the input ERs of 2 dB, 5 dB and 9 dB, while Fig. 2-16 gives the extinction ratio (ER) improvement. Both figures are obtained for a signal with a bitrate of 2.5 Gbit/s (RZ,  $2^{23}-1$  PRBS). Clearly, the input signal is regenerated. Both the power level and the noise at the logic “0” are tremendously suppressed, and a strong improvement of the ER is demonstrated. For the input signals with ERs of 5 dB and 9 dB, 8 dB improvement in ER is obtained. Even for a very deteriorated input signal with almost closed eyes (input ER = 2 dB), clearly opening eyes can be obtained with the 2R regenerator and an ER improvement of 7 dB is still achieved. This result is in contrast with that in [21], where the maximum improvement of the ER was 4 dB for an input ER of 6 dB.

As the noise at the logical “0” is strongly suppressed after the 2R regenerator, there is no doubt that an improvement in signal-to-noise ratio (SNR) and thus an improvement in receiver sensitivity can be achieved, although no significant intensity noise suppression at the logical “1” is observed.

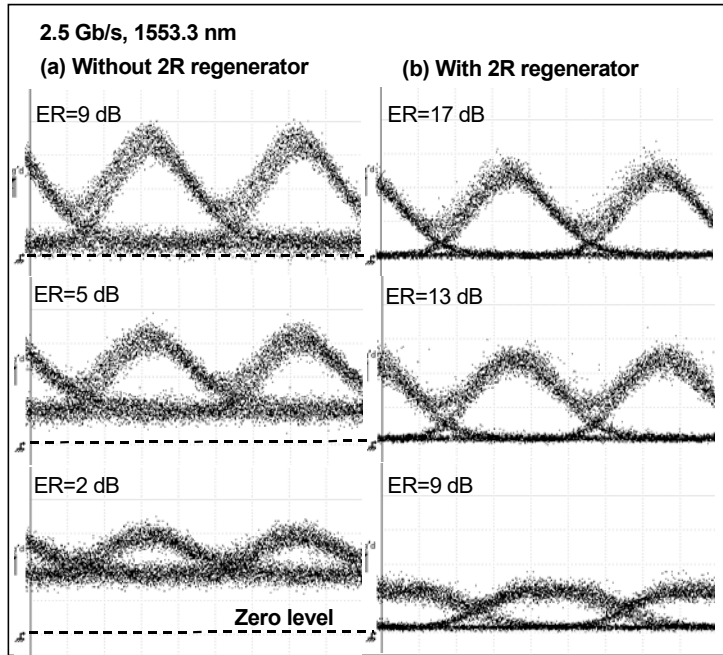


Fig. 2-15 Eye diagrams with and without the 2R regenerator for signals with different extinction ratios at 2.5 Gbit/s (PRBS=2<sup>23</sup>-1, RZ format). Signal wavelength: 1553.3 nm.

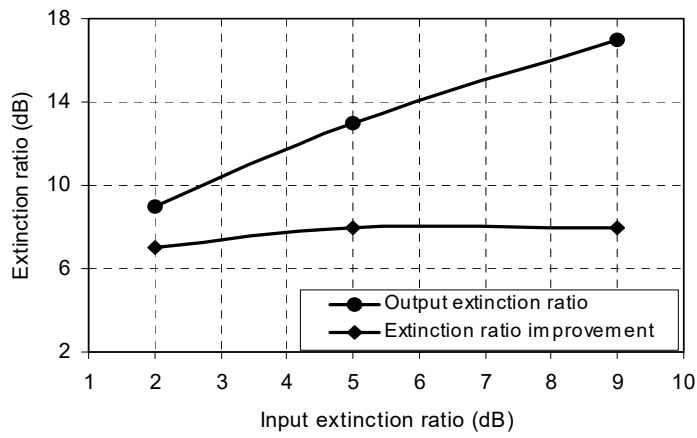


Fig. 2-16 Improvement in ER as a function of input ER at 2.5 Gbit/s.

### 2.3.4 Discussion

#### Noise of the logic “1”

It can be noticed that the noise suppression for a logical “1” is not as good as expected. This is due to extra noise induced by an instability of the laser mode near the saturation power of the GCSOAs. Fig. 2-17 shows the noise at the outputs of the GCSOAs and the 2R regenerator, respectively, for a CW input signal with different optical power. The injected currents to the two GCSOAs are 140 mA and 148 mA. The input saturation power of the GCSOAs is around 0.4 mW. One can see that for low input power of 0.5 mW to the 2R (0.25 mW to the GCSOAs) in the linear regime the noises at the outputs of GCSOAs and the 2R regenerator are very small. However, for a high input power of 1.0 mW, the power fluctuation at the GCSOAs becomes higher due to the instability of the laser mode and it causes a large noise at the output of the 2R regenerator. The instability of the laser mode near the threshold might result from some weak back reflection in the hybrid fiber-based device. We believe that an integrated version of the device would show better noise suppression at both logical “0” and “1”. On the other hand, the noise in the logical “1” can also be reduced using a cascaded SOA which operates at saturation condition. This has been successfully used for suppressing the noise in the logical “1” in SA-based 2R regenerators [23].

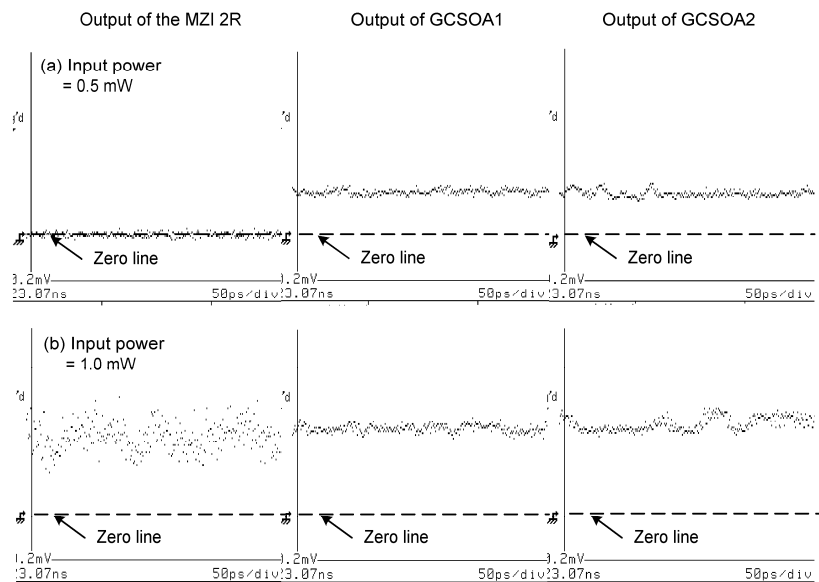


Fig. 2-17 Noises at the outputs of the GCSOAs and the 2R regenerator, respectively, for a CW input signal with different optical power. The injected currents to the two GCSOAs are 140 mA and 148 mA. The saturation input power of the GCSOAs is around 0.4 mW. The input powers given in the figure are the optical powers launched into the 2R regenerator.

### **Instability**

With a fiber-based MZI configuration, both arms of the interferometer are physically separated, and thus the 2R regenerator proposed above has a big issue of interference instabilities due to varying environmental conditions. By fixing the whole set-up on a plate and covering it with a plastic box, the output power instabilities have been reduced to some extent, but the output of the MZI still exhibits a significant fluctuation. This problem could be solved in two ways: utilizing active phase stabilization [24] or monolithically integrating the MZI. In the first method, a CW-pilot optical signal and an electrical feedback control circuit are added to the MZI. The pilot signal is passed through the MZI in opposite direction to the data signal. The pilot output power is held at a constant level by correcting the optical path length in one interferometer arm by a Peltier element directly attached to the optical fiber. The slow fluctuation of the phase and thus the fluctuation of the output power of the MZI are eliminated. As for the monolithically integrated MZI with GCSOAs in both arms, it has obviously more advantages than the fiber-based configuration, and we believe that it could be available in a not too far future.

### **Bitrate limitation due to relaxation oscillations**

The GCSOAs exhibit the relaxation oscillations occurring during the on-switching of the laser mode. These relaxation oscillations seriously affect the transient behavior of the GCSOA. Time domain simulations, shown in [18], indicated that the operation of the GCSOA-based 2R regenerator is limited to a bitrate below the relaxation oscillation frequency. We have measured the dynamic behavior of the GCSOA, as seen in Fig. 2-18, with an input consisting of periodic pulses driving the amplifier into saturation, clearly showing the relaxation oscillations with a resonance frequency of around 5 GHz and a total duration of about 0.4 ns.

The bitrate limitation of the all-optical 2R regeneration proposed above can be overcome by using some new designed gain-clamped SOAs, such as the linear optical amplifiers (LOA) [25]. In the LOA, a vertical cavity with a very short length is integrated with an optical amplifier and operates as the optical feedback, instead of the long cavity in the GCSOA. This results in a much higher relaxation oscillation frequency, and the LOA will not be limited for high-speed applications. In addition, two other types of GCSOAs are also reported: the hybrid integrated gain-clamped SOA [26] and the four-section GCSOA [27]. The hybrid integrated GCSOA uses UV-gratings written on PLC waveguides as external mirrors for laser oscillation, while the four-section GCSOA is similar to the normal GCSOA described in the previous section but with controllable feedback gratings. Both of them exhibit a variable gain and operation at 10 Gbit/s has been demonstrated for the first one. The property of variable gain of these devices is very promising to realize the “identical” amplification of the two arms of the MZI. Furthermore, it has been shown in recent investigation that DBR lasers can give very high bandwidths (e. g. , 30 GHz) and very high resonance frequencies [28]. If appropriately designed, even higher resonance frequencies should be possible in DBR-based GCSOAs. With such amplifiers, the regenerator proposed here should easily be capable of operation at 10 Gbit/s or at multiples of that bitrate.

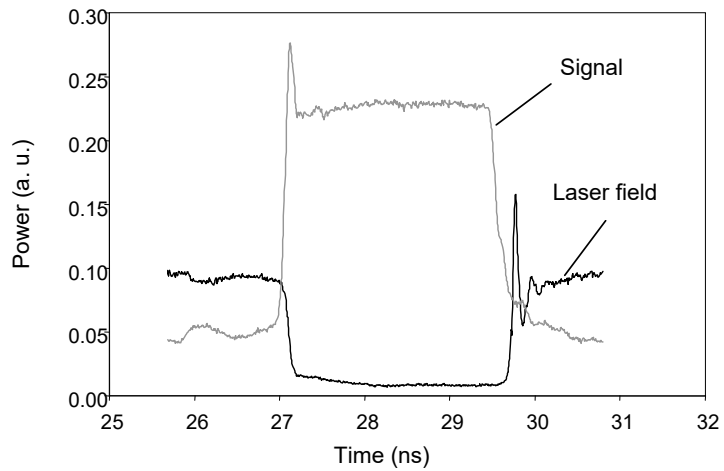


Fig. 2-18 Transient response of laser field and signal output power for a GCSOA (driven at 100 mA) and for rectangular input pulses with 200-MHz repetition rate and an extinction ratio of 10 dB.

In the following chapter, we will present an all-optical 2R regenerator based on an MZI with LOAs.

## 2.4 Summary

In this chapter, we first described the structure and operation characteristics of the GCSOAs. The GCSOAs exhibit specific properties in gain, phase shift, and polarization. In the linear regime, the gain, phase shift and the state of polarization are independent of the input power, while for input powers exceeding the saturation power, all of them change quickly as the input power increases.

Based on these specific properties, we introduced, in §2.2, an all-optical 2R regenerator that has a MZI structure. Both simulation and experiments show that the 2R regenerator has a digital-like nonlinear transfer function and a flexible adjustment of decision threshold. Dynamic measurements at 2.5 Gbit/s presented in §2.3 demonstrate significant intensity noise suppression at the logic “0” and a large improvement in the extinction ratio even for a very deteriorated input signal with small extinction ratio. 8 dB improvement in extinction ratio has been obtained for an input extinction ratio of 5 dB, and 7 dB improvement for an input extinction ratio of 2 dB. Furthermore, a good regeneration over a broad wavelength range of 20 nm is also demonstrated. Therefore, taking the simplicity of the device and the excellent

regeneration characteristics into account, this approach is a promising technique for all-optical 2R regeneration.

Finally, some discussions of the bitrate limitation due to the relaxation oscillations were made.

## References

- [1] J. C. Simon, P. Doussiere, P. Lamouler, I. Valiente, and F. Riou, "Travelling wave semiconductor optical amplifier with reduced nonlinear distortion," *Electron Lett.*, Vol. 30, No. 1, pp. 49-50, 1994.
- [2] P. Doussiere, A. Jourdan, G. Soulage, P. Garabédian, C. Graver, T. Fillion, E. Derouin, and D. Leclerc, "Clamped gain travelling wave semiconductor optical amplifier for wavelength division multiplexing application," *Semiconductor Laser conference, 14<sup>th</sup> IEEE International*, pp. 185-186, Maui, HI, USA, 1994.
- [3] L. F. Tiemeijer, P. J. A. Thijjs, T. V. Dongen, J. J. M. Binsma, E. J. Jansen, and H. R. J. R. van Helleputte, "Reduced intermodulation distortion in 1300 nm gain-clamped MQW laser amplifiers," *IEEE Photon. Technol. Lett.*, Vol. 7, No. 3, pp. 284-286, 1995.
- [4] B. Bauer, F. Henry, and R. Schimpe, "Gain stabilization of a semiconductor optical amplifier by distributed feedback," *IEEE Photon. Technol. Lett.*, Vol. 6, No. 2, pp. 182-185, 1994.
- [5] M. Bachmann, P. Doussiere, J. Y. Emery, R. N'Go, F. Pommereau, L. Goldstein, G. Soulage, and A. Jourdan, "Polarization-insensitive clamped-gain SOA with integrated spot-size convertor and DBR gratings for WDM applications at 1.55 $\mu$ m wavelength," *Electron. Lett.*, Vol. 32, No. 22, pp. 2076-2077, 1996.
- [6] J. L. Pleumeekers, M. A. Dupertuis, T. Hessler, P. E. Selbmann, S. Haacke, and B. Deveaud, "Longitudinal spatial hole burning and associated nonlinear gain in gain-clamped semiconductor optical amplifiers," *IEEE J. Quantum Electron.*, Vol. 34, No. 5, pp. 879-886, 1998.
- [7] D. T. Schaafsma, E. Miles, and E. M. Bradley, "Comparison of conventional and gain-clamped semiconductor optical amplifiers for wavelength-division-multiplexed transmission systems," *IEEE J. Lightwave Technol.* Vol. 18, No. 7, pp. 922-925, 2000.
- [8] G. Morthier, and J. Sun, "Repetition-rate dependence of the saturation power of gain-clamped semiconductor optical amplifiers," *IEEE Photon. Technol. Lett.*, Vol. 10, No. 2, pp. 282-284, 1998.
- [9] M. Zhao, G. Morthier, and R. Baets, "Analysis and optimization of intensity noise reduction in spectrum-sliced WDM systems using a saturated semiconductor optical amplifier," *IEEE Photon. Technol. Lett.*, Vol. 14, No. 3, pp. 390-392, 2002.
- [10] M. Zhao, G. Morthier, R. Baets, and J. Dekoster, "Investigation of the intensity noise reduction using a saturated semiconductor optical amplifier in spectrum sliced WDM systems," *Tech. Dig. Conference on Lasers and Electro-Optics, CLEO '01*, pp. 383 – 384, Baltimore, MD, USA, 2001.
- [11] D. Wolfson, S. L. Danielsen, C. Joergensen, B. Mikkelsen, and K. E. Stubkjaer, "Detailed theoretical investigation of the input power dynamic range for gain-clamped semiconductor optical amplifier gates at 10 Gb/s," *IEEE Photon. Technol. Lett.*, Vol. 10, No. 9, pp. 1241-1243, 1998.
- [12] G. Soulage, P. Doussiere, A. Jourdan, and M. Sotom, "Clamped gain travelling wave semiconductor optical amplifier as a large dynamic range optical gate," in *Proc. European Conference on Optical Communication, ECOC'94*, Vol. 1, pp. 451-454, Firenze, Italy, Sept. 25-29, 1994.

- [13] D. Wolfson, "Detailed theoretical investigation and comparison of the cascability of conventional and gain-clamped SOA gates in multiwavelength optical networks," *IEEE Photon. Technol. Lett.*, Vol. 11, No. 11, pp. 1494-1496, 1999.
- [14] <http://www.alcatel.com/telecom/optronics/products/datasheets/8-orm/A1921SOA.pdf>.
- [15] H. Soto, D. Erasme, and G. Guekos, "Cross-polarization modulation in semiconductor optical amplifiers," *IEEE Photon. Technol. Lett.*, Vol. 11, No. 8, pp. 970-972, 1999.
- [16] M. Zhao, J. DeMerlier, G. Morthier, and R. Baets, "Dynamic birefringence of the linear optical amplifier and application in optical regeneration," *IEEE Journal of Selected Topics in Quantum Electronics*, Vol. 8, No. 6, (November/December), 2002.
- [17] P. Vankwikelberge, G. Morthier, and R. Baets, "CLADISS-A longitudinal, multi-mode model for the analysis of the static, dynamic and stochastic behavior of diode lasers with distributed feedback," *IEEE J. Quantum Electron.*, Vol. 26, pp. 1728-1741, 1990.
- [18] G. Morthier, J. Sun, T. Gyselings, and R. Baets, "A novel optical decision circuit based on a Mach-Zehnder or Michelson interferometer and gain-clamped semiconductor optical amplifiers," *IEEE Photon. Technol. Lett.*, Vol. 10, No. 8, pp. 1162-1164, 1998.
- [19] B. Lavigne, D. Chiaroni, L. Hamon, C. Janz, and A. Jourdan, "Experimental analysis of SOA based 2R and 3R optical regeneration for future WDM networks," in *Tech. Dig. OFC*, San Jose, CA, USA, paper Th07, 1998.
- [20] B. Lavigne, D. Chiaroni, P. Guerber, L. Hamon, and A. Jourdan, "Improvement of regeneration capabilities in semiconductor optical amplifier-based 3R regenerator," in *Tech. Dig. OFC*, San Diego, CA, USA, paper TuJ3, 1999.
- [21] D. Wolfson, P. B. Hansen, A. Kloch, and K. E. Stubkjaer, "All-optical 2R regeneration based on interferometric structure incorporating semiconductor optical amplifiers," *Electron. Lett.*, vol. 35, pp. 59-60, 1999.
- [22] D. Wolfson, T. Fjelde, A. Kloch, C. Janz, A. Coquelin, I. Guillemot, F. Gaborit, F. Poingt, and M. Renaud, "Experimental investigation at 10 Gb/s of the noise suppression capabilities in a pass-through configuration in SOA-based interferometric structures," *Photon. Technol. Lett.*, vol. 12, No. 7, pp. 837-839, 2000.
- [23] Z. Bakonyi, G. Onishchukov, C. Knoll, M. Golles, F. Lederer, and R. Ludwig, "In-line saturable absorber in transmission systems with cascaded semiconductor optical amplifiers," *IEEE Photon. Technol. Lett.*, Vol. 12, No. 5, pp. 570-572, 2000.
- [24] Stefan Dien, "All-optical signal processing by gain-transparent semiconductor switches," *PhD thesis*, pp 74-76, HHI, Technische Universität Berlin, 2000.
- [25] D. A. Francis, S. P. DiJaili, J. D. Walker, "A single-chip linear optical amplifier," *Techn. Dig. Conference on Optical fiber communication OFC2001*, postdeadline papers, PD13, Anaheim, March 19-22, 2001.
- [26] I. Ogawa, T. Tanaka, T. Kitagawa, T. Hashimoto, R. Kasahara, and Y. Tohmori, "Hybrid integrated gain-clamped SOA module using UV-gratings on PLC platform," *Tech. Dig., Optical amplifiers and their applications*, paper JW2, Vancouver, Canada, July 14-17, 2002.
- [27] A. R. Davies, K. A. Williams, R. V. Penty, I. H. White, M. Glick, D. McAuley, and P. J. Williams, "Gain-clamped operation of a linear laser amplifier with electrical variable gain," *Tech. Dig., Optical amplifiers and their applications*, paper JW3, Vancouver, Canada, July 14-17, 2002.
- [28] O. Kjebon, R. Schatz, S. Lourduoss, S. Nilsson, B Stalnacke, and L. Backbom, "30 GHz direct modulation bandwidth in detuned loaded InGaAsP DBR-lasers at 1.55  $\mu\text{m}$  wavelength," *Electron. Lett.*, vol. 33, pp. 488-489, 1997.

## **Chapter 3**

# **All-optical 2R regeneration based on an MZI with LOAs in both arms**

Based on a MZI with GCSOAs in each arm, an all-optical 2R regenerator has been proposed in the previous chapter. Excellent static and dynamic regeneration characteristics have been demonstrated experimentally for such a regenerator. However, due to the problem with relaxation oscillations in the amplifiers the maximum speed of this regenerator is rather limited. These speed limitations can be overcome using a recently introduced type of gain clamped SOA, the linear optical amplifier (LOA) [1-3], which is based on integrating an amplifier and a vertical cavity surface emitting laser (VCSEL) on an InP substrate. We have therefore experimentally investigated MZIs with LOAs in both arms. First, the LOA and its characteristics are described in more detail in §3.1. Secondly, the operation principle of the regenerator is briefly described in §3.2. In §3.3, the experimental demonstration of the regenerative capabilities is given. An ER improvement of 8 dB has been obtained with an input extinction ratio of 7 dB for static operation. Experimental results for bit-rates of both 2.5 Gbit/s (NRZ,  $2^9-1$  PRBS) and 10Gbit/s (NRZ,  $2^{31}-1$  PRBS) are presented. With a degraded input signal, a receiver sensitivity improvement of 1 dB at a bit-error-rate (BER) of  $10^{-9}$  is found for 10 Gbit/s, showing the regeneration capability for high bit rate. The effects of polarization on the performance of the regenerator and the stability of the fiber-based setup are also discussed in this section. Finally, a summary is given in §3.4.

### **3.1 LOA and its characteristics**

#### **3.1.1 Description of a LOA**

The LOA is an amplifier with an integrated VCSEL on an InP substrate, as seen in Fig. 3-1. The VCSEL and the amplifier share the same active region. The VCSEL has high reflectivity DBR mirrors positioned above and below the active region. The VCSEL operates along the entire length of the amplifier and the lasing action is perpendicular to the propagation of the amplified light. The circulating optical power of the VCSEL overlaps with the amplifier waveguide and acts as an optical feedback to maintain a constant local gain in the amplifier.

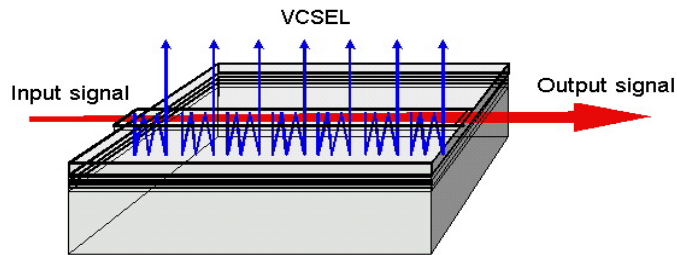


Fig. 3-1 LOA device structure

Obviously, similar to the normal GCSOA, the LOA operates by gain clamping which is achieved by a laser oscillation in the cavity, away from the gain peak, effectively pinning the carrier density and fixing the available gain. An important difference between LOAs and GCSOAs is that a vertically coupled cavity with a very short length is employed in the LOA, instead of the long cavity in the GCSOA. The LOA has a potential of operating at high bitrate, which has been experimentally demonstrated [3]. On the other hand, the large dimensions of the VCSEL make the saturation in the LOA more gradual. This is due to the fact that gain clamping in LOAs occurs much more locally and such that near the saturation level a part of the LOA can be clamped, while a part can be saturated. The detailed characteristics of the LOA are experimentally demonstrated in the following section.

The LOAs were grown using standard MOCVD manufacturing processing. The devices used in our experiments are supplied by Genoa Corp., CA USA. The LOA chips are approximately  $1 \text{ mm} \times 0.5 \text{ mm} \times 0.15 \text{ mm}$ .

### 3.1.2 Operating characteristics of the LOAs

The LOA has specific characteristics in gain, polarization, and phase due to gain clamping, which are the most important features for its applications in MZI-based optical regeneration. Similar to that of the GCSOA, the gain of the LOA is independent on injection current and optical input power in the linear regime below the saturation power, but changes rapidly with increasing input power once the linear regime is exceeded. Increasing the injection current results in a linear increase in the saturation power, while the gain remains constant. Both the phase shift and the state of polarization at the output of the LOA are independent of the input power in linear regime, but change with varying injection current to the LOA. In this section, these characteristics are experimentally demonstrated.

#### Gain

The experimental setup for measuring the gain of LOAs is shown in Fig. 3-2. A CW light beam from a tunable laser (Model Tunics-plus, Photonetics) is amplified and then coupled into the LOA. The variable attenuator (ATT) is used to change the

input power to the LOA. The optical band pass filter (OBPF2) is added for filtering out the ASE from the LOA. The output of the LOA is detected with a power meter.

Two different LOAs were measured, and the gain as a function of input power was measured for different injection currents. The two LOAs have similar saturation characteristics. Here we just show the typical results of one of the two LOAs, LOA#1. Figs. 3-3 and 3-4 give the measured output power and gain, respectively, as a function of input power. It can be seen that, as predicted, the gain is independent of both the input power and the injection current when the input power is below a certain input power level, i. e. the saturation input power, for a given injection current. By increasing the injection current, both saturation input power and saturation output power increase. The gains in linear regime at 1550 nm for LOA#1 and LOA#2 are 12.7 dB and 12.4 dB, respectively.

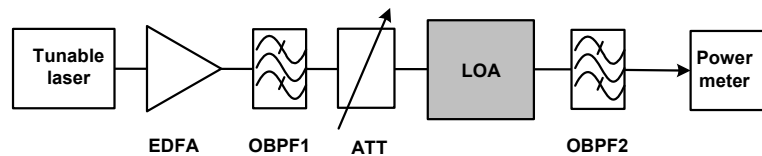


Fig. 3-2 Experimental set-up for the gain measurements.

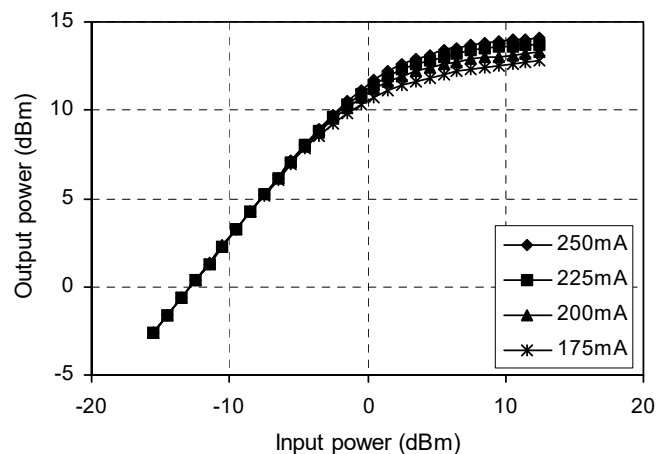


Fig. 3-3 Output power from LOA#1 as a function of input power for different injection currents, wavelength of the input: 1550 nm.

Comparing the saturation characteristics of the LOA (e. g. Fig. 3-3) and the GCSOA (e. g. Fig. 2-3), we can see that the saturation in LOAs is indeed more gradual than that in GCSOAs. This has the consequence, which will be seen in §3.3.1, that the transition between the digital zero and one in LOA-based 2R regeneration can't be as sharp as with GCSOAs.

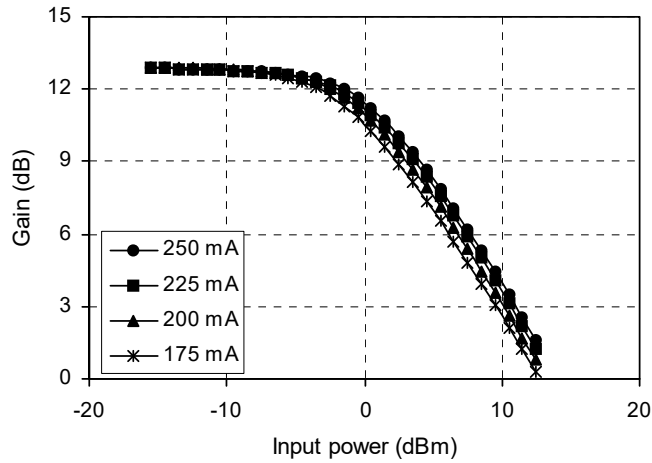


Fig. 3-4 Gain of LOA#1 versus input power for different injection currents, wavelength of the input: 1550 nm.

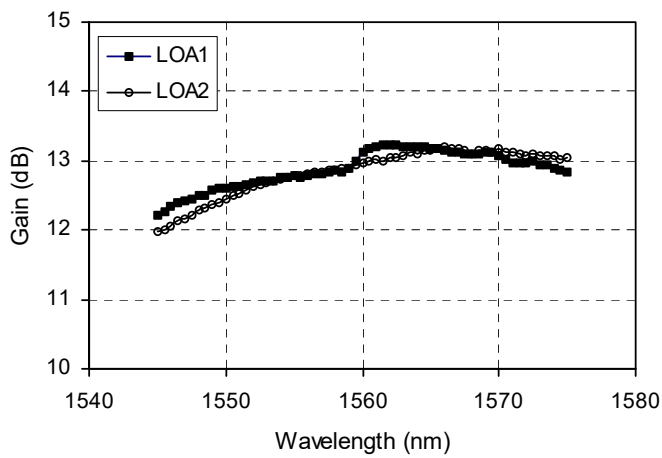


Fig. 3-5 Wavelength dependence of the gain at low input power (-6 dBm), injection current to the LOAs, 250 mA.

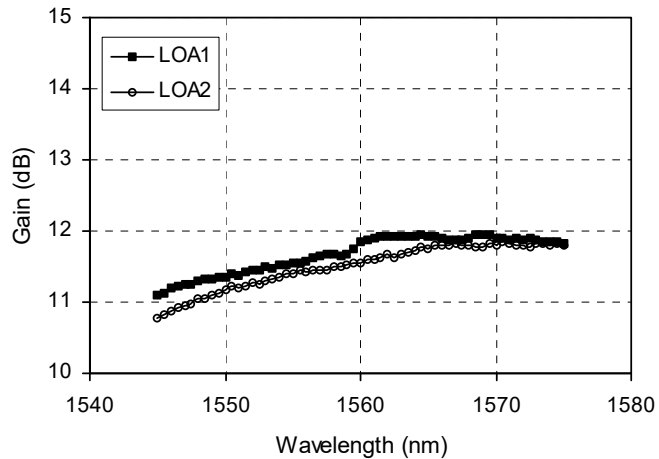


Fig. 3-6 Wavelength dependence of the gain at high input power (0 dBm), injection current to the LOAs, 250 mA.

We have also measured the wavelength dependence of the gain. Fig. 3-5 shows the gain as a function of signal wavelength for an input power of  $-6$  dBm in the linear regime at 250 mA, while Fig. 3-6 gives the results for a high input power (0 dBm) at which the LOA is saturated. One can see that within a wavelength range of 30 nm (1545 nm – 1575 nm) the gain flatness is  $\sim 1.2$  dB for both LOAs in the linear regime, while the gain difference between the two LOAs keeps below 0.2 dB, which is more important for the MZI-based 2R regeneration with LOAs. For a high input power, the LOA is saturated and the gain flatness is  $\sim 0.8$  dB, and the gain difference is  $< 0.3$  dB.

The polarization dependence of the gain (PDG) is 0.1 dB at 1557 nm, and the maximum PDG is 0.7 dB at 1577 nm for LOA#1. For LOA#2, the PDG is 0.3 dB at 1558 nm, and the maximum PDG is 0.9 at 1578 nm (Ref. datasheet of the LOAs from Genoa Corp.).

### State of polarization

The state of polarization at the output of the LOA is determined by the input polarization state and the effective birefringence of the LOA. In a practical LOA, a small difference between the TE and TM effective indices exists owing to the guiding properties of the amplifier waveguides. Even though this effective birefringence is very small, and does not affect the polarization independent gain, a significant change in the state of polarization at the output of the LOA can be induced. In addition, for a given device the effective birefringence depends on the carrier density. Detailed theoretical and experimental analyses of the polarization characteristics of the LOA are given in §4.1 and §4.2 in Chapter 4. Here in this section, we just show some conclusions and related important results.

For a LOA, the gain is clamped and both the free carrier density and the total photon density (photon density of both laser and optical signal) are constant when the input power level varies in the linear regime. Since there is no carrier density change, there will not be an effective birefringence change, and neither a variation of the state of polarization at the output. Once the linear power range is exceeded, the gain and thus the carrier density will drop rapidly. A significant change in the effective birefringence and thus a change in the polarization state of the output will be caused. The evolutions of the state of polarization at the output of the LOA with varying the input power can be seen in Fig. 4-3 in §4.1.1.

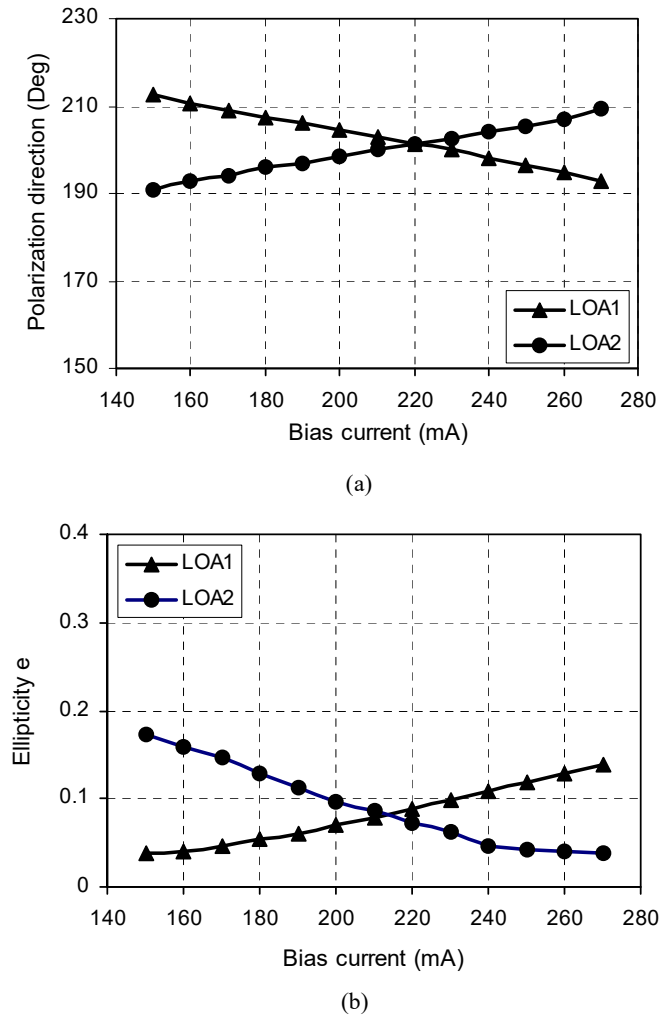


Fig. 3-7 The evolution of (a) the polarization direction (azimuth  $\theta$ ) and (b) the ellipticity  $e$  with the variation of the injection current. Input power  $-10$  dBm, signal wavelength: 1550 nm.

For a given input power in the linear regime, the gain remains constant but, due to gain suppression, the carrier density also increases a little with increasing injection current to the LOA. Therefore, the effective birefringence changes with the injection current, and thus the state of polarization at the output of the LOA changes when changing the injection current. Fig. 3-7 gives the measured evolutions of the state of polarization at the output of the LOAs versus the injection current in the linear regime. Clearly, the polarization direction (azimuth  $\theta$ , Ref. §4.1.1) rotates with increasing the injection current to the LOA. The rotation, however, for the two different LOAs is in the opposite direction. This could be due to the reasonable difference in effective birefringence between the two individual devices. The ellipticity (Ref. §4.1.1) of the output from the LOAs varies within a range from 0.037 to 0.14 for LOA#1 and from 0.17 to 0.037 for LOA#2 with changing the injection current from 150 mA to 270 mA. It will be seen in section §3.3 that these variations of the state of polarization with injection current give some negative influence on the threshold adjustment of the LOA-based MZI regenerator.

### **Phase shift**

For a given LOA, the phase shift experienced by the optical signal while travelling through the device depends on the effective index which is determined by the local carrier density. As for the GCSOA, the gain of the LOA is clamped and the free carrier density are constant when the input power level varies in the linear regime, and thus, the phase shift stays constant in the linear regime. Once the linear power range is exceeded, the gain and thus the carrier density will drop rapidly. A significant change in the effective index and thus in the phase shift will result. This specific characteristic of the phase shift plays an important part in the LOA-based 2R regeneration.

### **Speed**

The LOA exhibits high frequency relaxation oscillations due to the short cavity length of the clamping laser. This makes the LOAs suitable for high bitrate applications. To examine the availability for high-speed operations, we measured the eye-diagrams at the output of the LOA for 10 Gbit/s (NRZ,  $2^{31}-1$  PRBS), as shown in Fig. 3-8 (b) and (c). As a comparison, the eye-diagram at the input of the LOA is also measured, and given in Fig. 3-8(a). The bandwidth of the receiver used in the measurements is 15 GHz. The results show clearly no relaxation oscillation is found within this optical bandwidth. (Note that an overshoot exists at the “1” levels when the LOA operates in saturation). It means that the LOAs in our experiments can operate at a bitrate of at least 10 Gbit/s. Actually, new LOAs developed very recently can operate up to and beyond 40 Gbit/s [4].

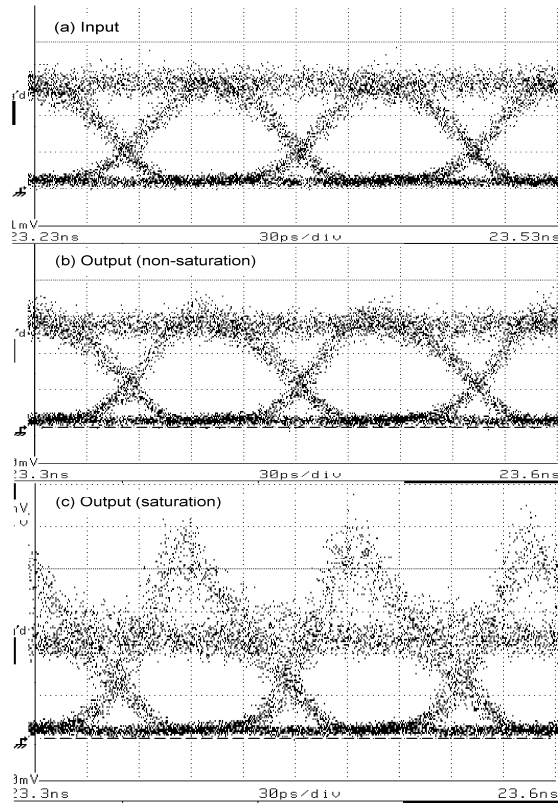


Fig. 3-8 Eye-diagrams at the input and the output of the LOA for 10 Gbit/s (NRZ,  $2^{31}-1$  PRBS). Signal wavelength, 1550 nm; injection current, 250 mA; Attenuation after the LOA  $\sim 13$  dB; Bandwidth of the optical receiver, 15 GHz.

## 3.2 2R regenerator based on an MZI with LOAs

### 3.2.1 Structure and operation principle

The principle structure of the regenerator is similar to the 2R regenerator presented in Chapter 2, but with two identical LOAs in both arms instead of GCSOAs, as illustrated in Fig. 3-9(a). Ideally, the ‘identical’ LOAs in both arms give an identical amplification in the linear regime, i.e. below the saturation level. The LOAs are given a different injection current though and they therefore exhibit a different saturation power level, as shown in Fig. 3-9(b). In the linear regime, where both interferometer arms exhibit an equal amplification, there is hence an interference between two signals with equal amplitude and a phase shift of  $\pi$  results in complete destructive interference. This perfect interference is obtained for all input power levels below the saturation levels of both LOAs, as opposed to the case of other MZI-based regenerators. At input power levels above the saturation level of both

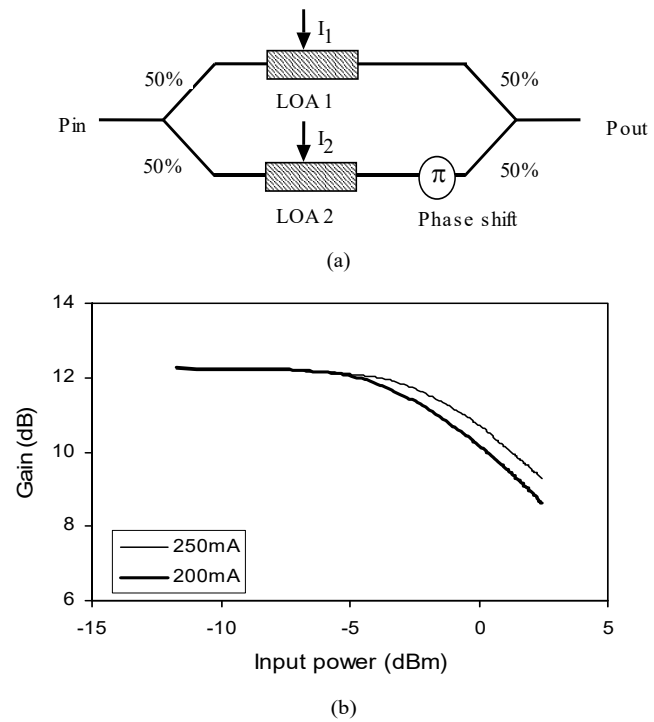


Fig. 3-9 Principle of MZI -based regenerator with LOAs. (a) structure of the 2R regenerator, (b) measured saturation characteristics of the LOA at different injection currents.

amplifiers, both arms give a rather constant output power, which in addition is different for both arms due to the different injection currents. Moreover, the phase difference between both arms is no longer  $\pi$ , but still remains constant. This results in a constant and rather high output power level at the output of the interferometer.

An important difference between normal gain clamped SOAs and LOAs is that the saturation in LOAs is more gradual, as mentioned in the above section. This has the consequence that the transition between the digital zero and one can't be as sharp as with GCSOAs, but also and more importantly that regenerative performance is not limited by relaxation oscillations.

### 3.3 Experimental demonstration of the 2R regenerator

The practical configuration of the LOA-based MZI regenerator and the entire experimental set-up is shown schematically in Fig. 3-10. The regenerator is constructed using fiber-based 3dB couplers and fiber-pigtailed and packaged LOAs, as seen in Fig. 3-11. The fibers are SMF fibers and the total arm lengths are about 1.3 m. Considering a slight difference in the gain between the two LOAs and a small

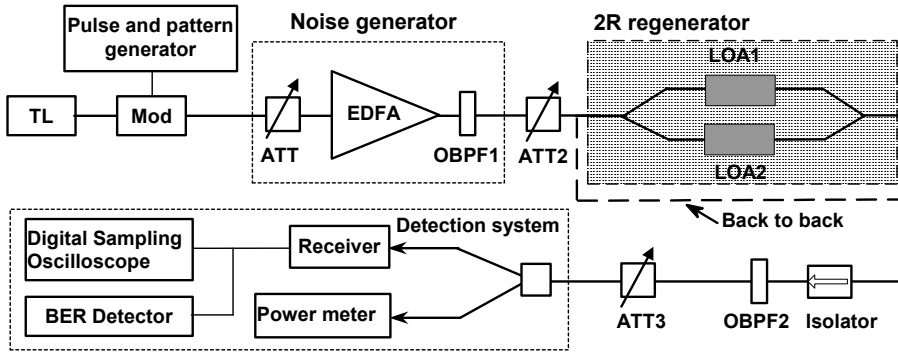


Fig. 3-10 Experimental set-up (the dashed line indicates the setup without the regenerator)

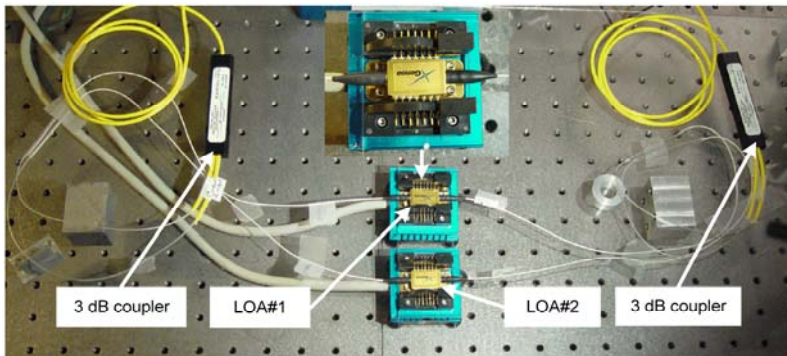


Fig. 3-11 Photograph of the experimental setup: the part of MZI-based 2R regenerator with LOAs

deviation from 3 dB of the splitting ratio of the couplers, the LOAs are arranged to give the same amplification in the two arms. The phase shift of  $\pi$  at low input power levels is obtained by slightly heating one of the LOAs.

A tunable laser (TL) is used to generate the injected light at a wavelength of 1550 nm. The optical data signal is first transmitted through an EDFA. A variable attenuator before the EDFA is used as to control the signal to noise ratio at the input so as to simulate the degradation of the signal. The ER of the input data signal is controlled by changing the driving pulse amplitude (i. e., the electrical pulse signal amplitude) of the external modulator. A second variable attenuator (ATT2) is used to control the power level before the signal is sent through the MZI. The third variable attenuator is for adjusting the received power. The two optical band pass filters (OBPF) have a 3 dB bandwidth of 0.3 nm. A Digital Sampling Oscilloscope (Tektronix 11801B) and an Error Detector (Advantest D3286) are used in the detection system for measuring the eye-diagrams and BER, respectively. The regeneration characteristics of the 2R regenerator are investigated for static operation and dynamic operation at both 2.5 Gbit/s (NRZ,  $2^9-1$  PRBS) and 10 Gbit/s (NRZ,  $2^{31}-1$  PRBS). The receivers used for dynamic measurements at 2.5 Gbit/s and 10 Gbit/s are Tektronix ORR24 and HP11982A optical receivers, respectively.

### 3.3.1 Static transfer characteristics

Fig. 3-12 shows the measured static regeneration characteristic for injection currents of 200 mA and 250 mA through the two LOAs, respectively. It can be seen that a nonlinear transfer function can be achieved with the LOA-based MZI. The extinction ratio can be improved from 7 dB at the input to 15 dB at the output, while the output power remains below  $-10$  dBm for input power levels below  $-5$  dBm and remains a little above 5 dBm for input powers above 1 dBm. For comparison with that of the MZI with GCSOAs as described in the previous chapter, the transfer function on a linear scale is also given in Fig. 3-12 as an inset. Due to the gradual saturation of the LOA, the output power shifts from the low to the high level more slowly than that for the GCSOA-based MZI.

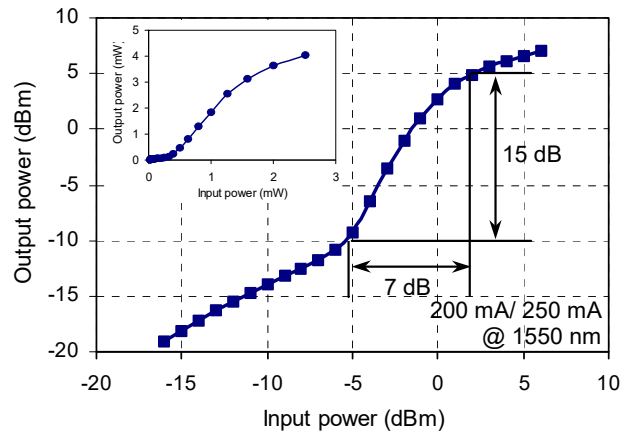


Fig. 3-12 Static transfer function of the regenerator. Losses from both the optical band-pass filter and the isolator after the MZI were not taken in to account in the output power.

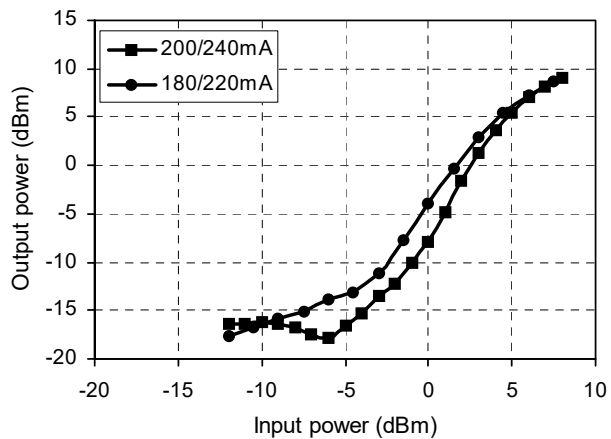


Fig. 3-13 Static transfer functions of the regenerator for different injection currents to the LOAs. Losses from both the optical band-pass filter and the isolator after the MZI were not taken in to account in the output power. Signal wavelength: 1550 nm

The small variation of the low output power level, i. e. the logical "0" level, with input power is due to the imperfect destructive interference. In fact, there is some small, reasonable difference of the polarization between the two arms, which makes the destructive interference incomplete at the low power level.

Fig. 3-13 gives the static regeneration characteristics for different injection currents to the two LOAs. A significant shift of the transfer curve ( $\sim 1$  dB at the input power around  $-3$  dBm) can be seen when the injection currents change from 200/240 mA into 180/220 mA. This implies that the threshold of the transfer between logical "0" level and logical "1" level can be adjusted by simply changing the injection current to the LOAs. It should be pointed out that the low power level changes for different injection currents. This is due to the fact that the polarization evolution with injection current of the two LOAs is not the same (Ref. Fig. 3-7), and thus the destructive interference at the low power level changes when the injection currents are changed. This performance degradation could be reduced with an integrated configuration with two identical LOAs.

### 3.3.2 Dynamic performance

#### Extinction ratio improvement

Experimental investigation of the dynamic performance of the LOA-based MZI has been carried out for both 2.5 Gbit/s and 10 Gbit/s. Fig. 3-14 shows the eye-diagrams with and without the regenerator at 2.5 Gbit/s for different input ER. Clearly, the input signal is regenerated and the extinction ratio is improved significantly.

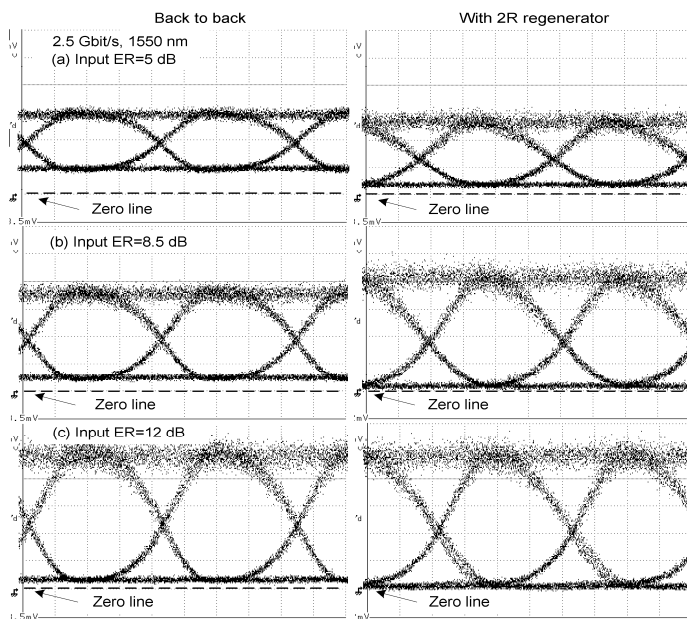


Fig. 3-14 Eye-diagrams with and without 2R for 2.5 Gbit/s with different input ER. Signal wavelength: 1550 nm; injection currents to the LOAs: 200 mA/250 mA.

Fig. 3-15 gives the ER improvement versus the input ER. For an input ER of around 8 dB, an ER improvement of over 4 dB can be achieved. It can be remarked that the eye diagram after the regenerator shows a slightly higher noise and a slightly larger timing jitter than that before the regenerator. This could be due the fact that the input signal is quasi-perfect and the LOAs add some ASE noise at the output. Furthermore, a small difference in the lengths of both fiber arms might exist, which might increase the timing jitter. This difference can in principle be further eliminated, e.g. using variable delay lines or using an integrated version of the MZI.

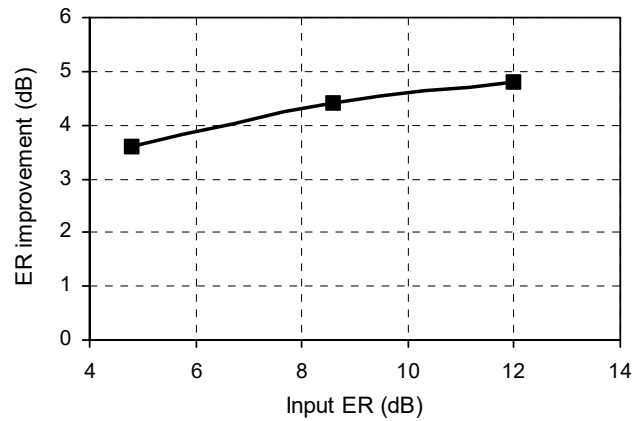


Fig. 3-15 ER improvements versus input ER for 2.5 Gbit/s. Signal wavelength: 1550 nm; injection currents to the LOAs: 200 mA/250 mA.

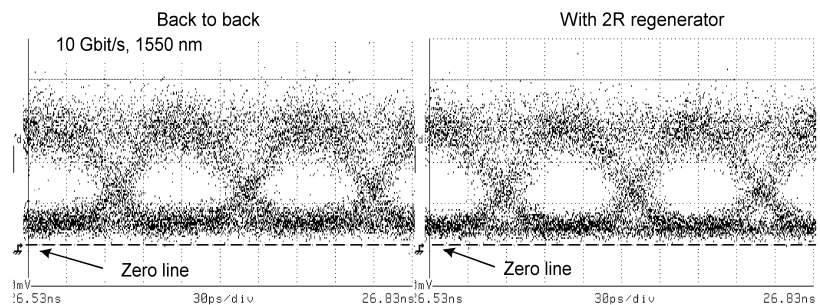


Fig. 3-16 Eye-diagrams with and without 2R for 10 Gbit/s. Signal wavelength, 1550 nm; injection currents to the LOAs, 200 mA/250 mA.

Eye-diagrams after the 2R regenerator with a seriously degraded input signal for 10 Gbit/s is shown in Fig. 3-16. The degraded input signal is obtained by decreasing the input power level ( $\approx -30$  dBm) to the EDFA, and has an ER of about 7 dB. One can see that the noise is suppressed and the eyes become much more open. An ER improvement of 1.5 dB has been obtained. All of the results clearly show the potential regeneration capability for 10 Gbit/s. It should be noted that the ER improvement for 10 Gbit/s is smaller than that for 2.5 Gbit/s. This could be due to the polarization relaxation of the LOAs (Ref. §4.3.3, Fig. 4-14), as the devices used here are not specifically designed for the application proposed here. The difference of the polarization relaxation between the LOAs in both arms makes the destructive interference incomplete at the low power level. LOAs with high speed and weak polarization relaxation effect could be fabricated, that are better suited for optical regeneration based on the MZI with LOAs.

In addition to the ER improvement and noise suppression, a net gain of the signal has also been obtained. In the eye-diagram measurement for the operation with 2R regenerator at 10 Gbit/s, an extra attenuation of about 10 dB has to be added to that for the back to back operation to get the same received power. This implies that a net gain of about 10 dB can be achieved with the LOA-based 2R regenerator.

### Receiver sensitivity improvement

BER measurement is another efficient way to characterise the regeneration capability of the 2R regenerator. Fig. 4-17 gives the results from the BER measurements for the operation of back-to-back (BTB) and operation with the 2R at a bitrate of 10 Gbit/s. Here the input power to the EDFA is about  $-21$  dBm, 8 dB higher than that for measuring the eye-diagrams in Fig. 3-16. One can see that a negative power penalty of about 1 dB at a BER of  $10^{-9}$  can be achieved for a degraded input signal. That means a receiver sensitivity improvement of  $\sim 1$  dB can be obtained. However, the BER with 2R exhibits an error floor at around  $3 \times 10^{-10}$ .

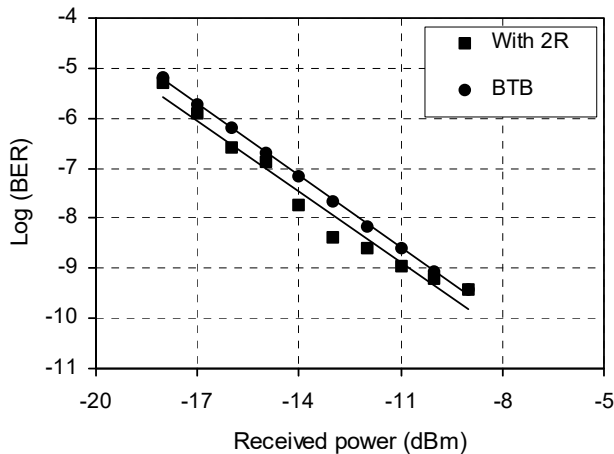


Fig. 3-17 BER versus received power for operations with 2R and BTB at 10 Gbit/s. Signal wavelength: 1550 nm; Injection current: 200 mA/250 mA.

### 3.4 Discussion

In the previous section, regeneration capabilities of the LOA-based MZI have been experimentally verified. However, the operation performance for a high bitrate (i. e. 10 Gbit/s) has some limitations due to non-identical polarization behaviours (i. e., polarization relaxation, polarization rotation) of the individual LOAs used in our experiments. In order to improve the high-speed performance, LOAs with high speed and weak polarization relaxation effect could be helpful. Furthermore, with the multi-channel integration technique [5] double-channel integrated "identical" gain-clamped optical amplifiers could be developed, that are better adapted to the optical regeneration proposed above.

As the fiber-based MZI with GCSOAs described in the previous chapter, the 2R regenerator proposed here suffers from interference instabilities due to temperature fluctuation and air flow also. The output of the MZI exhibits a significant fluctuation. By fixing the whole set-up on a plate and covering it with a plastic box, the output power instabilities have been reduced a lot, but it is still not enough. As mentioned in Chapter 2, this problem could be solved by using active phase stabilization [6] or monolithically integrating the MZI. This work would be part of our further efforts in the optical regeneration project.

### 3.5 Summary

The LOA exhibits specific characteristics in gain, polarization, and phase due to gain clamping, and has a high operation speed. Detailed experimental investigations of these characteristics were described in §3.1.2. Based on the specific characteristics of the LOAs, an all-optical 2R regenerator using a MZI with LOAs in both arms was demonstrated experimentally in §3.2 and §3.3. An ER improvement of 8 dB had been obtained with an input extinction ratio of 7 dB for static operation. For dynamic operations at bit-rates of both 2.5 Gbit/s (NRZ,  $2^9-1$  PRBS) and 10 Gbit/s (NRZ,  $2^{31}-1$  PRBS), both eye-diagram and BER were measured. Significant improvements of ER, noise, and receiver sensitivity were obtained. For 2.5 Gbit/s, an ER improvement of over 4 dB could be achieved with the input ER of around 8 dB. With a degraded input signal, a receiver sensitivity improvement of 1 dB at a bit-error-rate (BER) of  $10^{-9}$  was found for 10 Gbit/s, showing the regeneration capability for high bit rate. The effects of polarization on the performance of the regenerator and the instability of the fiber-based setup were also discussed. It is expected that further optimization and stabilization of the interferometer will lead to even better regeneration.

## References

- [1] D. A. Francis, S. P. DiJaili, J. D. Walker, "A single-chip linear optical amplifier," *Techn. Dig. Conference on Optical fiber communication OFC2001*, postdeadline papers, PD13, Anaheim, March 19-22, 2001.
- [2] J. J. J. Crijns, L. H. Spiekman, G. N. van den Hoven, E. Tangdionga, H. de Waardt, "8 Cascaded Linear Optical Amplifiers in a 200-km,  $8 \times 10$ -Gb/s, Metro WDM Ring Featuring Dynamic Switching of Channels", *Proc. European Conference on Optical communications, ECOC2002*, P. 6.4.6, Copenhagen, Denmark, September 9-12, 2002.
- [3] J. Leuthold, K. Dreyer, G. Hoven, and J. Lambe, "Linear all-optical wavelength conversion based on linear optical amplifier," *Techn. Dig. Conference on Optical fiber communication OFC2002*, ThDD5, pp. 597-598, Anaheim, March 2002.
- [4] LOAs-datasheet; [www.genoa.com](http://www.genoa.com)
- [5] I. Ogawa, T. Tanaka, T. Kitagawa, T. Hashimoto, R. Kasahara, and Y. Tohmori, "Hybrid integrated gain-clamped SOA module using UV-gratings on PLC platform," *Technical digest, Optical amplifiers and their applications 2002*, paper JW2, Vancouver, Canada, 2002.
- [6] Stefan Dien, "All-optical signal processing by gain-transparent semiconductor switches," *PhD thesis*, pp 74-76, HHI, Technische Universität Berlin, 2000.

## **Chapter 4**

# **All-optical 2R regeneration based on polarization rotation in a LOA**

In the previous chapters, optical regeneration was realized by using both gain and phase nonlinearities in the GCSOAs and LOAs with MZI configurations. Devices used there are desired to be with polarization insensitive gain, and polarization variation with the intensity of the input signal is an undesired effect. Although a reasonable polarization independent gain is technologically achievable, a total absence of effective birefringence (a difference between TE and TM effective indices) is virtually impossible to obtain [1] in the devices. The effective birefringence results from the guiding properties of the amplifier waveguides and varies with intensity of the input wave and the injection current to the device, resulting in a polarization rotation at the output of the device. This has been verified by our experimental results with both GCSOA and LOAs, where significant changes of the state of polarization of the output light are observed with power level of the input light and with the injected currents. As discussed in section §3.3, this polarization rotation is undesired and causes, in some sense, a degradation of the performance of the optical regeneration. However, one can wonder whether this effect can be used as a new form of non-linear operation to generate new functionalities. The answer is positive. Recently it has been proposed to make use of the polarization rotation in an SOA [1] for all-optical switching [2,3], optical gating [4,5], wavelength conversion [6], and demultiplexing [7]. In this chapter, we demonstrate all-optical 2R-regeneration based on such a polarization rotation in a single LOA [8]. In this chapter, first, polarization rotation induced by nonlinear birefringence in LOAs is analysed theoretically and experimentally in §4.1. Secondly, the operation principle of the polarization rotation based-2R regeneration is described in §4.2. In §4.3, the experimental demonstration of the regenerative capabilities is given. An ER improvement of 15 dB has been obtained with an input extinction ratio of 5 dB for static operation. Experimental results for bit-rates of both 2.5 Gbit/s (NRZ,  $2^9-1$  PRBS) and 10 Gbit/s (NRZ,  $2^{31}-1$  PRBS) are presented, respectively. With a degraded input signal, a receiver sensitivity improvement of over 3 dB at a bit-error-rate (BER) of  $10^{-9}$  is found for 2.5 Gbit/s. For 10 Gbit/s, zero power penalty is observed. Significant improvements of ER are obtained for both 2.5 Gbit/s and 10 Gbit/s. The features of simple configuration, stable operation and good regenerative capabilities make this new scheme a promising technique for all-

optical regeneration in future optical networks. Finally, this chapter is summarized in §4.4.

## 4.1 Polarization rotation in a LOA

### 4.1.1 Theoretical analysis

For the sake of generality, we consider a travelling wave LOA. The aim of this section is to derive the relative variation of the state of polarization of the output light with the input optical power (or the gain) for a given input linear polarization. The effect of the LOA on the incident light can be described by the  $2 \times 2$  Jones matrix  $J$ , which relates the state of polarization of the light at the output to the state of polarization at the input. Given the definition of two orthogonal reference axes (e. g.,  $x$  and  $y$ ), perpendicular to the direction of propagation, as shown in Fig. 4-1, the complex amplitudes ( $E_x^o$  and  $E_y^o$ ) of the Jones vector of the output light are related to the input complex amplitudes ( $E_x^i$  and  $E_y^i$ ) by [9]

$$\begin{bmatrix} E_x^o \\ E_y^o \end{bmatrix} = J \begin{bmatrix} E_x^i \\ E_y^i \end{bmatrix} = \begin{bmatrix} j_{11} & j_{12} \\ j_{21} & j_{22} \end{bmatrix} \begin{bmatrix} E_x^i \\ E_y^i \end{bmatrix} \quad (4.1)$$

If the input polarization is parallel to the  $x$  axis (*i.e.*  $E_y^i=0$ ), the elements  $j_{11}$  and  $j_{21}$  are given by

$$j_{11} = \left( \frac{E_x^o}{E_x^i} \right), \quad (4.2a)$$

$$j_{21} = \left( \frac{E_y^o}{E_x^i} \right), \quad (4.2b)$$

respectively. The linear oscillation  $E_x^i$  at the input of the device has produced two orthogonal linear oscillations  $E_x^o$  and  $E_y^o$  along the  $x$  and  $y$  axes at the output of the device, respectively. Equation (4.2a) shows that  $j_{11}$  is determined by the relative amplitude and phase of the output vibration  $E_x^o$  with respect to those of the input vibration  $E_x^i$ ; while equation (4.2b) shows that  $j_{21}$  is determined by the relative amplitude and phase of the output vibration  $E_y^o$  with respect to those of the input vibration  $E_x^i$ . If, instead of being parallel to the  $x$  axis, the input polarization is parallel to the  $y$  axis, the elements  $j_{12}$  and  $j_{22}$  are determined by

$$j_{12} = \left( \frac{E_x^o}{E_y^i} \right), \quad (4.3a)$$

$$j_{22} = \left( \frac{E_y^o}{E_y^i} \right). \quad (4.3b)$$

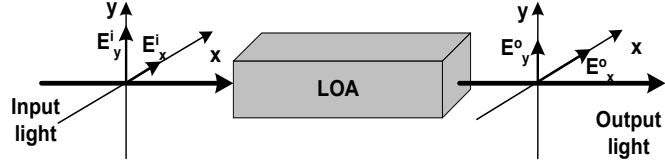


Fig. 4-1 The state of polarization of the input and output of the LOA.

In this case, the input linear oscillation  $E_y^i$  (along the  $y$  axis) has generated two orthogonal linear vibrations  $E_x^o$  and  $E_y^o$  along the  $x$  and  $y$  axes at the output of the device, respectively. Equation (4.3a) and (4.3b) tell us that  $j_{12}$  and  $j_{22}$  are determined by the relative amplitude and phase of the output vibration  $E_x^o$  and  $E_y^o$  with respect to those of the input vibration  $E_y^i$ . An alternative equivalent form of equation (4.1) is

$$\begin{bmatrix} E_x^o \\ E_y^o \end{bmatrix} = C e^{j\beta} \begin{bmatrix} B_{11} e^{j\delta_{11}} & B_{12} e^{j\delta_{12}} \\ B_{21} e^{j\delta_{21}} & 1 \end{bmatrix} \begin{bmatrix} E_x^i \\ E_y^i \end{bmatrix} \quad (4.4)$$

where  $C$  and  $B_{1l}$  are real numbers and are determined by the gain of the device.  $\delta_{1l}$  is determined by the differential phase shift between the linear vibrations along  $x$  and  $y$  axes.  $\delta_{mn}$  and  $B_{mn}$  ( $m, n=1,2, m \neq n$ ) are determined by the conversion between the linear vibrations along  $x$  and  $y$  axes. For simplicity, we only discuss  $\delta_{1l}$ , which represents the influence of the effective birefringence. If the  $x$  and  $y$  axes are chosen to correspond to the TM and TE polarization directions, respectively,  $\delta_{1l}$  will represent the differential phase shift between the TM and TE mode (i. e. , the TM mode with respect to the TE mode). For uniform refractive indices along the waveguide, one has:

$$\delta_{11} = kL(n_{TM}^a - n_{TE}^a). \quad (4.5)$$

where  $k=2\pi/\lambda$  and  $n_{TE}^a$  and  $n_{TM}^a$  are the TE and TM effective indices averaged along the LOA.  $L$  is the length of the LOA.

Let us consider a small uniform amplifier section at position  $z$  of length  $\Delta z$  for a given input optical power. The gain experienced by the optical signal while travelling through this section increases with the local carrier density  $N(z)$  :

$$G(z) = G_0 (N(z) - N_t) (1 - \beta S) \quad (4.6)$$

where  $G_0$  is the differential gain,  $N_t$  is the transparency carrier density, and  $\beta$  and  $S$  are gain suppression and photon density, respectively. The total gain  $G_T$  of the amplifier is given by the summation (or integration) of  $G(z)$  along the amplifier.

Furthermore, the effective local refractive indices of the active region for TE and TM modes increase linearly *with*  $N(z)$  :

$$n_{TE}(z) = n_{0TE} + \Gamma_{TE} N(z) \left( \frac{\partial n}{\partial N} \right), \quad (4.7a)$$

$$n_{TM}(z) = n_{0TM} + \Gamma_{TM} N(z) \left( \frac{\partial n}{\partial N} \right), \quad (4.7b)$$

where  $n_0$  is the effective refractive index of the waveguide for zero free carrier density,  $\Gamma$  is the confinement factor and  $(\partial n / \partial N)$  is the rate of change of the refractive index of the active region with the carrier density  $N(z)$ . The local effective index is different for the TE and TM components of the optical signal owing to the TE/TM asymmetry in both the confinement factors and the unperturbed effective refractive indices of the LOA. Thus, the LOA exhibits an effective birefringence that changes with the carrier density.

The TM/TE differential phase shift for the section is

$$\delta_{TM/TE}(z) = k\Delta z [n_{TM}(z) - n_{TE}(z)] \quad (4.8)$$

The total TM/TE differential phase shift  $\delta_{tl}$  is the summation of  $\delta_{TM/TE}(z)$  along the LOA:

$$\delta_{tl} = k \int_0^L [n_{TM}(z) - n_{TE}(z)] dz \quad (4.9)$$

Clearly, the TM/TE differential phase shift  $\delta_{tl}$  changes with the carrier density due to the effective birefringence in the LOA. Thus, the state of polarization of the output light changes with the carrier density of the LOA.

For the LOAs, the gain is clamped and both the free carrier density and the total photon density (photon density of both laser and optical signal) are constant in the linear regime when the input power level varies. Since there is no carrier density change, there will not be an effective birefringence change, and neither a variation of the state of polarization at the output. Once the linear power range is exceeded, the gain and thus the carrier density will drop rapidly. A significant change in the effective birefringence and thus in the polarization state of the output will be caused.

In addition to the induced birefringence effects mentioned above, another effect, induced TE/TM conversion, has been also shown to contribute to the polarization variation in SOAs [1]. The association of induced birefringence and induced TE/TM conversion accentuates the non-linear polarization variation of the device. The former effect induces a modification of the state of polarization when a light with an input polarization different from TE or TM travels through the device. The latter effect results in some polarization rotation even for TE and TM input mode. Both modifications vary with the intensity of the light.



For our analysis here, only the first three parameters are important and useful. The change of the state of polarization at the output of the LOA can be concisely specified by changes of these three elliptical parameters. In the following sections we will use them to describe the state of polarization of the output light from the LOA. For simplicity, the change in the state of polarization is called the polarization rotation, i. e., the rotation of the orientation of the ellipse accompanied with a change in its ellipticity.

#### 4.1.2 Experimental results

The evolution of the state of polarization at the output of the LOA with input power level has been experimentally investigated. The experimental setup is shown in Fig. 4-3, which is similar to the experimental setup for measuring the polarization properties of a GCSOA in §2.1.2. A CW light beam from a tunable laser (Model Tunics-plus, Photonetics) at 1550nm is amplified and then coupled into the LOA (which is the same as that used in the LOA-based MZI in chapter 3) with its input polarization set to be at some angle to the TE axis. The exact coupled input signal polarization is difficult to measure since the LOA has a pigtail of standard SM-fiber. However, there is a certain polarization for which the polarization effect is maximized, and it is this condition that is used in the experiment. The variable attenuator is used to change the input power to the LOA. The polarization controller after the LOA linearises the polarization of the output, elliptically polarized, when the LOA operates with a low input power in the linear regime. The polarizer before the power meter is used as an analyzer to check the evolution of the state of polarization of the output light from the LOA. By rotating the analyzer around the light beam axis, a minimum and a maximum detected power,  $P_{\min}$  and  $P_{\max}$ , can be found. At the minimum, the state of polarization at the input of the analyzer must be oriented orthogonal to the transmission axis of the analyzer. The elliptical polarization parameters,  $\theta$ ,  $e$  and  $A$  can be thus determined from the azimuth angle of the analyzer and the measured optical power  $P_{\min}$  and  $P_{\max}$ . In our experiment, only the change of the azimuth  $\theta$  with respect to that in linear regime is measured as a function of the input power and the bias current to the LOA. It will be seen in the following sections that it is this relative change of the state of polarization that is important for the polarization rotation based-2R regeneration. The evolution of  $e$  is equivalently described by the evolution of  $(P_{\min}/P_{\max} - \rho)^{1/2}$  with the variation of the input power. The extinction ratio,  $\rho$ , of the polarizer is  $<0.001$ .

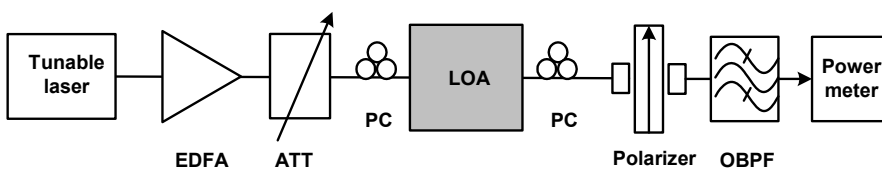


Fig. 4-3 Experimental set-up for measuring the polarization rotation of the LOA. ATT: Tunable attenuator; PC: Polarization controller; OBPF: optical band pass filter. The polarizer is rotatable around the light beam axis. Two collimators are used for the in- and out-of-fiber coupling of the polarizer.

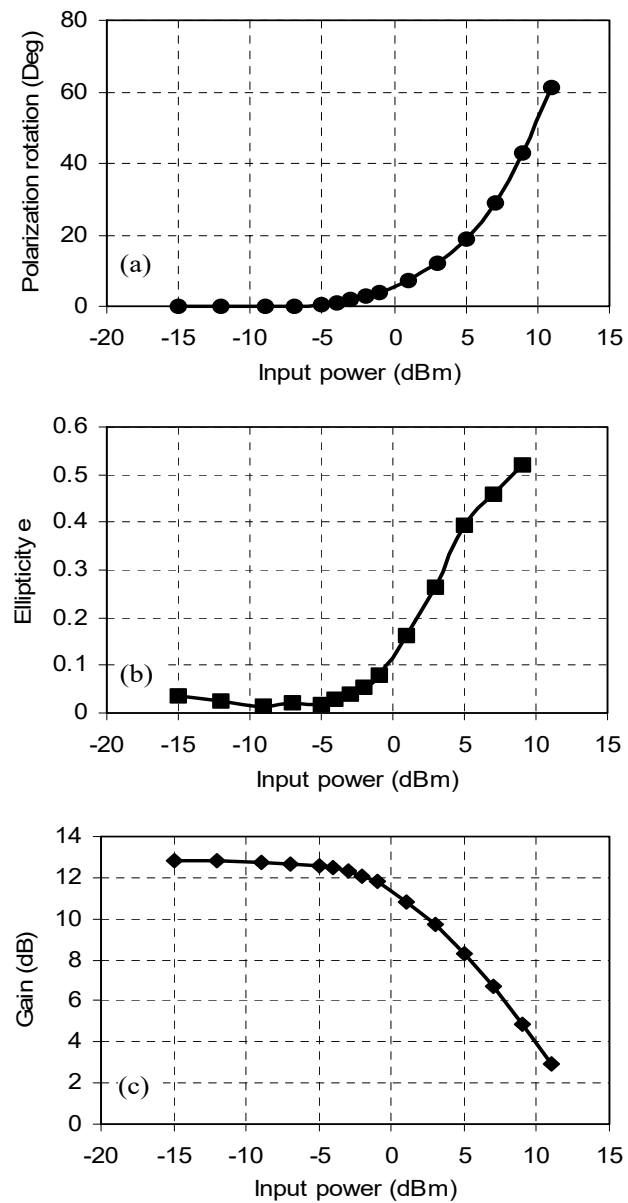


Fig. 4-4 Evolution of the state of polarization at the output of the LOA with varying input power, (a) the relative evolution of the azimuth  $\theta$  with respect to that for the linear regime; (b) the evolution of ellipticity  $e$  with the variation of the input power; and (c) saturation characteristic of the LOA. Bias current to the LOA: 250 mA; signal wavelength: 1550 nm.

Fig. 4-4(a) shows the relative evolution of the azimuth  $\theta$  with respect to that for the linear regime, while Figs. 4-4(b) gives the evolution of  $e$  with the variation of the input power. As a comparison, the saturation characteristic is given in Fig. 4-4(c). The bias current to the LOA is 250 mA. It can be clearly seen that in the linear regime both  $\theta$  and  $e$  are independent of the variation of the input power. That means there is no change in the state of polarization when the input power increases in the linear regime. Once the linear regime is exceeded, both  $\theta$  and  $e$  change rapidly, showing a significant polarization rotation and a remarkable change in the degree of ellipticity with increasing input power. This agrees with the theoretical prediction in the above section. As  $A$  is a measure of the strength of the elliptical vibration and its square is proportional to the power of the light, its evolution depends on the saturation characteristic of the LOA.

It should be noted that the evolutions of the state of polarization shown above are not the exactly those of the LOA itself. They contain some contributions from the polarization controller after the LOA. It will be seen, however, that it is the combined evolution of the state of polarization that is important and useful.

Obviously, by setting the analyzer with its transmission axis orthogonal to the orientation of the linearly polarized output light of the LOA, the optical controlled polarization rotation will result in a nonlinear transmission through the polarization controller/polarizer (analyzer) combination, which sets the basis for the application in optical signal processing. In the following sections, we will present an all-optical 2R regenerator based on the above polarization rotation.

## 4.2 Operation principle of the polarization rotation-based all-optical 2R regenerator with a single LOA

The regenerator basically consists of a LOA followed by a polarization controller and a polarizer, as shown in Fig 4-5. The operation of this regenerator is based on the polarization rotation of the LOA (as shown in the previous section): while the polarization state of the output in the linear regime is independent of the input power level, it changes rapidly when the LOA becomes saturated due to birefringence effects and TE/TM conversion effects. For a linearly polarized injected light beam, the polarization orientation and the degree of ellipticity of the output from the LOA will not change with varying input power level in the linear regime, as shown in Fig. 4-4. Hence, by using a polarization controller after the LOA to make the LOA output be linearly polarized (as mentioned in §4.1.2) and by setting the polarizer (i. g., the transmission axis of the polarizer being orthogonal to the direction of the linear polarization) so as to block the output beam, a very low output power (or a logical “0”) is obtained below the input saturation power of the LOA. The output power level of the logical “0” depends on the extinction ratio of the polarizer and the filtered ASE from the LOA. For an efficient polarizer, the power level of the logical “0” is only limited by the filtered ASE. Beyond the saturation power of the LOA, the state of polarization at the output of the LOA is changed due to a change in the birefringence. Both the orientation (azimuth) and the ellipticity of the polarization

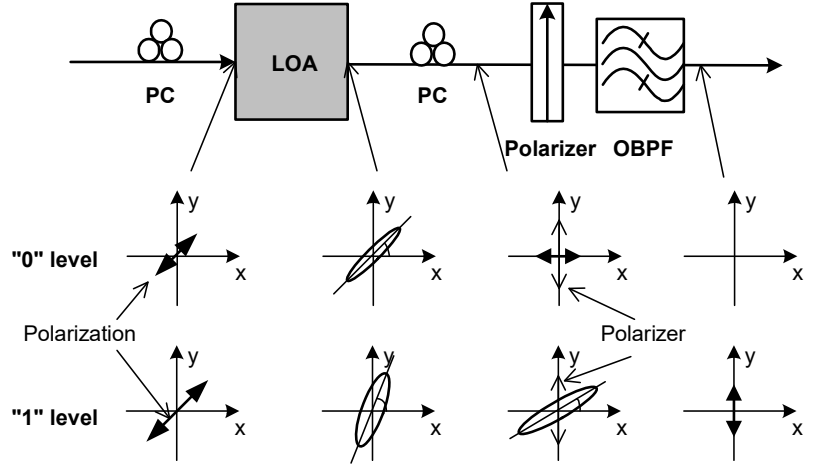


Fig. 4-5 Principle structure of an all-optical 2R regenerator based on the polarization nonlinearity of the LOA. Top: Basic structure, bottom: changing of the state of polarization at different positions of the 2R.

vary rapidly with the input power. The polarizer can no longer block the output from the LOA. Hence, a high power level (or a logical “1”) is obtained at the output of the polarizer. At the same time, the LOA is saturated and its gain quickly drops with increasing input power, and thus the high power level of the output becomes saturated. As a result, an optical regeneration is realized. This can be analytically described as follows.

Assuming the transmission axis of the polarizer is orthogonal to the  $x$  axis (as seen in Fig. 4-5), it is easy to show, according to (Eq. 4.12), that the output power of the 2R regenerator can be given by

$$P_{out} = P_{in} G K_a^2 (T_{//} \sin^2 \theta + T_{\perp} \cos^2 \theta) + P_{in} G K_b^2 (T_{//} \cos^2 \theta + T_{\perp} \sin^2 \theta) + P_{ASE}/2 \quad (4.13)$$

where  $G$  and  $P_{in}$  are the gain and input power of the LOA, respectively.  $T_{\perp}$  and  $T_{//}$  are the transmission coefficients of the polarizer for input linear polarization orthogonal and parallel to the transmission axis of the polarizer, respectively. Their ratio is defined as the extinction ratio of the polarizer,  $\rho = T_{\perp}/T_{//}$ .  $P_{ASE}$  is the optical power of the filtered ASE from the LOA.

$$K_a^2 = \cos^2 \varepsilon = \frac{1}{1 + e^2}, \quad (4.14)$$

$$K_b^2 = \sin^2 \varepsilon = \frac{e^2}{1 + e^2}. \quad (4.15)$$

In the linear regime, the polarization of the output of the LOA is linearised by the polarization controller after the LOA, that is,  $e=0$ ,  $K_b=0$ , and  $K_a=1$ . If setting the

polarizer such as to make its transmission axis be orthogonal to the polarization direction,  $\theta = 0$ , the output power in the linear regime is thus given by

$$P_{out} = P_{in}GT_{\perp} + P_{ASE}/2 = P_{in}GT_{\parallel}\rho + P_{ASE}/2. \quad (4.16)$$

$P_{out}$  depends on the extinction ratio of the polarizer and the filtered ASE from the LOA, and thus a very low output power is obtained. For a perfect polarizer,  $T_{\parallel} = 1$ ,  $\rho = 0$ ,  $P_{out}$  is near zero and just limited by  $P_{ASE}$ . For a practical polarizer, such as in our setup,  $T_{\parallel} \approx 0.9$ ,  $\rho < 0.001$ ,  $P_{out} \approx -34 \text{ dBm} \sim -30 \text{ dBm}$  for the input power from  $-13 \text{ dBm}$  to  $-5 \text{ dBm}$ .

When the linear regime is exceeded, the LOA is saturated and the state of polarization of the output from the LOA changes rapidly and nonlinearly with the input power. Both  $e$  and  $\theta$  are no longer zero and change nonlinearly with the input power (as seen in §4.1.1 and §4.1.2). A high power level is obtained at the output of the 2R:

$$P_{out} = P_{in}GT_{\parallel} \frac{1}{1+e^2} (\sin^2 \theta + e^2 \cos^2 \theta) \quad (4.17)$$

Here,  $P_{ASE}$  and  $T_{\perp}$  ( $\ll T_{\parallel}$ ) are omitted due to their very small values.

For high input power, the output is with a high power level and increases with the induced increase of  $\theta$  ( $< \pi/2$ ) and  $e$  ( $\leq 1$ ). But meanwhile the gain,  $G$ , of the LOA decreases with increasing input power, which makes the output power of the 2R saturate.

In the 2R regenerator, the polarization controller before the LOA is added for adjusting the initial polarization of the input signal beam and thus getting an optimum polarization rotation effect.

Fig. 4-6 shows the calculated static regenerative characteristic of the 2R, which is based on the measured  $e$ ,  $\theta$ , and the gain  $G$  given in Fig. 4-4. In the calculation, the extinction ratio of the polarizer was assumed to be  $\rho = 0.0006$  ( $-32 \text{ dB}$ ) and  $T_{\parallel} = 0.9$ . The filtered ASE from the LOA was set to be  $-42 \text{ dBm}$ . For comparison, static regenerative characteristics for different orientations of the polarizer are also given. It can be seen clearly that an optical regeneration is obtained based on the polarization rotation of the LOA. A significant improvement of extinction ratio can be achieved. For example, an improvement of about  $19 \text{ dB}$  can be obtained with an input extinction ratio of  $10 \text{ dB}$ . The output of the 2R regenerator is sensitive to the orientation of the polarizer in a null condition and thus the regeneration at the logical "0" sensitively depends on the setting of the polarizer. A small deviation of its orientation from being orthogonal to the linear polarization direction will lead to an increase of the "0" level and a change of the regeneration characteristic. For  $2 \text{ dB}$  change in the logical "0" level, the tolerance of the polarizer's orientation is about  $\pm 2^\circ$ .

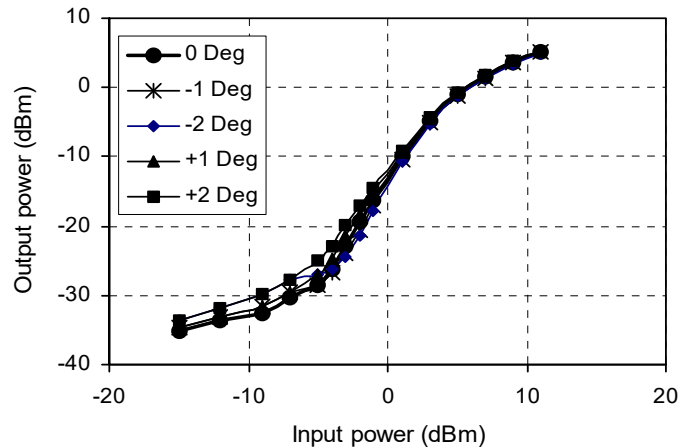


Fig. 4-6 Calculated static regeneration characteristics for different orientation of the polarizer. Extinction ratio of the polarizer, 32 dB;  $T_{//} = 0.9$ ; Filtered ASE, -42 dBm. “0 Deg” means that the transmission axis of the polarizer is orthogonal to the polarization direction of the light; “ $\pm 1, \pm 2$  Deg” represent the deviations of its orientation from being orthogonal to the linear polarization direction.

The advantages of this new scheme of all-optical 2R regeneration are its immunity against small signal distortion in the “0” level and a potentially large extinction ratio (ER) improvement. This results from the flat gain response for small signal powers and the sudden drop in gain as soon as the linear power range is exceeded. The gain of the LOA is clamped and thus does not change in the linear regime. Since there is no gain change, there will not be a polarization state change either. The sudden drop in gain causes a significant change in polarization state of the output of the LOA, as seen in Fig. 4-4. This results in a quasi-ideal regeneration at the “0” level and a high ER improvement.

### 4.3 Experimental demonstration of the regenerative capabilities

The experimental set-up used for demonstrating optical regeneration is shown in Fig. 4-7. A tunable laser source (Model Tunics-plus, Photonetics), an external modulator, and a pulse pattern generator (Advantest D3186) are combined and used as a transmitter. A variable attenuator and an EDFA are used as to control the signal to noise ratio at the input so as to simulate the degradation of the signal. The ER of the input data signal is controlled by changing the driving pulse amplitude (i. e., electrical pulse signal amplitude) of the external modulator. The LOA used in our experiments, as seen in Fig. 4-8, is supplied by Genoa Corp., USA. It is biased with 250mA. The optical band pass filter (OBPF2) after the 2R regenerator has a 3 dB bandwidth of 0.3 nm and is used to reduce the ASE from the LOA. The polarizer has an extinction ratio of 30dB. A Digital Sampling Oscilloscope (Tektronix 11801B)

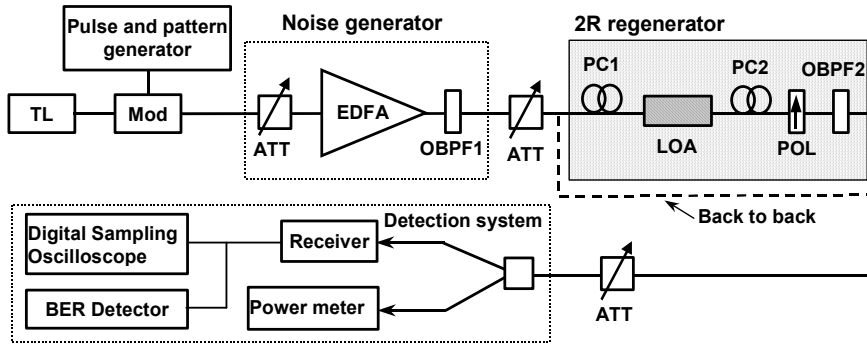


Fig. 4-7 Experimental setup. TL: tunable laser, ATT: Attenuator, Mod: Mach-Zehnder modulator, PC: polarization controller, Pol: polarizer, OBPF: optical band pass filter.

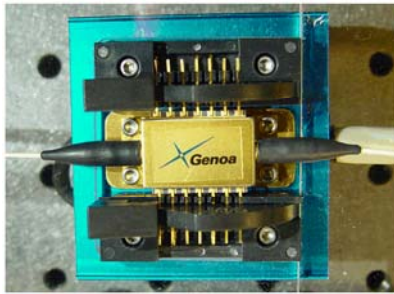


Fig. 4-8 Photograph of the LOA used in the experiments of the 2R regeneration based on polarization rotation.

and an Error Detector (Advantest D3286) are used in the detection system for measuring the eye-diagrams and BER, respectively. The regeneration characteristics of the 2R regenerator are investigated for static operation and dynamic operation at both 2.5 Gbit/s (NRZ,  $2^9-1$  PRBS) and 10 Gbit/s (NRZ,  $2^{31}-1$  PRBS). For 10 Gbit/s, measurements for the RZ signal with a word pattern of (1010010101010010) have also been carried out. The receivers used for dynamic measurements at 2.5 Gbit/s and 10 Gbit/s are Tektronix ORR24 and HP11982A optical receivers, respectively.

### 4.3.1 Static regeneration characteristics

Fig. 4-9 gives the measured static transfer characteristics of the 2R regenerator. It can be seen that a quasi-perfect regeneration is achieved. An ER improvement of 19 dB can be obtained for the input ER of 10 dB. Even for a very low input ER (e.g., 5 dB) an ER improvement of more than 15 dB can be achieved.

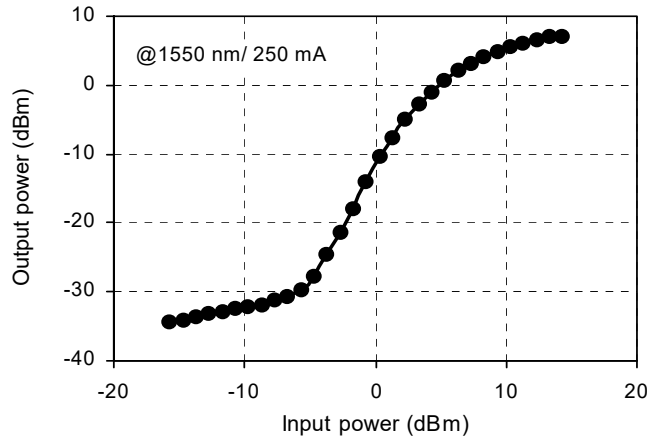


Fig. 4-9 Static regeneration characteristic. Bias current to the LOA: 250 mA, wavelength: 1550 nm. Losses of the optical filter and polarizer are 3.2 dB and 2.2 dB, respectively.

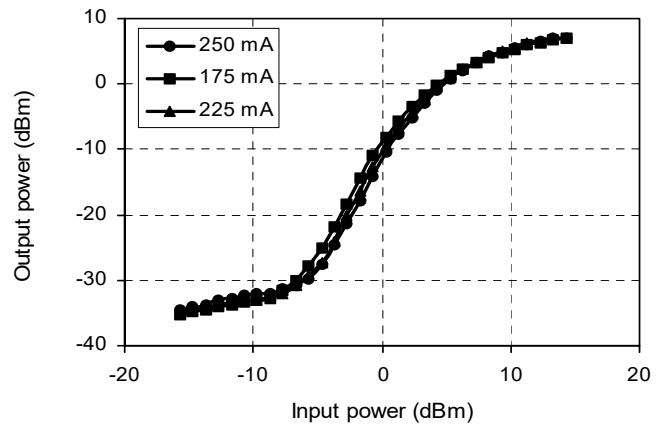


Fig. 4-10 Static regeneration characteristic for different bias currents to the LOA. Wavelength: 1550 nm. Losses of the optical filter and polarizer are 3.2 dB and 2.2 dB, respectively.

In principle, the saturation input power increases with increasing bias current to the LOA, and thus the decision threshold of the 2R can be adjusted simply by changing the bias current. Fig. 4-10 shows the static regenerative characteristics for three different bias currents to the LOA. Only a small shift ( $\sim 1.5$  dB) of the decision threshold is found when changing the bias current from 175 mA to 250 mA. This weak response is due to the fact that the LOA used in our experiment is not specifically designed for the application proposed above and its saturation input power is not so sensitive to the bias current (as seen in Fig 3-3 of Chapter 3). LOAs with high polarization nonlinear effects (high birefringence, high TE/TM conversion) and larger shift of saturation input power with bias current could be

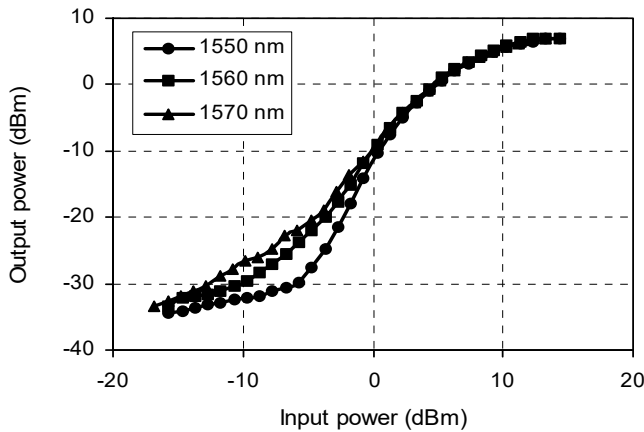


Fig. 4-11 Static regeneration characteristic for different signal wavelengths. Bias current to the LOA: 250 mA. Losses of the optical filter and polarizer are 3.2 dB and 2.2 dB, respectively.

fabricated, that are better adapted to the optical regeneration based on the polarization rotation.

Fig. 4-11 shows the static regenerative characteristics for different wavelengths. Good regeneration has been obtained from 1550 nm to 1570 nm. A small difference in the regeneration at the “0” level is due to the different polarization rotation for different signal wavelengths. Actually, the operation wavelength range of the 2R regenerator is determined by the optical bandwidth of the LOA and the polarization rotation in that wavelength range. As shown in Chapter 3 (as seen in Fig. 3-5 and Fig. 3-6), the optical bandwidth of the LOA is 30 nm. Experimental measurements show that significant polarization rotation can be obtained over that wavelength range. The 2R regeneration can be achieved over the optical bandwidth of the LOA. It should, however, be noted that the state of polarization at the output of the LOA is sensitive to the signal wavelength. To get a good regeneration for different wavelength, the polarization controller after the LOA has to be adjusted for every signal wavelength.

### 4.3.2 Regenerative capabilities at 2.5 Gbit/s

The regenerative capabilities of the regenerator under dynamic operation at 2.5 Gbit/s are demonstrated in Figs. 4-12 to 4-14. Fig. 4-12 shows the eye diagrams with and without the 2R regenerator for degraded signals with different input extinction ratios, while Fig. 4-13 shows the ER improvements as a function of the input ER for the same input optical power of 3 dBm. Both figures are obtained for a signal with a bitrate of 2.5 Gbit/s. Clearly, the input signal is regenerated. The “0” levels in the input signal have been lowered. The eyes become much more open after the 2R regenerator. A significant improvement of the ER is demonstrated. For an input signal with an ER of 4 dB, 8 dB improvement in the ER is obtained. Even for a very deteriorated input signal with an extinction of 3 dB, an extinction ratio improvement

of 5 dB is still achieved. For an input ER higher than 4 dB, the improvement of ER becomes lower. This is mainly due to the fact that the logical “0” level of the output signal has already reached its limit and the output ER goes to saturation to some extent.

Fig. 4-14 contains the results from the BER measurement for two different degraded input signals. Comparing the BER results for the operation of BTB and operation with the 2R, one can see that a negative power penalty of 3.3 dB at a BER of  $10^{-9}$  can be achieved for the degraded signal with 3 dB ER. That means an improvement of more than 3 dB in the receiver sensitivity can be obtained with the proposed 2R-regenerator. For a slightly degraded input signal with an ER of 4 dB, the power penalty is about -2 dB.

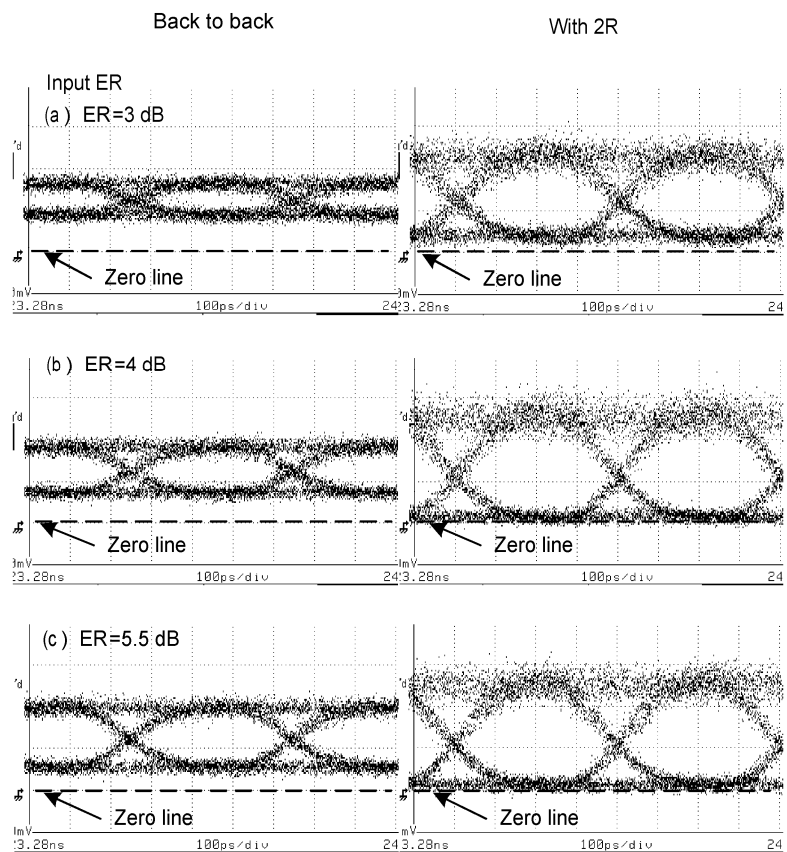


Fig. 4-12 Eye diagrams with and without 2R regenerator for different input signal ER at a bitrate of 2.5 Gbit/s (NRZ,  $2^9$ -1 PRBS). All of the eye diagrams are measured with the same received optical power.

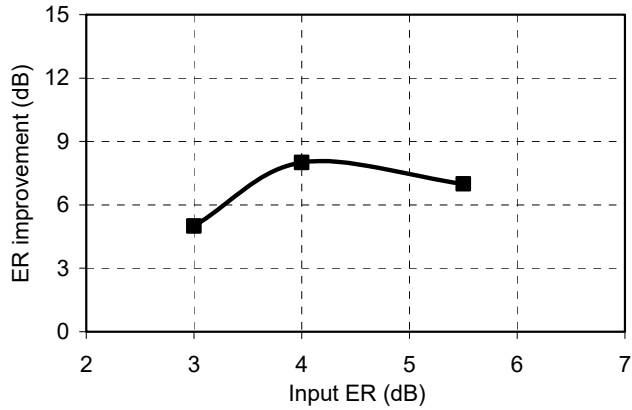


Fig. 4-13 ER improvement as a function of the input ER for 2.5 Gbit/s. Input power to the 2R: 3 dBm; Bias current to the LOA: 250 mA; Signal Wavelength: 1550nm.

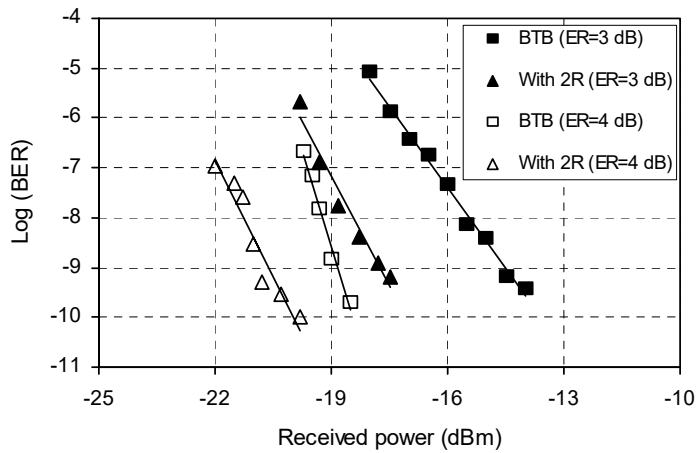


Fig. 4-14 BER as a function of the received power with and without 2R at 2.5 Gbit/s for different degraded input signals, ■ -- with the degraded input signal with the ER of 3 dB, □-- with the slightly degraded input signal with the ER of 4 dB. Input power: 3 dBm; signal wavelength: 1550 nm.

### 4.3.3 Regenerative capabilities at 10 Gbit/s

Experiments for 10 Gbit/s (NRZ,  $2^{31}-1$  PRBS) have also been carried out. Due to the low sensitivity of the receiver (HP11982A), an optical pre-amplifier (EDFA) was used before the receiver for BER measurements. Fig. 4-15 shows the eye diagrams with and without the 2R regenerator for degraded signals with different input ER. It can be clearly seen that the CW component in the input signal is removed and the noise at logical "0" is suppressed after the 2R regenerator. The eyes become much more open and the input signal is regenerated.

From Fig. 4-15, one can see a clear “tail” at the falling edge of the output signal for the input signal with low ER (with high logical “0” level). When the logical “0” level of the input signal gets lower, the “tail” becomes weaker. This “tail” results from a polarization relaxation (the state of polarization of the output light of the LOA can not be simultaneously recovered when the signal goes to logical “0”), since the logical “0” level at the output of the 2R sensitively depends on the state of polarization. This can be also shown with another simple experiment. In that experiment, the polarizer is turned around the light beam axis and it can not totally block the output beam from the LOA for the input logical “0”. The output “0” level of the 2R increases and the “tail” vanishes as the polarizer is being rotated, as shown in Fig. 4-16. Both observations demonstrate that the “tail” belongs to a polarization different from that of the regular “0”, which arises from the polarization relaxation.

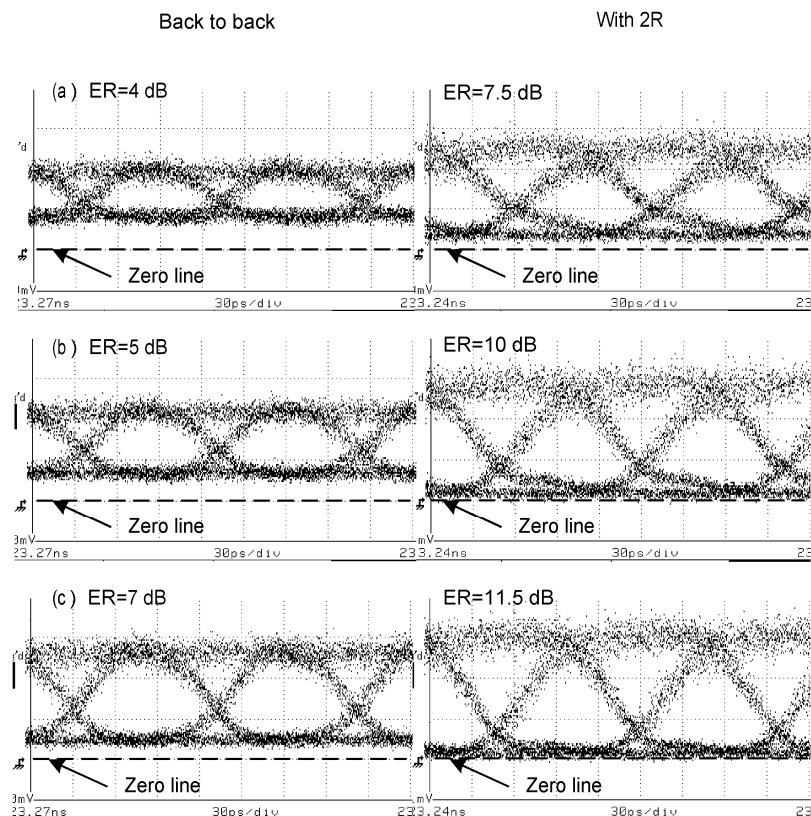


Fig. 4-15 Eye diagrams with and without 2R regenerator for 10 Gbit/s (NRZ,  $2^{31}-1$  PRBS) for different input signal with different extinction ratios. Input power: 5 dBm; Bias current to the LOA: 250 mA. All of the eye diagrams are measured with the same received optical power.

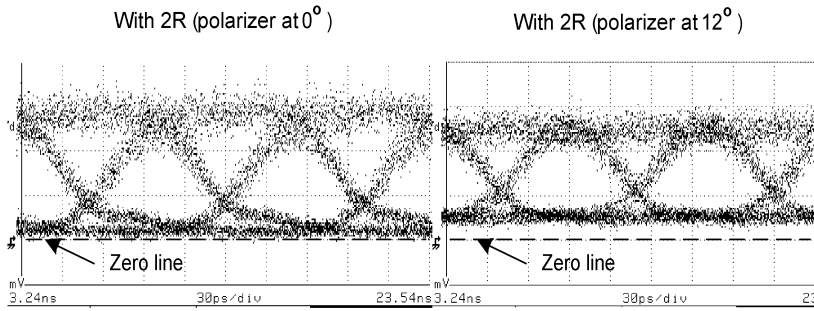


Fig. 4-16 Comparison between the eye diagrams for different polarizer orientations. The input signal is the same as that in Fig. 4-10 (b), input ER=5 dB. Both eye diagrams are measured with the same received optical power.

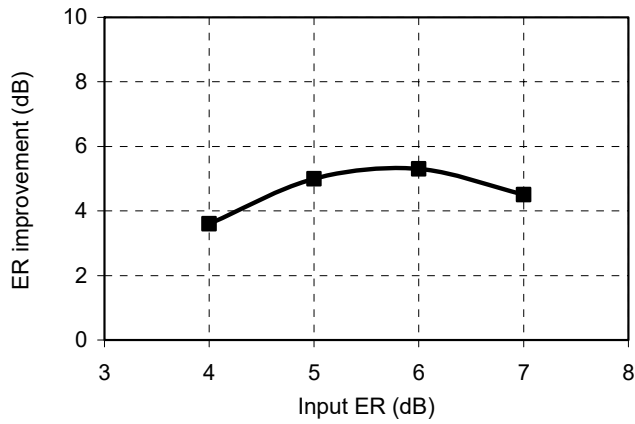


Fig. 4-17 ER improvement as a function of the input ER for 10 Gbit/s. Input power to the 2R: 5 dBm; Bias current to the LOA: 250 mA; Signal Wavelength: 1550nm.

Fig. 4-17 shows the improvement of ER. For an input signal with an ER of 6 dB, more than 5 dB improvement in ER is obtained. Even for a very deteriorated input signal with an extinction of 4 dB, an extinction ratio improvement of > 3 dB is still achieved. For the same reason as for 2.5 Gbit/s, the ER improvement for 10 Gbit/s drops with the increase of the input ER after its peak at 5.3 dB for the input ER of 6 dB. The output ER is larger than 11 dB at the input ER of 7 dB.

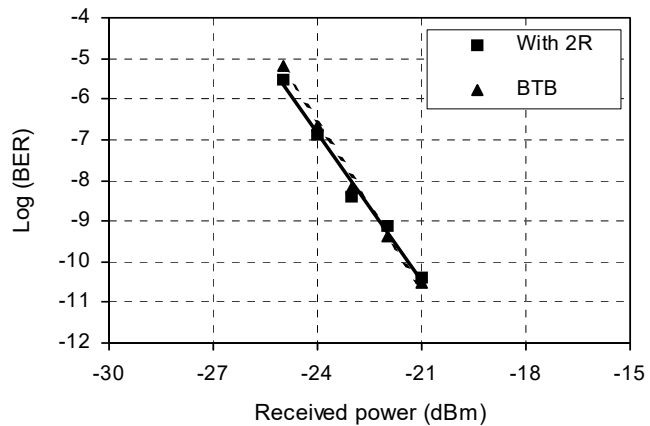


Fig. 4-18 BER as a function of the received power with and without 2R at 10 Gbit/s. Input power to the 2R: 5 dBm; Input ER: 5 dB; Bias current to the LOA: 250 mA; Signal Wavelength: 1550nm.

Fig. 4-18 gives the BER measurement results with and without the 2R regenerator for a degraded signal with 4 dB ER, showing a zero power penalty at a BER of  $10^{-9}$ . Here no negative power penalty is found. This is due to the polarization relaxation mentioned above and the induced pattern distortion at the falling edge of the signal, as seen in Fig. 4-15. In order to minimise this undesired effect, it is necessary to enhance the speed and reduce the polarization relaxation effect in the LOA. This could be a further effort for optimising the LOA for the polarization rotation-based optical regeneration at high bitrates.

Experiments for a “quasi” RZ signal with a word pattern of (1010010101010010) have also been carried out for 10 Gbit/s. Fig. 4-19 demonstrates the eye diagrams at the input and output of the 2R regenerator for the input signals with different ER. Note the time delay in the eye diagrams after the 2R regenerator. As it can be seen, the degraded input signal is regenerated. The “0” level of the input signal is significantly reduced. An ER improvement of more than 5 dB can be achieved for an input ER of 6 dB. The noise at the logical “0” level is suppressed. All of these demonstrate the regenerative capability for RZ signals. Noise suppression at the logical “1” level has not been found due to the weak regeneration of the 2R at the logical “1”. It can be improved, however, by using a narrow optical band pass filter as in the saturable absorber based 2R regeneration for the RZ signal [10].

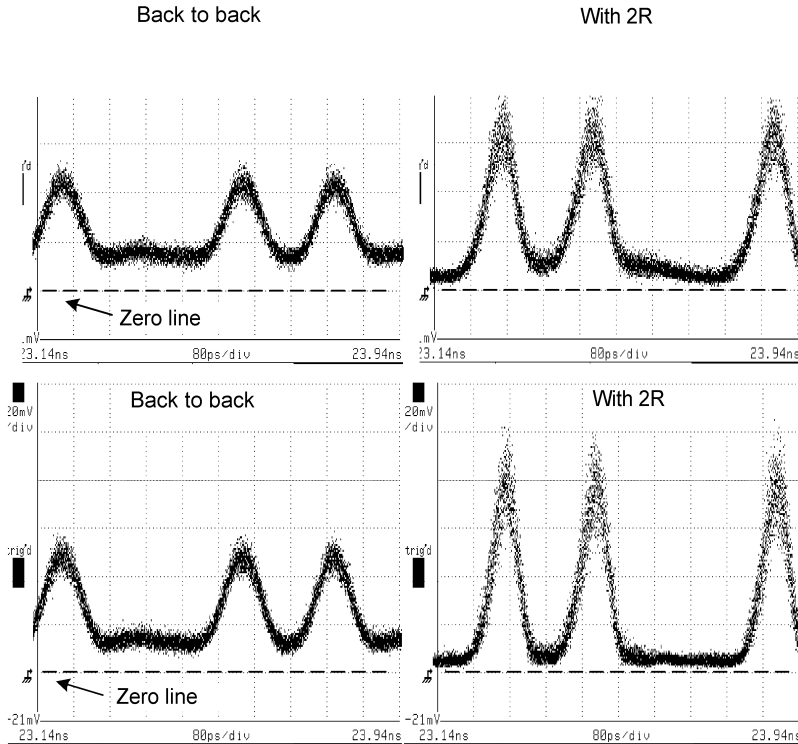


Fig. 4-19 Eye diagrams with and without 2R regenerator for 10 Gbit/s quasi-RZ signal with a word pattern of (1010010101010010) for input signals with different extinction ratios. Input extinction ratio: 5 dB (top), and 6 dB (bottom). Input power: 5 dBm, Bias current to the LOA: 250 mA. All of the eye diagrams are measured with the same received power.

#### 4.4 Summary

The LOA exhibits polarization rotation due to the non-linear effective birefringence. Both orientation and ellipticity of the elliptical polarization of the output light from the LOA change with increasing input power when the LOA is saturated, but not in the linear regime. Based on this nonlinear change of the state of polarization with input optical power, an all-optical 2R regenerator can be realized by using a single LOA. Under static operation, an ER improvement of 19 dB has been obtained for the input ER of 10 dB, and a 15 dB ER improvement for the input ER of 5 dB. With a degraded input signal, a receiver sensitivity improvement of over 3 dB at a bit-error-rate (BER) of  $10^{-9}$  has been found for 2.5 Gbit/s. For 10 Gbit/s, zero power penalty is observed. Significant improvements of ER are obtained for both 2.5 Gbit/s and 10 Gbit/s. The 2R regenerator can be used for both NRZ and RZ formats, and its operating wavelength range can be up to 30 nm. In addition, the decision threshold of the 2R regenerator can, in principle, be adjusted simply by changing the bias current to the LOA. The features of simple configuration, stable operation and high

regenerative capabilities make this new scheme a promising technique for all-optical regeneration in future optical networks.

It is clear however that control of input polarization is required in this new scheme, which may be disadvantageous in some circumstances. But it could be extended to an input polarization insensitive 2R regenerator with a polarization diversity scheme.

## References

- [1] H. Soto, D. Erasme, and G. Guekos, "Cross-polarization modulation in semiconductor optical amplifiers," *IEEE Photon. Technol. Lett.*, Vol. 11, No. 8, pp. 970-972, 1999.
- [2] D. Erasme, H. Soto, and G. Guekos, "All-optical switching and XOR-gating using cross-polarization modulation in a semiconductor optical amplifier," *Proc. Conference on Lasers and Electro Optics CLEO/Europe*, CTuD3, Nice, France, September 10-15, 2000.
- [3] H. Soto, J. C. Dominguez, D.Erasme, and G. Guekos, "Demonstration of an all-optical switch using cross-polarization modulation in semiconductor optical amplifiers," *Microwave and Opt. Technol. Lett.*, Vol. 29, No. 3, pp. 205-208, 2001.
- [4] H. Soto, D.Erasme, and G. Guekos, "5-Gb/s XOR optical gate based on cross-polarization modulation in semiconductor optical amplifiers," *IEEE Photon. Technol. Lett.*, Vol. 13, No. 3, pp. 335-337, 2001.
- [5] H. Soto, C. A. Diaz, J. Topomondzo, D.Erasme, L. Schares, and G. Guekos, "All-optical AND gate implementation using cross-polarization modulation in a semiconductor optical amplifier," *IEEE Photon. Technol. Lett.*, Vol. 14, No. 4, pp. 498-500, 2002.
- [6] M. F. C. Stephens, M. Asghari, R. V. Penty, and I. H. White, "Demonstration of ultrafast all-optical wavelength conversion utilizing birefringence in semiconductor optical amplifiers," *IEEE Photon. Technol. Lett.*, Vol. 9, No. 4, pp. 449-451, 1997.
- [7] M.F.C. Stephens, A.E. Kelly, D. Nettet, A. Wonfor, and R.V. Penty, "Demonstration of Time Division Demultiplexing from 40Gb/s to 10Gb/s via Polarisation Switching in a Semiconductor Optical Amplifier," *Proc. Conference on Lasers and Electro Optics CLEO/Europe*, pp.383, Glasgow, Scotland, UK, September 13-18, 1998.
- [8] D. A. Francis, S. P. DiJaili, J. D. Walker, "A single-chip linear optical amplifier," *Techn. Dig. Conference on Optical fiber communication OFC2001*, PD-13, Anaheim, USA, March 19-22, 2001.
- [9] R. M. A. Azzam, and N. M. Bashara, "Ellipsometry and polarized light", (North-Holland Personal Library, 1988), pp. 7, 27, 69.
- [10] O. Leclerc, "Optical regeneration & WDM dispersion-managed transmission systems," *Proc. European Conference on Optical communications, ECOC 2001*, Tutorial TuM.1.1, Amsterdam, October 1-4, 2001.

## **Chapter 5**

# **Noise suppression in spectrum-sliced WDM systems**

Spectrum slicing is an attractive WDM technique in which optical filters are used to obtain a spectral slice of light from a broadband source and modulators encode data onto the slice [1,2]. Spectrum slicing is a strong candidate for future FTTH access networks [3-6], and has potential for cost-sensitive local area network applications, because the need for multiple semiconductor lasers stabilized at specific wavelengths is avoided and the potential exists for a network that uses a single shared source. The spectrum slicing technique was first presented and demonstrated by M. H. Reeve and co-workers in British Telecom Research Laboratories, United Kingdom in 1988 [1]. It has been investigated and further developed in the past years. Spectrum slicing of both coherent broadband sources such as femtosecond mode-locked lasers [7-10], Fabry-Perot lasers [11], and super-continuum generators [12-15] and incoherent broadband sources such as EDFAs [16, 17], LEDs [18, 19] and superluminescent LEDs [20] has been demonstrated. The coherent broadband sources are costly and complex, probably limiting the scope for their use to high performance WDM transmission systems. The incoherent broadband sources are more widely available and low cost, making them potentially suitable in cost-sensitive access and other network applications. Recently, spectrum-sliced WDM systems using incoherent broadband sources for passive optical networks and local access networks have been reported [21-26]. However, light spectrally sliced from an incoherent source is thermal-like and, therefore, exhibits excess intensity noise that limits the achievable bit error rate for a given slice bandwidth [27, 28]. Previously, this limitation could have been overcome only at the expense of system capacity, i.e., by increasing the optical bandwidth or by reducing the bitrate of the channel. We have investigated a technique for reducing excess intensity noise in the spectrum-sliced WDM system, which is based on the specific noise properties of a saturated SOA. In this chapter, we first define the spectrum slicing and briefly review the intensity noise properties of light spectrally sliced from an incoherent broadband source, its limitation on the transmission performance of the spectrum-sliced WDM system and existing solutions for the intensity noise reduction in section §5.1. In §5.2, a theoretical analysis of the noise suppression using a saturated SOA is given. The influence of the injected current and the input power level of the SOA on the noise reduction and its bandwidth is studied, and the optimum condition for a high noise suppression ratio and a large bandwidth is derived. Experimental

results of relative intensity noise (RIN), SNR, and BER improvements have confirmed the theoretical predictions. Finally, a summary is given in §5.3.

## 5.1 Intensity noise limits in spectrum-sliced WDM systems

### 5.1.1 Spectrum-sliced WDM system

A schematic diagram of a spectrum-sliced WDM system is shown in Fig. 5-1. The broadband light source is efficiently split into many WDM channels by using a  $1 \times N$  WDM demultiplexer, each channel is modulated individually, and the channels are multiplexed back into a single-mode fiber by using an  $N \times 1$  WDM multiplexer in a central office. Each channel of the transmission system takes a slice from the output spectrum of the broadband light source. After transmission, the multiplexed signals enter another  $1 \times N$  WDM demultiplexer, and the demultiplexed signals are sent to the corresponding subscribers' sites through the single-mode fibers. As mentioned above, the broadband light source used in spectrum-sliced WDM system can be an incoherent ASE source (e. g., LEDs, superluminescent LEDs, or EDFAs) or a coherent broadband source (e. g., femtosecond mode-locked lasers, Fabry-Perot (FP) lasers, or super-continuum generators). The WDM multi- and demultiplexers can be waveguide grating routers (WGR's) or other multi-channel optical bandpass filters.

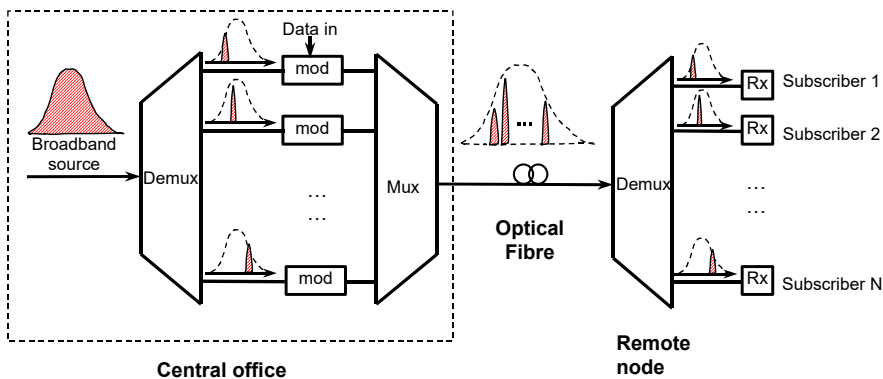


Fig. 5-1 Schematic diagram of the spectrum-sliced WDM system based on a broadband light source (downstream transmission).

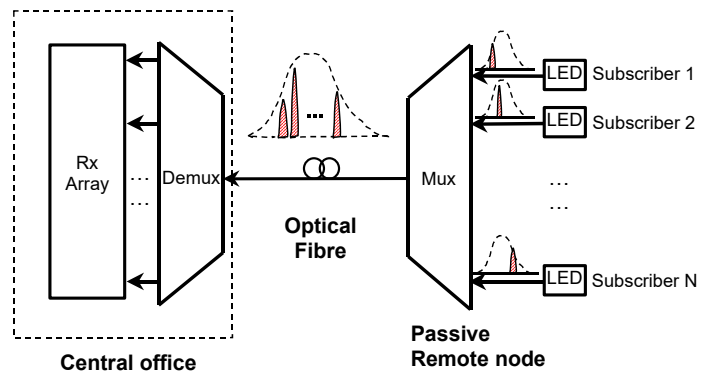


Fig. 5-2 Schematic diagram of an upstream transmission system using spectral slicing.

Obviously, the system shown in Fig. 5-1 is for downstream transmission. The spectrum-sliced WDM system for upstream transmission is schematically displayed in Fig. 5-2. In the upstream transmission, a central office is connected by a single fiber to a remote node that contains a waveguide router. There are  $N$  input ports of the router, and a single fiber runs from each input port to a subscriber. Each router port has multiple passbands separated from one another by the router's free spectral range (FSR), and the passbands of one port are separated from those of the adjacent ports by the channel spacing (CS) of the router. The light from the LED's is spectrally sliced at the router in the remote node, and the signals are multiplexed onto the fiber that goes to the central office. The central office contains a router that demultiplexes the different wavelengths and routes the light from each LED to a separate detector.

The system depicted is an example of a passive optical network (PON), that is, it is a point-to-multipoint system with no active elements between the endpoints. The cost of the system is quite sensitive to the cost of the upstream transmitter because there is one transmitter at each subscriber, so inexpensive broadband ASE sources (e. g. LEDs, or SLEDs) could be an ideal choice.

Spectral slicing of the broadband ASE sources has certain limitations. One is that the optical power of each channel is low as it just takes a slice of the total output spectrum and hence optical power of the ASE source. This limits the area a PON can serve without further amplification. This problem could be solved using high power broadband ASE sources [16, 29-31].

A second problem that arises in spectral slicing is that interference due to linear crosstalk can be quite high. It has been noted that the tails of a Gaussian optical passband contribute to crosstalk [32]. In the waveguide router [33], the passband shape is Gaussian only over a limited wavelength range and there is a finite maximum rejection level for out-of-band light. Both the passband shape and the finite out-of-band rejection lead to crosstalk in the demultiplexer. In addition, the finite rejection and passband shape of the multiplexer lead to non-ideal spectral slicing, and therefore contribute additional interference. That is, after multiplexing,

some of the light from LED#1 will appear in the optical passbands of channels 2, 3, and so on. As a result, even a perfect optical demultiplexer could not produce a crosstalk-free signal at the central office or the subscribers' sites. Finally, in a PON, there will be no electrical power at the site of the multiplexer, so the temperature of the multiplexer cannot be controlled. Changes in temperature will lead to changes in the positions of the optical passbands of the multiplexer [5]. If the demultiplexer tracks these changes imperfectly, the resulting channel misalignment will lead to increased crosstalk as well as increased slicing loss. This issue has been extensively investigated [32, 34, 35], and the crosstalk could be reduced using a router with small temperature dependence or using some wavelength tracking techniques to reduce the misalignment between the multiplexing and the demultiplexing routers.

A third important issue of the spectrum-sliced WDM system based on the incoherent broadband source is the intensity noise limit. The broadband ASE light sources make the spectrum-sliced WDM system cost effective. However, the optical slice of the incoherent light source exhibits a high intensity noise due to the spontaneous-spontaneous beating when it is detected in the receiver [27, 36-38]. This intensity noise, termed excess intensity noise, is inversely proportional to the optical bandwidth of the slice of incoherent light source. For moderate distances and data rates, the excess intensity noise does not pose a problem. But it places limits on the achievable performance when the spectrum-sliced WDM system operates at a high bitrate (2.5 Gbit/s and beyond) and over a long distance.

Spectrum-sliced WDM systems using coherent broadband sources such as femtosecond mode-locked lasers and Fabry-Perot (FP) lasers exhibit so called mode partition noise due to spectral filtering of multiple modes [39,40]. Similar to the excess intensity noise of the sliced incoherent ASE source, the mode partition noise causes a large degradation of the SNR of the transmission system.

In the following sections, we will focus our discussion and analysis on the excess intensity noise limits to the transmission performance of the incoherent ASE source-based spectrum-sliced WDM system and on the suppression of this excess intensity noise.

### 5.1.2 Limits on the transmission performance caused by excess Intensity noise

#### Theoretical analysis

Fig. 5-3 shows a schematic diagram of a single spectrum-sliced WDM channel from an incoherent ASE source. Light from a broadband, incoherent ASE source is filtered to produce a spectral slice that is fed to an optical intensity modulator to encode data onto the slice. It arrives at an optical bandpass filter normally identical to that used to produce the transmitted spectrum. The filter is followed by an ideal square-law detector and an electrical low-pass filter. If the ASE is unpolarized and has a linewidth substantially greater than the modulation bandwidth, as is the case in a spectrum sliced system, then the mean-square photocurrent fluctuations produced in a photodetector in a bandwidth  $B_c$  can be written as [26, 38]

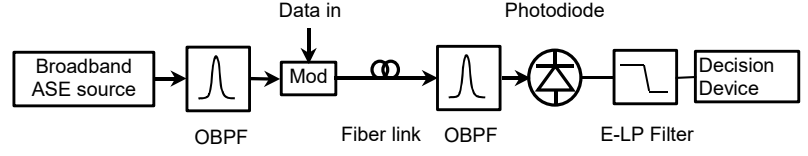


Fig. 5-3 Schematic diagram of a single spectrum-sliced WDM channel using incoherent ASE source. OBPF: optical bandpass filter; Mod: intensity modulator; E-LP filter: electrical low-pass filter.

$$\langle \Delta I_s^2 \rangle = \frac{4KT}{R_L} B_e + 2q \langle I_s \rangle B_e + \langle I_s \rangle^2 \frac{B_e}{\Delta \nu} \quad (5.1)$$

Here the first two terms are the well-known thermal noise and shot noise, and the third term represents excess intensity noise due to the mutual beating between spontaneous emission components.  $\langle I_s \rangle$  is the optical mean power of the signal. The thermal noise, the shot noise, and the excess intensity noise can be considered as "white" noise sources at frequencies of electronic interest. In the case of spectrum-sliced system,  $B_e$  is the noise equivalent bandwidth of the electrical low-pass filter, and is defined by [28]

$$B_e = \frac{1}{2\pi |G(0)|^2} \int_0^\infty |G(\omega)|^2 d\omega \quad (5.2)$$

where  $\omega$  is the angular baseband electrical frequency.  $G(\omega)$  is the frequency response of the receiver noise filter.

The term  $\Delta \nu$  is determined by the optical linewidth of the source, and is defined by

$$\Delta \nu = \left[ \int_{-\infty}^{\infty} P(\nu) d\nu \right]^2 / \int_{-\infty}^{\infty} P^2(\nu) d\nu \quad (5.3)$$

where  $P(\nu)$  is the power spectral density of the optical field.

The SNR of the received signal can be written as

$$SNR = \frac{\langle I_s \rangle^2}{\langle \Delta I_s^2 \rangle} = \frac{\langle I_s \rangle^2}{(4KT/R_L)B_e + 2e\langle I_s \rangle B_e + \langle I_s \rangle^2 B_e / \Delta \nu} \quad (5.4)$$

In traditional LED transmission systems, the spontaneous-spontaneous beat noise is negligible because of the large optical bandwidth. However, it becomes dominant over electrical noise (shot noise and thermal noise) when the optical bandwidth per channel is significantly reduced as in the proposed spectrum-sliced WDM system.

For a given spectrum-sliced WDM channel,  $B_e$  can normally be assumed to be 0.75 times the transmission bitrate  $B$  [28], and hence the  $SNR$  is inversely proportional to the bitrate  $B$ . For very low signal powers, the excess intensity noise is small, and the electrical noise dominates over the excess intensity noise. The  $SNR$  is given by

$$SNR_{sh} = \frac{\langle I_s \rangle}{2qB_e} \quad (\text{Shot-noise-limited}) \quad (5.5)$$

For high signal powers, the excess intensity noise becomes dominant, and the excess intensity noise limited  $SNR$  is given as

$$SNR_{ex} = \frac{\Delta V}{B_e} \quad (\text{excess-noise-limited}) \quad (5.6)$$

For partially polarized light, the  $SNR_{ex}$  in (5.6) must be decreased by a factor  $(1+p^2)/2$  where  $p$  is the degree of polarization [28]. Using polarized ASE, therefore, decreases  $SNR_{ex}$  by a factor of two.

The  $SNR_{ex}$  is constant for all values of received power and is proportional to the optical linewidth of the signal. Obviously, the constant  $SNR_{ex}$  will result in an error floor, which limits achievable transmission performances such as transmission distance and bitrate. Since the excess intensity noise dominates, the electrical noise of the receiver can be neglect, and there is no noise when the signal is not present (i. e., for the logical "0"). The  $BER$  can be given by [41]

$$BER = \frac{1}{2} \operatorname{erfc}(Q/\sqrt{2}) \quad (5.7)$$

$$Q \approx \frac{\langle I_s \rangle}{\sqrt{\langle \Delta I_s^2 \rangle}} = \sqrt{SNR_{ex}} \quad (5.8)$$

At a given bitrate,  $SNR_{ex}$  may be increased by increasing the optical linewidth of the spectral slice, and thus the error floor is reduced. However, increasing the optical linewidth will also increase the errors due to dispersion-induced intersymbol interference. In addition, dispersion also causes a decrease in the  $SNR_{ex}$ . This leads to dispersion-induced errors in addition to those produced by intersymbol interference alone [28]. For a given optical link, there is a tradeoff in linewidth

between increasing the  $SNR_{ex}$  and reducing dispersion-induced intersymbol interference. Consequently, the spectrum-sliced WDM system is limited to low bitrate and short distance transmission due to excess intensity noise. This will be confirmed by both simulation and experimental results described in the following.

### Experimental and simulation results

The setup used for the transmission experiment using a single spectrum sliced WDM channel is shown in Fig. 5-4. The amplified spontaneous emission (ASE) from a SLED, as shown in Fig. 5-5 (1550MHFD, Opto speed) was spectrally sliced using a fibre Bragg grating (FBG) filter. The slice of light was NRZ-modulated using a LiNbO<sub>3</sub> external modulator with a  $2^{23}-1$  pseudorandom-bit-sequence (PRBS) pattern, and then detected using a receiver with electrical low pass filters and an oscilloscope (Tektronix 11801B digital sampling oscilloscope).

Fig. 5-6 shows the optical spectra of the broadband incoherent light from the SLED and the optical slice filtered out from this light source. The central wavelength of the slice is 1550.9 nm and its 3 dB-bandwidth is 0.5 nm. Fig. 5-7 gives the eye diagrams of the spectrum-sliced WDM channel for different bitrates at back to back operation. There is a considerable contribution of intensity noise to the high level of the eye. At low bitrates, e.g. several hundreds of Mbit/s, the eyes are open well, but at high bitrates, e. g. 2.5Gbit/s, the intensity noise becomes significant and the eyes are almost closed. The eye diagrams for different slice bandwidths are shown in Fig. 5-8. Larger slice bandwidth results in a higher signal to noise ratio and thus a better eye diagram. These results are consistent with the theoretical analysis described above.

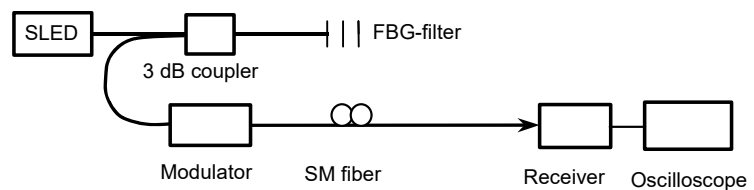


Fig. 5-4 Setup for the fibre link experiment with spectrum-sliced WDM



Fig. 5-5 Photograph of the SLED used for spectral slicing.

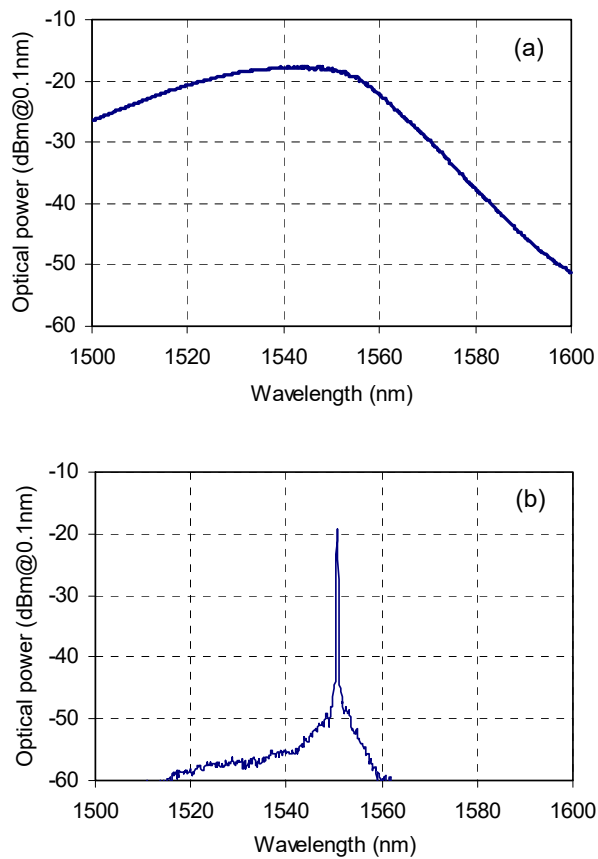


Fig. 5-6 Optical spectra of the SLED and the optical slice. The central wavelength of the slice: 1550.9 nm; 3 dB-bandwidth: 0.5 nm.

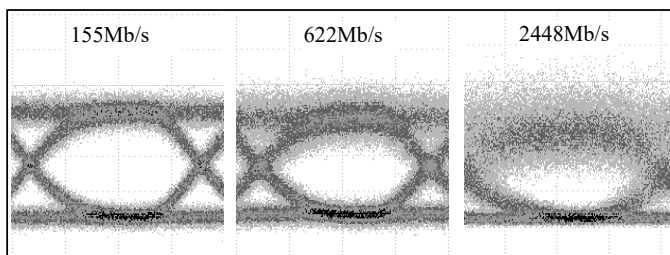


Fig. 5-7 Eye diagrams for different bitrates at back to back operation. Optical slice bandwidth: 0.5nm ( $\Delta\nu=63.8$  GHz), signal wavelength: 1550 nm.

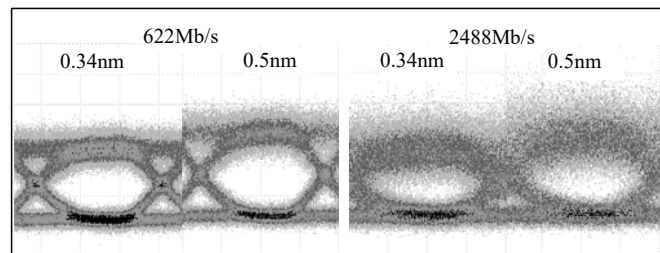


Fig. 5-8 Eye diagrams for different bandwidths of the optical slice and different bitrates. Back to back operation. Signal wavelength: 1550 nm.

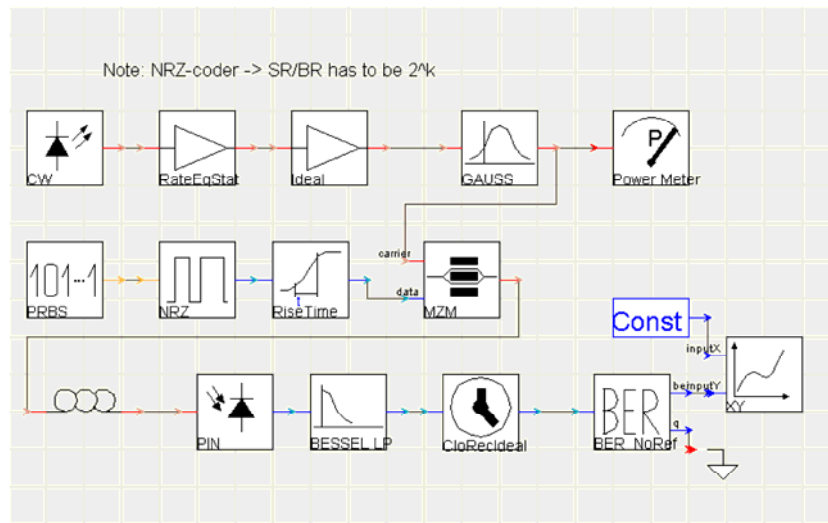


Fig. 5-9 Simulation setup of a single spectrum-sliced WDM channel. Broadband source: ASE from EDFA; optical filter:Gaussian, 1537nm; signal: PRBS-order 8; extinction ratio of Mod: 30dB; detector: PIN, shot noise on; thermal noise:  $1e-12A/\sqrt{Hz}$ ; E-LP-filter:Bessel, bandwidth,  $0.75 \times$  bitrate; fiber link: standardSMF.

With PTDS (Photonic Transmission Design Suite, currently called VPI) from Virtual Photonics Incorporated [42], simulations of the transmission of a single spectrum-sliced WDM channel were also performed. The simulation setup is shown in Fig. 5-9. Fig. 5-10 gives the simulation results for back to back operation. In the figure, BER curves as a function of received power are given for bitrates of 1.25 Gbit/s and 2.5 Gbit/s, respectively. One can see clearly that there is an error floor in the high received power region where the excess intensity noise dominates, and the error floor can be lowered by decreasing the bitrate.

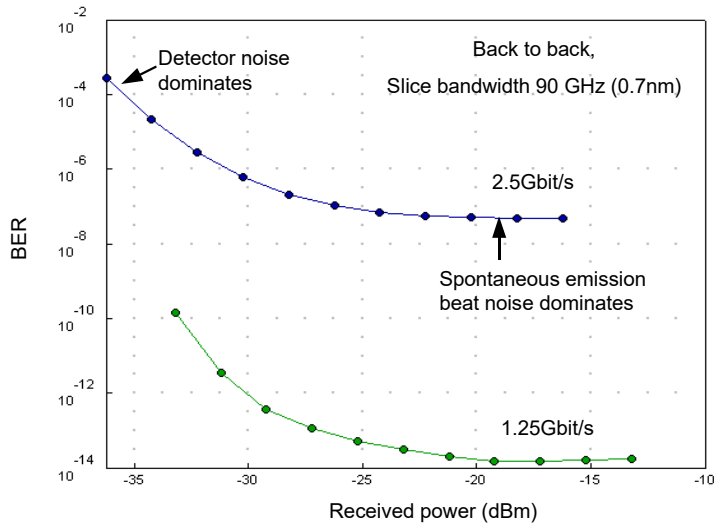


Fig. 5-10 BER versus received power for the bitrates of 1.25 Gbit/s and 2.5 Gbit/s for back to back operation. Optical slice bandwidth: 90 GHz (0.7 nm).

As mentioned in the above section, the excess intensity noise limited SNR and thus the BER can be improved by increasing the slice bandwidth. However, increasing the optical linewidth will also increase the error due to dispersion-induced intersymbol interference. For a given optical link, there is thus a tradeoff in linewidth between increasing the  $SNR_{ex}$  and reducing dispersion-induced intersymbol interference. Fig. 5-11 shows BER as a function of slice bandwidth for different fiber (standard single mode fiber) lengths of the optical link operating at 625 Mbit/s, while Fig. 5-12 gives that for a bitrate of 2.5 Gbit/s. In the simulation, the received power was  $-15$  dBm and thus the excess intensity noise dominated over the receiver noise. It can be seen that for narrow slice bandwidths, the BER is dominated by the excess intensity noise and decreases with increasing slice bandwidth; whereas for larger slice bandwidths, dispersion becomes the limiting factor. For a given bitrate and fiber link length, there is an optimum slice bandwidth that minimizes the BER. The optimum slice bandwidth decreases with increasing fiber link length, and the minimum BER increases. Consequently, the achievable transmission distance is limited for a given bitrate. From the simulation results given above, transmission over 100 km with a BER of  $10^{-9}$  can be achieved for a bitrate of 625 Mbit/s with a slice bandwidth of 0.8 nm. But for a bitrate of 2.5 Gbit/s, less than 10 km transmission with a BER of  $10^{-9}$  can be achieved with a slice bandwidth of 1.4 nm.

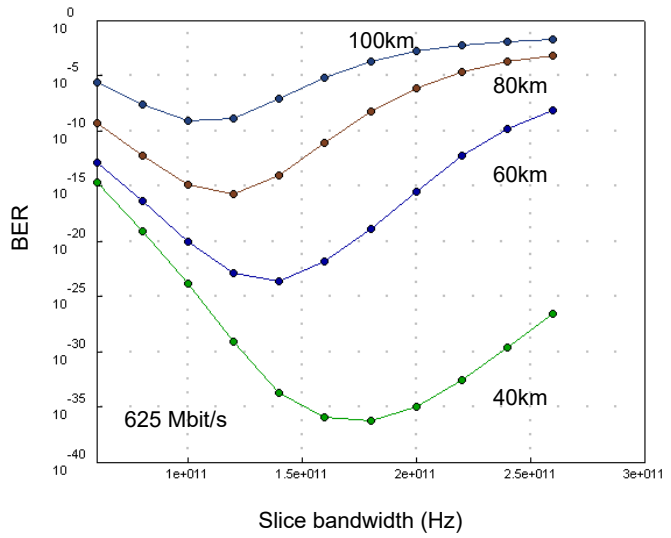


Fig. 5-11 BER versus optical slice bandwidth for different optical fiber link lengths at a bitrate of 625 Mbit/s.

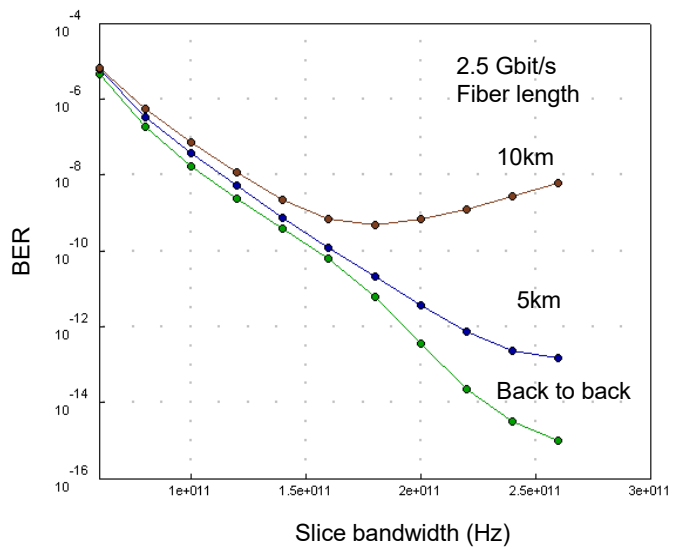


Fig. 5-12 BER versus optical slice bandwidth for different optical fiber link lengths at a bitrate of 2.5 Gbit/s.

It should be pointed out that the simulation described here is just based on a simple Gaussian mode, and the achievable transmission performance such as the transmission distance of the spectrum-sliced WDM channel could have been over estimated. This is because the probability density function (PDF) of detected thermal light can be approximated by a Gaussian only close to the mean and there are significant deviations in the tails [43]. Nevertheless, from a qualitative point of view the simulation agrees well with the theoretical results.

### 5.1.3 Possible solutions of intensity noise suppression

The spectrum-sliced incoherent light has a large intensity noise that strongly limits transmission bitrate and distance of the spectrum-sliced WDM system. In order to break the limitations and improve the performance of spectrum-sliced WDM, three different techniques have been reported recently: a feedforward modulation technique [44, 45], an intrachannel four-wave mixing (IC-FWM) technique [46], and a technique based on a saturated SOA [47,48].

#### Feedforward modulation technique

The feedforward modulation technique of intensity noise reduction is an electrical method that is shown in Fig. 5-13 [44]. The feedforward noise reduction (FFNR) circuit is shown in the shaded region and consists of a fiber coupler, an optical attenuator, photodetector and electrical gain and phase matching elements. A fraction of the filtered incoherent light is tapped off and the excess intensity noise detected. The remaining light forms the primary signal and propagates through the modulator. The excess intensity noise detected by the FFNR circuit results from excursions in the optical power above (over-shoots) and below (drop-outs) the average power. Reducing the primary signal during signal over-shoots and increasing the primary signal during drop-outs reduces the excess intensity noise of the primary signal. As the average power is unaffected, the SNR of the primary signal is improved. This technique can achieve a wideband reduction of excess intensity noise. For transmission at 2.5 Gbit/s, the BER can be reduced for a given received optical power by over three orders of magnitude. A four-fold increase in capacity has been demonstrated owing to the less optical bandwidth required than a spectral slice without noise reduction. Obviously this technique, however, needs complicated microwave circuits at the transmitter with a critical timing control.

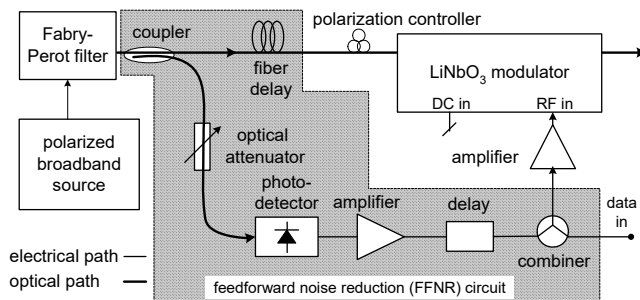


Fig. 5-13 Schematic diagram of a spectrum-sliced transmitter with feedforward noise reduction.

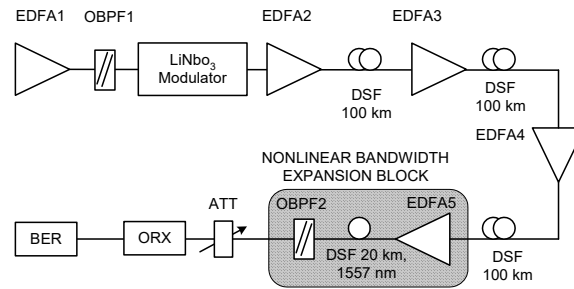


Fig. 5-14 Schematic diagram of the intrachannel four-wave mixing technique for intensity noise reduction in a spectrum-sliced WDM channel. OF: optical filter; DSF: dispersion-shifted fiber; ATT: optical attenuator; ORX: optical receiver.

### IC-FWM technique

The basic idea of the IC-FWM technique is that the optical slice has much narrower optical bandwidth than the conventional limit during its transmission through the fiber link of the spectrum-sliced WDM channel. When the slice arrives at the receiver side, its optical bandwidth is expanded using an optical nonlinear bandwidth expansion block that is based on the intrachannel four-wave mixing. Even though the SNR is poor during the transmission, sufficient SNR can be obtained through the optical bandwidth expansion at the receiver. The schematic diagram of the IC-FWM technique is shown in Fig. 5-14. The shaded region shows the nonlinear bandwidth expansion block. It consists of 20-km DSF and an EDFA. The optical filter (OF2) has much larger bandwidth than that of the first optical filter in the transmitter and is used to filter out some noise from the EDFAs. Transmission for 2.5 Gbit/s incoherent spectrum-sliced channel with only 0.1 nm slice bandwidth has been demonstrated using this technique [46]. Since the optical bandwidth of the transmission channel is reduced, the maximum number of spectrum-sliced WDM channel can be increased and the dispersion penalty can be reduced simultaneously. The drawback of this technique is that a dispersion-shifted fiber and a high power EDFA are needed at the receiver.

### Saturated SOA-based technique

On the contrary, the saturated SOA-based technique is a more simple and efficient technique to reduce the intensity noise. In this technique, an SOA operating at saturation is used at the transmitter before the optical modulator. The gain-saturation characteristics of the SOA suppress the intensity noise and increase the intensity-noise-limited SNR very effectively. This technique was proposed in 1997 [47], and experimentally demonstrated in the passed several years [48-52]. Such techniques have the advantage of simplicity, high efficiency and potentially low cost since the saturated SOA can be used simultaneously for both noise reduction and signal modulation. Therefore, it is very practical and useful for application in cost-sensitive local area networks. However, previous reports on the noise reduction considered

only the dependence of the noise reduction on the gain compression (input power level) of the SOA or consisted of a simple experimental demonstration. In the following section, we present a more complete analysis of the noise reduction in spectrum-sliced WDM systems. The influence of the injected current and the input power level of the SOA on the noise reduction and its bandwidth is studied theoretically and experimentally, and the optimum condition for a high noise suppression ratio and a large bandwidth is derived.

## 5.2 Intensity noise suppression using a saturated SOA

### 5.2.1 Analytical theory

Intensity noise suppression using a saturated SOA is based on the specific noise properties of the saturated SOA. We consider a travelling wave SOA. An optical beam is incident and propagates through the SOA. Neglecting the contribution of the spontaneous emission from the SOA itself, the propagation of optical power,  $P$ , and the carrier density,  $N(z, t)$  in the amplifier can be described by the following equations [53]:

$$\frac{\partial P}{\partial z} - \frac{1}{v_g} \frac{\partial P}{\partial t} = [\Gamma g(N) - \alpha_{int}] P \quad (5.9)$$

$$\frac{\partial N(z, t)}{\partial t} = \frac{J}{qd} - \frac{N(z, t)}{\tau_d} - \frac{\Gamma g(N) P}{h\nu A} \quad (5.10)$$

where  $\Gamma$  is the mode confinement,  $g(N)$  the gain coefficient,  $\alpha_{int}$  the internal loss,  $J$  the injected current density,  $d$  the active layer thickness of the SOA,  $A$  the active region area,  $q$  the electronic charge and  $\tau_d$  the carrier lifetime.

Now we consider the case where there is a large saturating power of the optical beam and a small modulation (perturbing signal) representing the noise superimposed on it. The optical power,  $P$ , and the carrier density,  $N$ , can be linearized and described as

$$P = P_0 + \frac{1}{2\pi} \int_{-\infty}^{+\infty} \Delta P(\Omega) e^{j\Omega t} d\Omega \quad (5.11)$$

$$N = N_0 + \frac{1}{2\pi} \int_{-\infty}^{+\infty} \Delta N(\Omega) e^{j\Omega t} d\Omega \quad (5.12)$$

where  $P_0, N_0$  are the time-averages and  $\Delta P(\Omega)$  and  $\Delta N(\Omega)$  stand for the noise.  $\Omega$  is the angular frequency at which the perturbing signal varies. By substituting (5.11) and (5.12) into (5.9) and (5.10) and considering the component with angular frequency  $\Omega$ , we get the small signal equations for  $\Delta P \equiv \Delta P(\Omega)$  and  $\Delta N \equiv \Delta N(\Omega)$  as

$$\frac{\partial \Delta P}{\partial z} = j \frac{\Omega}{v_g} \Delta P + [\Gamma g(N) - \alpha_{\text{int}}] \Delta P + \Gamma g' \Delta N P_0(z) \quad (5.13)$$

$$\Delta N = - \frac{\Gamma g(N_0) \Delta P}{h \nu A} \frac{1}{j\Omega + \frac{1}{\tau_d} + \frac{\Gamma g' P_0}{h \nu A}} \quad (5.14)$$

where  $g'$  is the differential gain coefficient.

Eq. (5.14) gives the magnitude of the perturbation to the carrier population, which describes the response of the carrier density due to the amplification of the perturbing signal. It shows that the response at position  $z$  has a high frequency roll-off with a 3-dB frequency of  $1/(2\pi\tau_{\text{eff}})$  governed by the local effective lifetime  $\tau_{\text{eff}}$

$$\frac{1}{\tau_{\text{eff}}} = \frac{1}{\tau_d} + \frac{1}{\tau_s} \quad (5.15)$$

where  $1/\tau_s = \Gamma g' P_0 / A h \nu$  is the contribution of the stimulated emission [54].

The behavior of the optical power fluctuation in the beam is governed by Eq. (5.13). The first two terms describe the usual amplification of the optical power fluctuation. The last term represents coupling of light from the CW component into the time varying component and acts to compress the gain, owing to the opposite-phase change of  $\Delta N$  with  $\Delta P$ . This gain compression effect is significant at low frequencies, but vanishes at high frequencies because of the high frequency roll-off of the response of the carrier population. In addition, the gain compression effect is depending on the optical power. It is significant only when the optical power is high. For very small optical power, it becomes negligible. This means that the intensity noise of a nonlinearly amplified optical signal at low frequencies can be much lower than that at high frequencies. Namely gain compression tends to suppress the random fluctuations in signal intensity. Based on this specific noise property, intensity noise in narrow band detection systems such as spectrum-sliced WDM systems can be thus reduced.

The intuitive explanation of the frequency dependent noise suppression is that for high optical power, the SOA is saturated and the gain coefficient is inversely proportional to the intensity of the propagating signal so that when the signal intensity increases due to noise, the gain is reduced so that the increase in intensity is suppressed, and vice versa. Obviously, this description can only be correct when the intensity fluctuations are sufficiently slow for the amplifier gain to adjust. Therefore,

the intensity noise suppression becomes small at high frequencies. The bandwidth of the intensity noise suppression is approximately determined by the effective lifetime (as seen in Eq. 5.15). For a given SOA, it increases with increasing optical power  $P_0$ . From Eq. (5.13) and (5.14), we have (with  $L$  the length of the SOA)

$$\frac{\Delta P(L)}{\Delta P(0)} = e^{j\frac{\Omega L}{v_g}} e^{-\alpha_{\text{int}} L} \exp \left\{ \int_0^L dz \frac{\Gamma g(N_0)(j\Omega + 1/\tau_d)}{j\Omega + \frac{1}{\tau_d} + \frac{\Gamma g' P_0(z)}{Ah\nu}} \right\} \quad (5.16)$$

From this the relative intensity noise (RIN) suppression ratio (electrical),  $\eta$ , can be derived as, in decibel,

$$\begin{aligned} \eta &= -10 \log \left( \left| \frac{\frac{\Delta P(L)}{P_0(L)}}{\frac{\Delta P(0)}{P_0(0)}} \right|^2 \right) \\ &= 20 (\log e) \int_0^L dz \frac{\Gamma g(N_0) \frac{\Gamma g' P_0}{Ah\nu} \left( \frac{1}{\tau_d} + \frac{\Gamma g' P_0(z)}{Ah\nu} \right)}{\Omega^2 + \left( \frac{1}{\tau_d} + \frac{\Gamma g' P_0(z)}{Ah\nu} \right)^2} \end{aligned} \quad (5.17)$$

where

$$P_0(L)/P_0(0) = \exp \left[ \int_0^L dz (\Gamma g(N_0) - \alpha_{\text{int}}) \right] \quad (5.18)$$

Eq. (5.17) shows that  $P_0$ ,  $\Gamma g(N_0)$  and  $\Gamma g'$  have to be as large as possible for getting a high noise reduction.  $A$  must be as small as possible. For a given SOA,  $P_0$  and  $\Gamma g(N_0)$  depend on the input power  $P_{\text{in}}$  and the injected current  $I_b$ . For a given injected current to the SOA,  $P_0$  increases with increasing input power,  $P_{\text{in}}$ .  $\Gamma g(N_0)$  changes little when  $P_{\text{in}}$  is low, yet sufficiently high to get amplifier saturation. The amount of the noise reduction is thus small but increases with increasing input power. For high input powers, that means in the case of saturation of the SOA,  $P_0$  increases very slowly and  $\Gamma g(N_0)$  decreases with the increase of the input power. The noise reduction has thus a small dependence on the input power to the saturated SOA. For a given input power, both  $P_0$  and  $\Gamma g(N_0)$  increase rapidly and thus the amount of the intensity noise reduction increases significantly by increasing the injected current. Increasing the injected current can also result in an increase in the bandwidth of the noise reduction since the bandwidth increases with the increase of  $P_0$ . So, increasing the bias current of the saturated SOA is an effective way to get a great reduction of

the intensity noise and thus a large increase of the SNR. These analytical predictions will be verified by the experimental results given in the following sections.

### 5.2.2 Experimental demonstration

Our experimental setup for the intensity noise reduction using a saturated SOA in the spectrum-sliced WDM system is shown in Fig. 5-15. The ASE light from a superluminescent LED (SLED) was spectrally sliced using a 0.5nm-bandwidth fiber Bragg grating (FBG) filter with 25 dB out of channel rejection. The spectrum-sliced incoherent light centered at 1550.9nm was amplified using an EDFA and then injected into a gain saturated SOA. The output of the SOA was modulated using a LiNbO<sub>3</sub> external modulator. To remove the ASE from the amplifiers, a 1.2-nm bandwidth filter was used before the modulator. The saturation characteristic of the SOA (GC-SOA Module-GC187, Alcatel) used in the experiments is shown in Fig. 5-16.

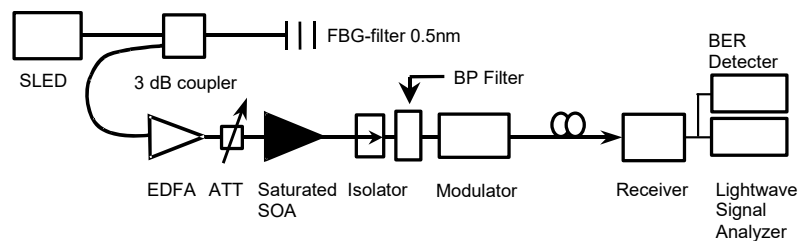


Fig. 5-15 Experimental setup for intensity noise reduction using a saturated SOA. ATT: attenuator.

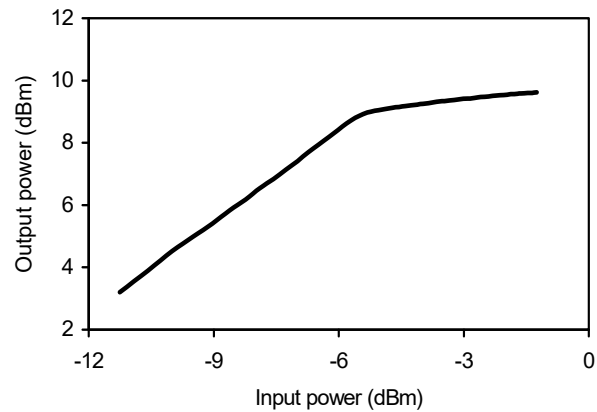


Fig. 5-16 Saturation characteristic of the SOA used for intensity noise reduction in a spectrum-sliced WDM channel.

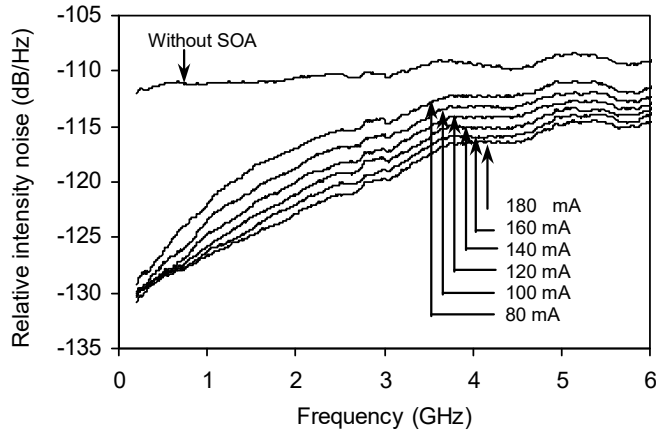


Fig. 5-17 Measured relative intensity noise without and with a gain-saturated SOA at different bias currents. Input power: 4.5 dBm.

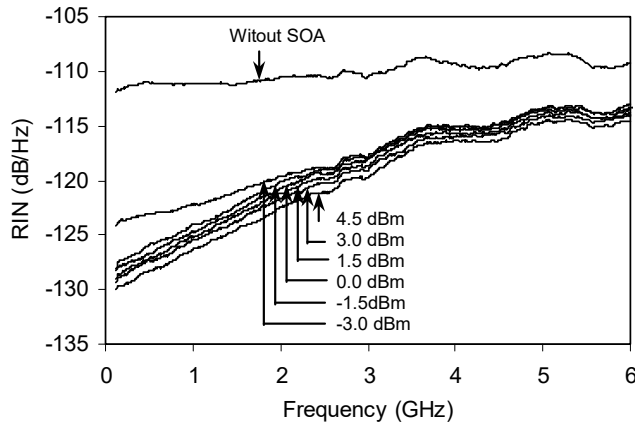


Fig. 5-18 Measured relative intensity noise without and with a gain-saturated SOA for different input powers to the SOA. Injection current: 180 mA.

In the experiments, we measured the RIN spectra of the spectrum-sliced light with and without the saturated SOA, respectively. Figs. 5-17 and 5-18 give the measured results for different injection currents and input powers to the SOA. One can see that the RIN level of the optical slice was around  $-110$  dB/Hz without the SOA. With the SOA, it was significantly suppressed at low frequencies over a bandwidth of several GHz. Figs. 5-19 and 5-20 show the noise suppression ratios as a function of frequency measured for different bias currents and different input powers to the SOA, respectively. Clearly, the bandwidth of the noise reduction increases by increasing the bias current of the SOA but not efficiently by increasing the input

power. The amount of the noise reduction depends on the bias current and the input power. The noise reduction can increase by increasing both of them, but the former is a more effective way. The experimental results are consistent with the analytical predictions. For very low frequencies and large optical power, the noise suppression ratio can be up to 18 dB. This is in relatively good agreement with the 20 dB estimated from Equation (5.17), where a measured fiber-to-fiber amplification of 7.5 dB, a chip-to-fiber coupling loss of 3 dB and an internal loss of  $25 \text{ cm}^{-1}$  of the SOA were used and  $\tau_d$  and  $\tau_s$  were assumed to be equal.

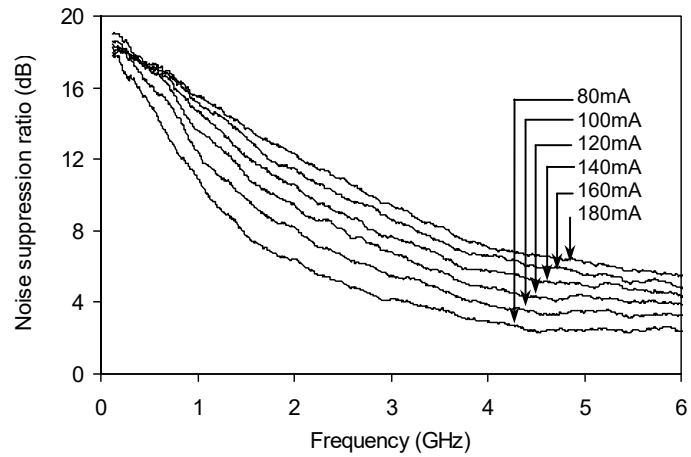


Fig. 5-19 Measured noise suppression ratios for different injection currents,  $I_b$ , for  $P_{in}=4.5 \text{ dBm}$ .

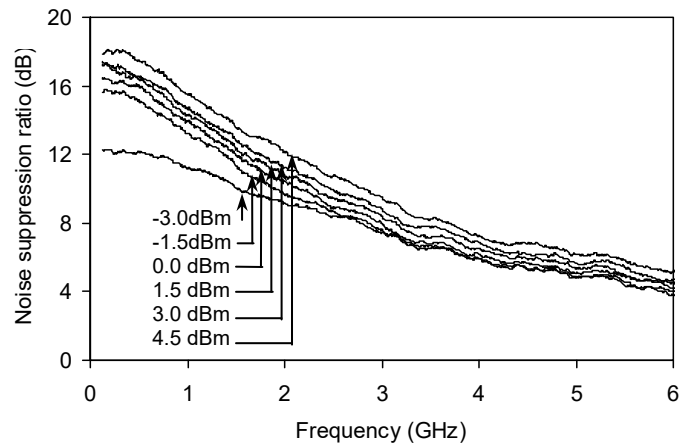


Fig. 5-20 Measured noise suppression ratios for different input powers,  $P_{in}$ , for  $I_b=180 \text{ mA}$ .

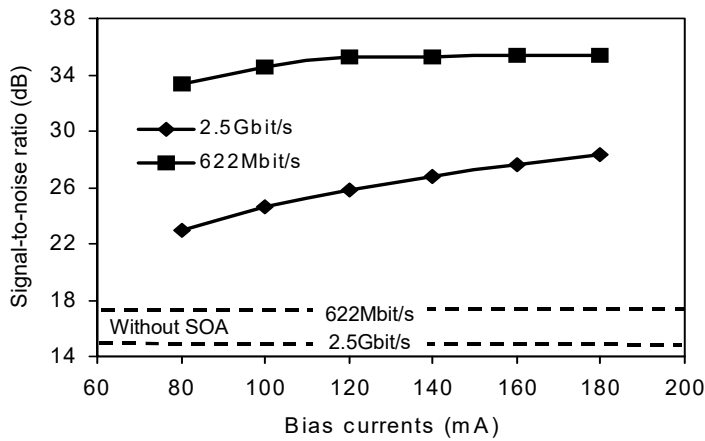


Fig. 5-21 SNR versus injection currents for two different bitrates at back to back operation.  $P_{in} = 4.5$  dBm.

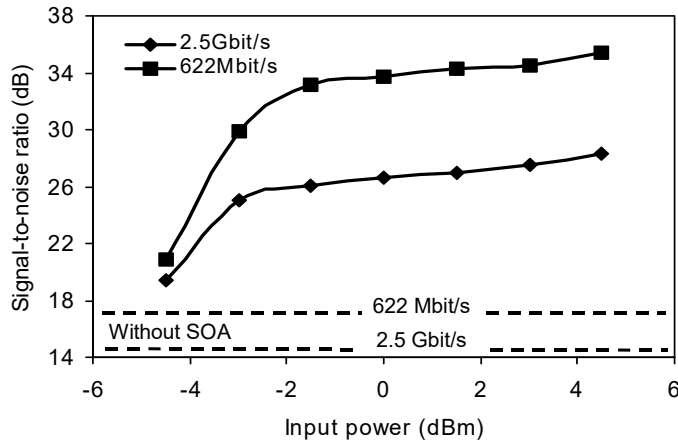


Fig. 5-22 SNR versus input powers for different bitrates at back to back operation.  $I_b = 180$  mA.

Fig. 5-21 and 5-22 show the intensity-noise-limited SNR's with and without SOA at bitrates of 622 Mbit/s and 2.5 Gbit/s for different bias currents and input powers to the SOA, respectively. The SNR can be enhanced significantly by increasing the bias current of the saturated SOA for high bitrate, e.g. 2.5 Gbit/s. But at a low bitrate, e. g. 622 Mbit/s, the enhancement in the SNR is not sensitive to the bias current. This is because the receiver bandwidth is very small for this bitrate and thus the increase of the bandwidth of the noise reduction gives less contribution to the SNR

enhancement. For a given bias current, as shown in Fig. 5-22, the improvement of the SNR is very small when the input power is very low and the SOA is unsaturated. For large input powers, the SOA is saturated and thus a large improvement of the SNR is obtained. With a high bias current of 180mA, an improvement on the SNR of 13.5 dB at a bitrate of 2.5 Gbit/s and 17.5 dB at 622 Mbit/s have been obtained experimentally in a single stage SOA for an input power of 4.5dBm.

The measured eye-diagrams at back to back operation with and without noise reduction are shown in Figs. 5-23 for the bitrate of 2.5 Gbit/s and in Fig. 5-24 for 622 Mbit/s. Clearly, the intensity noise is suppressed dramatically. The optical slice used here and furtheron has an optical bandwidth of 0.3 nm since we added an optical bandpass filter after the EDFA in the experimental setup of Fig. 5-15 to reduce the ASE from the EDFA.

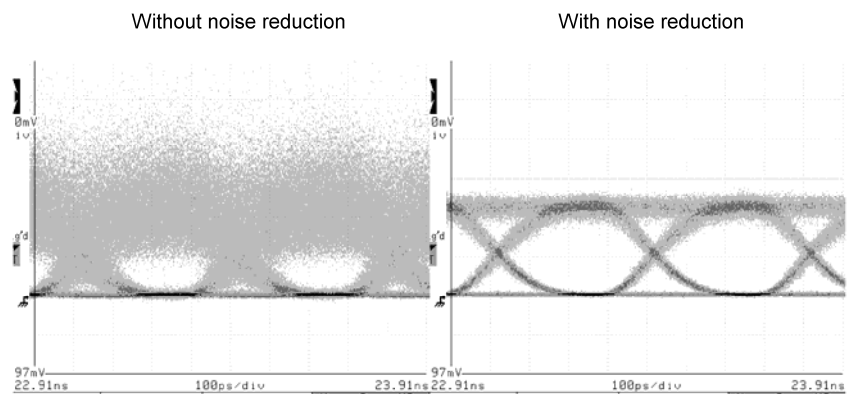


Fig. 5-23 Eye diagrams with and without noise reduction for 2.5 Gbit/s. Injection current to the SOA: 180 mA; input power: 4.5 dBm; optical slice bandwidth: 0.3 nm, received optical power: -9 dBm.

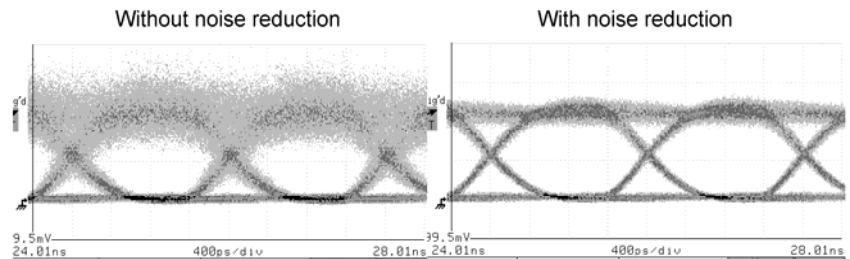


Fig. 5-24 Eye diagrams with and without noise reduction for 622 Mbit/s. Injection current to the SOA: 180 mA; input power: 4.5 dBm; optical slice bandwidth: 0.3 nm, received optical power: -9 dBm

In Fig. 5-25, the measured BER curves with and without noise reduction are plotted for 2.5 Gbit/s. The BER curve with noise reduction after 25 km SMF transmission is also given in the figure. Without the noise reduction for back-to-back operation, the error floor level is at  $2 \times 10^{-4}$ . With the noise reduction using the saturated SOA, the error floor is removed and error free operation is obtained. After the 25 km SMF transmission, the error floor comes back and is at  $4 \times 10^{-8}$ . The eye diagram after 25 km SMF transmission is given in Fig. 5-26, showing an increased time jitter due to dispersion of the fiber, but clear open eyes can still be seen. The dispersion of the fiber is 18 ps/nm·km for 1550 nm.

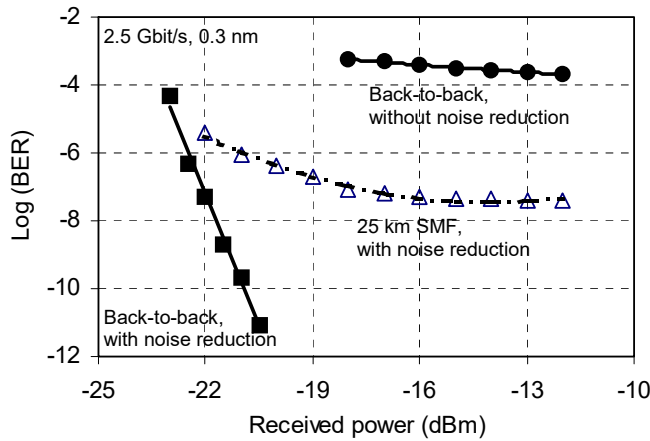


Fig. 5-25 Measured BER curves for 2.5 Gbit/s with and without noise reduction. Optical slice bandwidth: 0.3 nm; Input power to the SOA: 4.5 dBm; Injection current to the SOA: 180 mA.

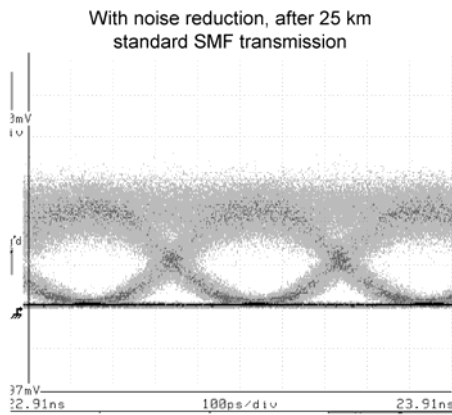


Fig. 5-26 Eye diagrams with noise reduction after transmission of 25 km standard single-mode fiber at a bitrate of 2.5 Gbit/s. Slice bandwidth: 0.3 nm, injection current to the SOA: 180 mA, Input power to the SOA: 4.5 dBm, received optical power: -9 dBm.

We also measured the BER for different injection currents and different input power to the SOA for 2.5 Gbit/s. Figs. 5-27 and 5-28 show the BER curves as a function of received power. One can see that increasing both injection current and input power to the SOA improves the BER, which agrees with the theoretical prediction. For a given input power, e. g., 4.5 dBm, a receiver sensitivity improvement of 1 dB at the BER of  $10^{-9}$  can be achieved by increasing the injection current from 80 mA to 180 mA. While for a given injection current, e. g., 180 mA, a receiver sensitivity improvement of 0.5 dB at the BER of  $10^{-9}$  is obtained when the input power increases from -1.5 dBm to 7.5 dBm. A comparison of the eye diagrams for different injection currents and for different input powers is presented in Fig. 5-29 and Fig. 5-30, respectively.

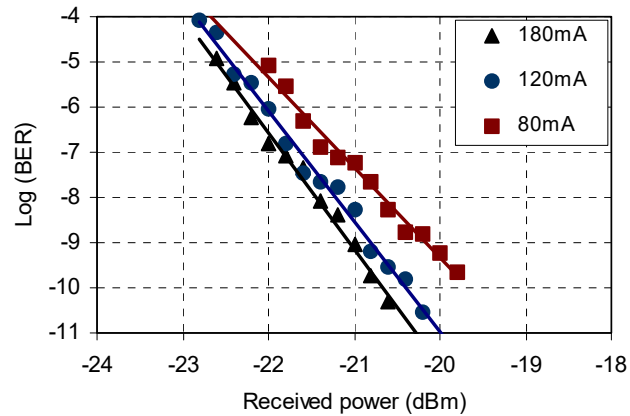


Fig. 5-27 Measured BER as a function of received power for different injection currents to the SOA at 2.5 Gbit/s. Input power to the SOA: 4.5 dBm; slice bandwidth: 0.3 nm; signal central wavelength: 1550.9 nm.

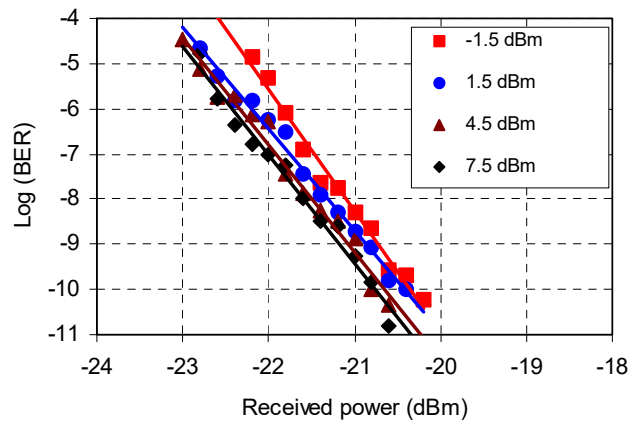


Fig. 5-28 Measured BER as a function of received power for different input powers to the SOA at 2.5 Gbit/s. Injection current to the SOA: 180 mA; slice bandwidth: 0.3 nm; central wavelength: 1550.9 nm.

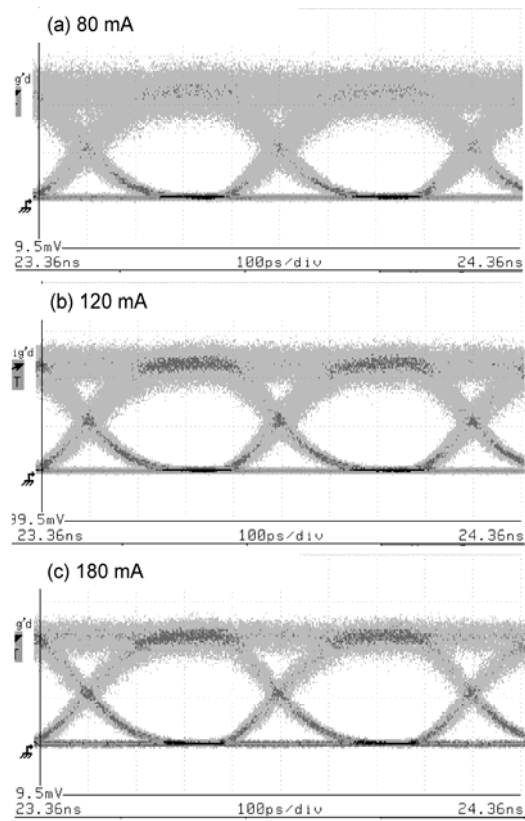


Fig. 5-29 Eye diagrams for different injection currents to the SOA at 2.5 Gbit/s. Input power to the SOA: 4.5 dBm; slice bandwidth: 0.3 nm; central wavelength: 1550.9 nm; received optical power: -9 dBm.

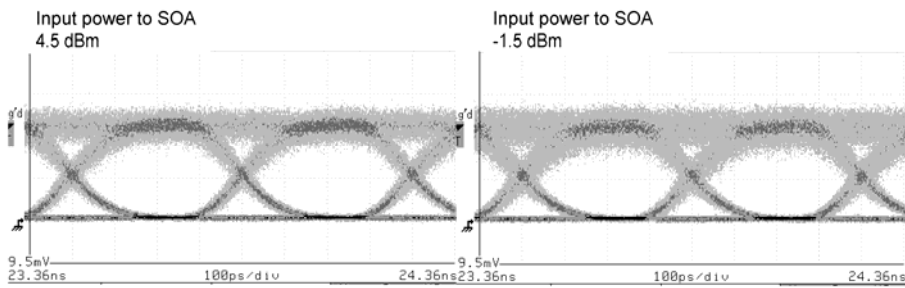


Fig. 5-30 Eye diagrams for different input powers to the SOA at 2.5 Gbit/s. Injection current to the SOA: 180 mA; slice bandwidth: 0.3 nm; central wavelength: 1550.9 nm; received optical power: -9 dBm.

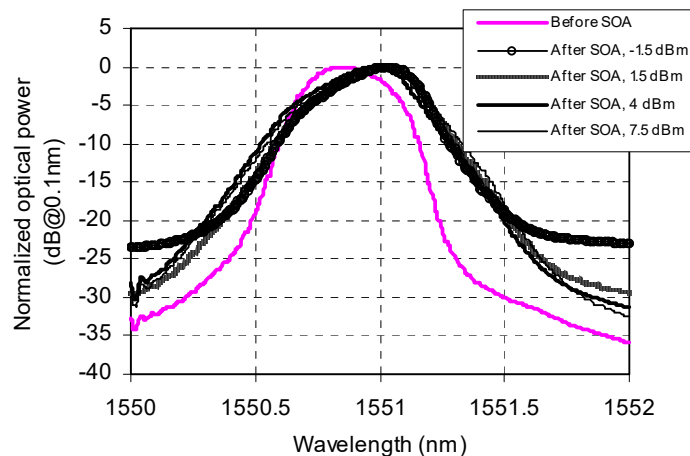


Fig. 5-31 Optical spectra before and after the SOA for different input powers to the SOA. Injection current to the SOA: 180 mA.

Fig. 5-31 shows the optical spectra before and after the SOA for different input powers to the SOA. The spectral curves are normalized to make their peak values the same. It can be seen that the optical slice is broadened after the SOA. Although the 3 dB-bandwidth does not change, the bandwidth at  $-10$  dB or below is significantly increased, and the bandwidth broadening increases with the increase of input power to the SOA. For an input power of  $-1.5$  dBm, the 10-dB bandwidth increases from 0.57 nm to 0.7 nm (23 % broadening), while for an input power of 7.5 dBm it increases to 0.8 nm (40 % broadening). This bandwidth broadening is due to the IC-FWM of the SOA [55]. It means that in addition to the gain saturation effect, IC-FWM also contributes to the intensity noise reduction using a saturated SOA in the spectrum-sliced WDM channel. Furthermore, the shape and the central wavelength of the optical slice are also changed a little bit after the SOA. The central wavelength shifts to the long-wavelength side. This could be explained by the fact that when a pulse passes through the SOA, its spectrum is shifted toward the long-wavelength side and the spectrum has developed a multippeak structure due to gain-saturation-induced self-modulation [56, 57]. The intensity fluctuations of the optical slice filtered out from the ASE source can be considered as a combination of a large number of optical pulses, and thus the optical spectrum of the slice is shifted toward the long-wavelength side. The distortion of the spectrum is due to the additional induced optical peak.

The achievable bitrate using a SOA for noise reduction depends on both intrinsic parameters (e. g.  $\tau_d$ ,  $Ig'$ ,  $A$ ) and operation conditions (e. g. bias current, input power) of the SOA and can be estimated from the measured RIN spectra. For a high bias current of 180 mA and an input power of 4.5 dBm, a bitrate of 5 Gbit/s with a SNR of 20 dB can be achieved with the SOA used in our experiments in a single stage. If cascaded saturated SOAs are used, the achievable bitrate can be increased.

### 5.3 Summary

Both theory and experiment show that spectrum-sliced incoherent light exhibits excess intensity noise that limits the achievable bit error rate for a given slice bandwidth in spectrum-sliced WDM systems. This limitation could have previously been overcome only at the expense of system capacity, i.e., by increasing the optical bandwidth or by reducing the bitrate of the channel. We have investigated a technique for reducing excess intensity noise in the spectrum-sliced WDM system, which is based on the specific noise properties of a saturated SOA. A simple theoretical model of the noise suppression using the saturated SOA is developed based on the rate equations. With this model, the influence of the input power level and the injection current to the SOA on the noise reduction and its bandwidth is studied. The intensity noise reduction can be improved by increasing both the injection current and the input power to the SOA. Experimental results of RIN, SNR, and BER have confirmed the theoretical predictions. RIN measurements show clearly the RIN reduction using the saturated SOA and the injection current dependence of the bandwidth of the RIN reduction. Experimental results of SNR show an increase of 13.5 dB in the intensity-noise-limited signal-to-noise ratio (SNR) for a bitrate of 2.5 Gbit/s and of 17.5 dB for a bitrate of 622 Mbit/s. We have also presented the BER and the eye diagram measurement results. For an optical slice with 0.3 nm bandwidth, the error floor level is at  $2 \times 10^{-4}$  without the noise reduction for back-to-back operation. With the noise reduction using the saturated SOA, the error floor is removed and error free operation is obtained. Transmission experiments show that after 25 km of SMF the error floor is at  $4 \times 10^{-8}$ . The BER measurement results for different injection currents and different input powers to the SOA for 2.5 Gbit/s show that increasing both injection current and input power to the SOA improves the BER, which agrees with the theoretical prediction. A receiver sensitivity improvement of 1 dB at the BER of  $10^{-9}$  has been demonstrated by increasing the injection current from 80 mA to 180 mA for an input power of 4.5 dBm. For a given injection current, e. g., 180 mA, a receiver sensitivity improvement of 0.5 dB at the BER of  $10^{-9}$  can be also obtained when the input power increases from -1.5 dBm to 7.5 dBm. All of these have demonstrated the improvement of the transmission performance of the spectrum-sliced WDM channel using the saturated SOA. Experimental results of the optical spectra of the slice before and after the SOA have shown that in addition to the gain-saturation characteristics of the SOA, the IC-FWM within the SOA is also an important mechanism for intensity noise reduction.

## References

- [1] M. H. Reeve, A. R. Hunwicks, W. Zhao, S. G. Methley, L. Bickers, and S. Hornung, "LED spectral slicing for single-mode local loop applications", *Electron. Lett.*, Vol. 24, No. 7, pp. 389-390, 1988.
- [2] S. S. Wagner and T. E. Chapuran, "Broadband high-density WDM transmission using superluminescent diodes," *Electron. Lett.*, Vol. 26, No. 11, pp. 696-697, 1990.
- [3] M. Zirngibl, C. H. Joyner, L. W. Stultz, C. Dragone, H. M. Presby, and I. P. Kaminow, "LARNet, a local access router network," *IEEE Photon. Technol. Lett.*, Vol. 7, No. 2, pp. 215-217, 1995.
- [4] P. P. Iannone, N. J. Frigo, and T. E. Darcie, "WDM passive-optical-network architecture with bidirectional optical spectral slicing," in *Techn. Dig. Conference on Optical fiber communication OFC95*, pp. 51-53, 1995.
- [5] M. Zirngibl, C. R. Doerr, and L. W. Stultz, "Study of spectral slicing for local access applications," *IEEE Photon. Technol. Lett.*, Vol. 8, No. 5, pp. 721-723, 1996.
- [6] N. J. Frigo, P. P. Iannone, and K. C. Reichmann, "Spectral slicing in WDM passive optical networks for local access," *Proc. European Conference on Optical communications, ECOC 98*, pp. 119-120, Madrid, Spain, September 20-24, 1998.
- [7] E. A. De Souza, M. C. Nuss, M. Zirngibl, and C. H. Joyner, "Spectrally sliced WDM using a single femtosecond source," in *Techn. Dig. Conference on Optical fiber communication OFC95*, postdeadline paper PD 16-1, Washington DC, USA, 1995.
- [8] H. Sanjoh, H. Yasaka, Y. Sakai, K. Sato, H. Ishii, and Y. Yoshikuni, "Multiwavelength light source with precise frequency spacing using a mode-locked semiconductor laser and an arrayed waveguide grating filter," *IEEE Photon. Technol. Lett.*, Vol. 9, No. 6, pp. 818-820, 1997.
- [9] W. T. Holloway, A. J. Keating, and D. D. Sampson, "Multiwavelength source for spectrum-sliced WDM access networks and LAN's," *IEEE Photon. Technol. Lett.*, Vol. 9, No. 7, pp. 1014-1016, 1997.
- [10] B. Mikulla, L. Leng, S. Sears, B. C. Collings, M. Arend, and K. Bergman, "Broadband high-repetition-rate source for spectrally sliced WDM," *IEEE Photon. Technol. Lett.*, Vol. 11, No. 4, pp. 418-420, 1999.
- [11] S. L. Woodward, P. P. Iannone, K. C. Reichmann, and N. J. Frigo, "A spectrally sliced PON employing Fabry-Perot lasers," *IEEE Photon. Technol. Lett.*, Vol. 10, No. 9, pp. 1337-1339, 1998.
- [12] T. Morioka, K. Mori, S. Kawanishi, and M. Saruwatari, "Multi-WDM-channel Gbit/s pulse generation from a single laser source utilizing LD-pumped supercontinuum in optical fibers," *IEEE Photon. Technol. Lett.*, Vol. 6, pp. 365-368, 1994.
- [13] L. Boivin, S. Taccheo, C. R. Doerr, P. Schiffer, L. W. Stulz, R. Monnard, and W. Lin, "400 Gbit/s transmission over 544 km from spectrum-sliced supercontinuum source," *Electron. Lett.*, Vol. 36, No. 4, pp. 335-336, 2000.
- [14] Y. Takushima and K. Kikuchi, "10-GHz, over 20-channel multiwavelength pulse source by slicing super-continuum spectrum generated in normal dispersion fiber," *IEEE Photon. Technol. Lett.*, Vol. 11, pp. 322-324, 1999.
- [15] T. Morioka, K. Mori, and M. Saruwatari, "More than 100-wavelength-channel picosecond optical pulse generation from single laser source using supercontinuum in optical fibers," *Electron. Lett.*, Vol. 29, pp. 862-864, 1993.

- [16] D. D. Sampson and W. T. Holloway, "100mW spectrally-uniform broadband ASE source for spectrum-sliced WDM systems," *Electron. Lett.*, Vol. 30, No. 19, pp. 1611-1612, 1994.
- [17] J. S. Lee, Y. C. Chung, and D. J. DiGiovanni, "Spectrum-sliced fiber amplifier light source for multichannel WDM applications," *IEEE Photon. Technol. Lett.*, Vol. 5, No. 12, pp. 1458-1461, 1993.
- [18] K. Y. Liou and G. Raybon, "Operation of an LED with a single-mode semiconductor amplifier as a broad-band 1.3- $\mu\text{m}$  transmitter source," *IEEE Photon. Technol. Lett.*, Vol. 7, No. 9, pp. 1025-1027, 1995.
- [19] K. Y. Liou, U. Koren, E. C. Burrows, J. L. Zyskind, and K. Dreyer, "A WDM access system architecture based on spectral slicing of an amplified LED and delay-line multiplexing and encoding of eight wavelength channels for 64 subscribers," *IEEE Photon. Technol. Lett.*, Vol. 9, No. 4, pp. 517-519, 1997.
- [20] P. D. D. Kilkelly, P. J. Chidgey, and G. Hill, "Experimental demonstration of a three channel WDM system over 110 km using superluminescent diodes," *Electron. Lett.*, Vol. 26, pp. 1671-1673, 1990.
- [21] D. K. Jung, S. K. Shin, C. H. Lee, and Y. C. Chung, "Wavelength-division-multiplexed passive optical network based on spectrum-slicing techniques," *IEEE Photon. Technol. Lett.*, Vol. 10, No. 9, pp. 1334-1336, 1998.
- [22] K. Y. Liou, J. B. Stark, U. Koren, E. C. Burrows, J. L. Zyskind, and K. Dreyer, "System performance of an eight-channel WDM local access network employing a spectrum-sliced and delay-line-multiplexed LED source," *IEEE Photon. Technol. Lett.*, Vol. 9, No. 5, pp. 696-698, 1997.
- [23] K. Y. Liou, U. Koren, K. Dreyer, E. C. Burrows, J. L. Zyskind, and J. W. Sulhoff, "A 24-channel WDM transmitter for access systems using a loop-back spectrally sliced light-emitting diode," *IEEE Photon. Technol. Lett.*, Vol. 10, No. 2, pp. 270-272, 1998.
- [24] P. P. Iannone, K. C. Reichmann, and N. J. Frigo, "High-speed point-to-point and multiple broadcast services delivered over a WDM passive optical network," *IEEE Photon. Technol. Lett.*, Vol. 10, No. 9, pp. 1328-1330, 1998.
- [25] K. C. Reichmann, P. P. Iannone, and N. J. Frigo, "Operational demonstration and filter alignment study of multiple broadcast services delivered over a WDM passive optical network," *IEEE Photon. Technol. Lett.*, Vol. 10, No. 9, pp. 1331-1333, 1998.
- [26] P. Healey, P. Townsend, C. Ford, L. Johnston, P. Townley, I. Lealman, L. Reviere, S. Perrin, and R. Moore, "Spectral slicing WDM-PON using wavelength-seeded reflective SOAs," *Electron. Lett.*, Vol. 37, No. 19, pp. 1181-1182, 2001.
- [27] P. P. Morkel, R. I. Laming, and D. N. Payne, "Noise characteristics of high-power doped-fiber superluminescent sources," *Electron. Lett.*, Vol. 26, No. 2, pp. 96-98, 1990.
- [28] G. J. Pendock and D. D. Sampson, "Transmission performance of high bit rate spectrum-sliced WDM systems," *IEEE J. Lightwave Technol.*, Vol. 14, No. 10, pp. 2141-2148, 1996.
- [29] L. Goldberg and D. Mehuys, "High power superluminescent diode source," *Electron. Lett.*, Vol. 30, No. 20, pp. 1682-1684, 1994.
- [30] C. H. Joyner, C. R. Doerr, J. C. Centanni, K. Dreyer, and L. W. Stulz, "Broad spectrum source for local access networks," *Electron. Lett.*, Vol. 32, No. 8, pp. 749-751, 1996.
- [31] K. Y. Liou, B. Glance, U. Koren, E. C. Burrows, G. Raybon, C. A. Burrus, and K. Dreyer, "Monolithically integrated semiconductor LED-amplifier for applications as

- transceivers in fiber access systems," *IEEE Photon. Technol. Lett.*, Vol. 8, No. 6, pp. 800-802, 1996.
- [32] G. Murtaza and J. M. Senior, "WDM crosstalk analysis for systems employing spectrally-sliced LED sources," *IEEE Photon. Technol. Lett.*, Vol. 8, No. 3, pp. 440-442, 1996.
- [33] C. Dragone, C. A. Edwards, and R. C. Kistler, "Integrated optics  $N \times N$  multiplexer on silicon," *IEEE Photon. Technol. Lett.*, Vol. 4, pp. 896-899, 1991.
- [34] R. D. Feldman, "Crosstalk and loss in wavelength division multiplexed systems employing spectral slicing," *IEEE J. Lightwave Technol.*, Vol. 15, No. 11, pp. 1823-1830, 1997.
- [35] Y. S. Jang, C. H. Lee, and Y. C. Chung, "Effects of crosstalk in WDM systems using spectrum-sliced light sources," *IEEE Photon. Technol. Lett.*, Vol. 11, No. 6, pp. 715-717, 1999.
- [36] C. R. Giles and E. Desurvire, "Propagation of signal and noise in concatenated Erbium-doped fiber optical amplifiers," *IEEE J. Lightwave Technol.*, Vol. 9, No. 2, pp. 147-154, 1991.
- [37] N. A. Olsson, "Lightwave systems with optical amplifiers," *IEEE J. Lightwave Technol.*, Vol. 7, No. 7, pp. 1071-1082, 1989.
- [38] M. Zhao, G. Morthier, B. Moeyersoon, and R. Baets, "Influence of intensity noise on link transmission performance of spectrum-sliced WDM systems," *Towards an Optical Internet (New Visions in Optical Network Design and Modeling)*, pp. 253-261, Edited by Admela Jukan, Kluwer Academic publishers, 2001.
- [39] K. Ogawa, "Analysis of mode partition noise in laser transmission systems," *IEEE J. Quantum Electron.*, Vol. QE-18, pp. 849-855, 1982.
- [40] Y. K. Chen, M. C. Wu, T. Tanbun-EK, R. A. Logan, and M. A. Chin, "Multicolor single-wavelength sources generated by a monolithic colliding pulse mode-locked quantum well laser," *IEEE Photon. Technol. Lett.*, Vol. 3, No. 11, pp. 971-973, 1991.
- [41] S. D. Personick, "Receiver design for digital fiber optic communication systems, I," *Bell Syst. Tech. J.*, Vol. 52, No. 6, pp. 843-874, 1973.
- [42] VPI transmissionMaker was supplied by Virtual Photonics Incorporated:  
[www.virtualphotonics.com](http://www.virtualphotonics.com)
- [43] T. Li, and M. C. Teich, "Bit-error rate for a lightwave communication system incorporating an erbium-doped fiber amplifier," *Electron. Lett.*, Vol. 27, pp. 598-600, 1991.
- [44] A. J. Keating, W. T. Holloway, and D. D. Sampson, "Feedforward noise reduction of incoherent light for spectrum-sliced transmission at 2.5 Gb/s," *IEEE Photon. Technol. Lett.*, Vol. 7, No. 12, pp. 1513-1515, 1995.
- [45] A. J. Keating and D. D. Sampson, "Reduction of excess intensity noise in spectrum-sliced incoherent light for WDM applications," *IEEE J. Lightwave Technol.*, Vol. 15, No. 1, pp. 53-61, 1997.
- [46] J. H. Han, J. W. Ko, J. S. Lee, and S. Y. Shin, "0.1-nm narrow bandwidth transmission of a 2.5-Gb/s spectrum-sliced incoherent light channel using an all-optical bandwidth expansion technique at the receiver," *IEEE Photon. Technol. Lett.*, Vol. 10, No. 10, pp. 1501-1503, 1998.
- [47] F. Koyama, "High power superluminescent diode for multi-wavelength light sources," in *Proc. Annual Lasers and Electro Optics Meeting, LEOS'97*, Vol. 1, pp. 333-334 (p. TuY2), San Francisco, CA, USA, November 10-13, 1997.

- [48] T. Yamatoya, F. Koyama, and K. Iga, "Noise suppression and intensity modulation using gain-saturated semiconductor optical amplifier," in *Tech. Dig. of Integrated Photonics Research, IPR 2000*, pp. 72-74 (p. OMD12), Canada, July, 2000.
- [49] S. J. Kim, J. H. Han, J. S. Lee and C. S. Park, "Intensity noise suppression in spectrum-sliced incoherent light communication systems using a gain-saturated semiconductor optical amplifier," *IEEE Photon. Technol. Lett.*, Vol. 11, No. 8, pp. 1042-1044, 1999.
- [50] S. J. Kim, J. H. Han, J. S. Lee and C. S. Park, "Suppression of intensity noise in 10 Gbit/s spectrum-sliced incoherent light channel using gain-saturated semiconductor optical amplifiers," *Electron. Lett.*, Vol. 35, No. 12, pp. 1000-1001, 1999.
- [51] Y. Katagiri, K. Suzuki, and K. Aida, "Intensity stabilisation of spectrum-sliced Gaussian radiation based on amplitude squeezing using semiconductor optical amplifiers with gain saturation," *Electron. Lett.*, Vol. 35, No. 16, pp. 1362-1363, 1999.
- [52] M. Zhao, G. Morthier, R. Baets, and J. Dekoster, "Investigation of the intensity noise reduction using a saturated semiconductor optical amplifier in spectrum sliced WDM systems" in *Proc. Conference on Lasers and Electro-Optics, CLEO 2001*, p. CThB3, Baltimore, Maryland, USA, May 8-10, 2001.
- [53] M. E. Bray and M. J. O'Mahony, "Cascading gain-saturation semiconductor laser-amplifier wavelength translators," *IEE Proc.-Optoelectron.*, Vol. 143, No. 1, pp. 1-6, 1996.
- [54] D. A. O. Davies, "Small-signal analysis of wavelength conversion in semiconductor laser amplifier via gain saturation," *IEEE Photon. Technol. Lett.*, Vol. 7, No. 6, pp. 617-619, 1995.
- [55] G. Grosskopf, R. Ludwig, R. G. Waarts, and H. G. Weber, "Four-wave mixing in a semiconductor laser amplifier," *Electron. Lett.*, Vol. 24, No. 1, pp. 31-32, 1988.
- [56] G. P. Agrawal and N. A. Olsson, "Self-phase modulation and spectral broadening of optical pulse in semiconductor laser amplifiers," *IEEE J. Quantum Electron.*, Vol. 25, No. 11, pp. 2297-2306, 1989.
- [57] J. Yu and P. Jeppesen, "Increase input power dynamic range of SOA by shifting the transparent wavelength of tunable optical filter," *IEEE J. Lightwave Technol.*, Vol. 19, No. 9, pp. 1316-1325, 2001.

## Chapter 6

# Conclusions

All-optical regeneration will be the key technique to face the challenges of capacity, transmission distance and scalability of future optical telecommunication networks. A number of solutions for optical regeneration have been proposed and experimentally demonstrated in recent years. Among the proposed solutions, those based on SOAs offer the highest integration potential and have been the focus of much research on all-optical regeneration. They also open possibilities for more complex optical signal processing.

The nonlinear transfer function of the optical regenerators is the key characteristic that governs regeneration efficiency. The SOA-based MZI is very promising for all-optical regeneration in high-bitrate optical networks due to the diversity of the functionality it offers. However, this device suffers from a rather slow nonlinear transfer response. To get a steeper nonlinear response, cascaded MZIs are needed. Furthermore, in most cases the optical regeneration is realized through wavelength conversion and an extra CW laser signal is needed. All of this results in increased cost and complexity.

As described in this thesis, we have developed some new all-optical 2R regenerators that have a steep nonlinear transfer function, operate on the signal itself instead of on a pump or external pulse sequence, and give the same benefits as SOA-based devices. In chapter 2, an all-optical 2R regenerator using an MZI with GCSOAs in both arms is presented. The operation of this regenerator is based on the specific property of a GCSOA that its amplification in the linear regime is independent of the injected current, whereas the saturation power increases linearly with the injected current. A digital-like nonlinear transfer function and a flexible adjustment of decision threshold are demonstrated. Dynamic measurements at 2.5 Gbit/s show a tremendous intensity noise suppression at the logic "0" and a large improvement in ER even for a very deteriorated input signal with small ER: e.g. 8 dB improvement in ER has been obtained for an input ER of 5 dB, and 7 dB improvement for an input ER of 2 dB. In chapter 3, an alternative implementation of the above GCSOA-based 2R regeneration is proposed, which has higher speed potential. In this 2R regenerator, two very recently introduced devices, LOAs, are used in the two arms of the MZI, instead of the GCSOAs. A significant improvement in ER and operation at 10 Gbit/s are demonstrated.

In addition to using the self-gain-modulation and the self-phase-modulation in the SOAs, we have demonstrated all-optical 2R-regeneration based on nonlinear

birefringence in a single LOA. Theoretical analysis and experimental demonstration show excellent regenerative capabilities of this device. An ER improvement of 15 dB has been obtained with an input ER of 5 dB for static operation. Experimental results for bit-rates of both 2.5 Gbit/s (NRZ,  $2^9-1$  PRBS) and 10 Gbit/s (NRZ,  $2^{31}-1$  PRBS) have been presented. With a degraded input signal, a receiver sensitivity improvement of over 3 dB at a BER of  $10^{-9}$  is found for 2.5 Gbit/s. For 10 Gbit/s, zero power penalty is observed. Significant improvements of ER are obtained for both 2.5 Gbit/s and 10 Gbit/s. The features of simple configuration, stable operation and strong regenerative capabilities make this new scheme a promising technique for all-optical regeneration in future optical networks.

The spectrum-sliced WDM technique is a strong candidate for the cost-sensitive local area networks, such as campus or metropolitan networks and fiber-to-the-home access networks, due to its advantages of low cost, high wavelength selectivity and temperature stability as compared to conventional DWDM systems. Spectrum-sliced incoherent light, however, exhibits a large intensity noise that places limits on the achievable system performances. We have investigated a technique for reducing excess intensity noise in the spectrum-sliced WDM system, which is based on the specific noise properties of a saturated SOA. A simple theoretical model of the noise suppression using the saturated SOA has been developed based on the rate equations. Experimental results of RIN, SNR, and BER have been carried out and demonstrated the improvement of the transmission performance of the spectrum-sliced WDM channel using the saturated SOA. For an optical slice with 0.3 nm bandwidth, the error floor level is at  $2 \times 10^{-4}$  without the noise reduction for back-to-back operation. With the noise reduction using the saturated SOA, the error floor is removed and error free operation is obtained. The BER measurements, performed for different injection currents and different input powers to the SOA for 2.5 Gbit/s, confirmed that increasing both the injection current and the input power to the SOA improves the BER. Experimental results of the optical spectra of the slice before and after the SOA have shown that the intensity noise reduction is due to both the gain-saturation characteristics and the IC-FWM in the SOA. As mentioned in this thesis, this noise suppression technique has the advantage of simplicity and high efficiency and is potentially low cost since the saturated SOA can be used simultaneously for both noise reduction and signal modulation. Therefore, this approach is very practical and useful for application in cost-sensitive local area networks.

There are several important issues for the 2R regenerators described in this thesis. First, the bitrate of the GCSOA-based 2R regenerator is limited by the relaxation oscillations. This bitrate limitation can be overcome by using some new designed gain-clamped SOAs such as LOA, as described in the thesis, and appropriately designed DBR-based GCSOAs that could deliver very high bandwidths (e. g., 30 GHz). Optical regeneration based on the MZI with LOAs can operate at high bitrate, 10 Gbit/s has been demonstrated, but unexpected polarization relaxation in the LOA degrades the regeneration performance. This polarization relaxation has also impact on the regenerative capability of the 2R regenerator based on nonlinear birefringence in a LOA. So, reduction of this impact could be one of the topics for future research.

---

Secondly, in both the GCSOA-based and the LOA-based 2R regeneration the noise suppression at the “1” levels were not as good as expected. Investigating how further to reduce this noise could be another topic for future research.

Finally, the experimental demonstration of the 2R regenerators described in this thesis uses optical fiber-based MZIs. A big issue of the fiber-based devices is instability. From a practical point of view, an integrated version could be more useful and more stable. Furthermore, as mentioned in Chapter 5, the saturated SOA used for intensity noise reduction in the spectrum-sliced WDM systems can also be used for simultaneous modulation. An integrated multi-functional SOA module for intensity noise suppression, intensity modulation and amplification would be very interesting for spectrum-sliced WDM local networks.

# List of Acronyms

|        |  |
|--------|--|
| ASE    | Amplified Spontaneous Emission               |
| BER    | Bit Error Rate                               |
| BTB    | Back to Back                                 |
| CS     | Channel Spacing                              |
| DBR    | Distributed Bragg Reflector                  |
| DFB    | Distributed Feedback                         |
| DWDM   | Dense Wavelength Division Multiplexing       |
| ECC    | Error Correcting Code                        |
| EDFA   | Erbium-Doped Fiber Amplifier                 |
| ER     | Extinction Ratio                             |
| ESCON  | Enterprise Serial Connection                 |
| FBG    | Fiber Bragg Grating                          |
| FFNR   | Feed-forward Noise Reduction                 |
| FP     | Fabry-Perot                                  |
| FSR    | Free Spectral Range                          |
| FTTH   | Fiber-to-the-Home                            |
| FWM    | Four Wave Mixing                             |
| GCSOA  | Gain Clamped Semiconductor Optical Amplifier |
| IC-FWM | Intra-channel Four Wave Mixing               |
| LED    | Light Emitting Diode                         |
| LOA    | Linear Optical Amplifier                     |
| MI     | Michelson Interferometer                     |
| MOCVD  | Metalorganic Chemical Vapor Deposition       |
| NRZ    | Non-Return-to-Zero                           |
| OADM   | Optical Add/Drop Multiplexer                 |
| OBPF   | Optical Band-pass Filter                     |
| OLT    | Optical Line Terminal                        |
| OXC    | Optical Cross-connect                        |

|       |  |
|-------|--|
| OSNR  | Optical Signal to Noise Ratio          |
| PDF   | Probability Density Function           |
| PDG   | Polarization Dependence of the Gain    |
| PLC   | Planar Lightwave (Lightguide) Circuit  |
| PMD   | Polarization Mode Dispersion           |
| PON   | Passive Optical Network                |
| PRBS  | Pseudo-Random Binary Sequence          |
| RIN   | Relative Intensity Noise               |
| RZ    | Return-to-Zero                         |
| SA    | Saturable Absorber                     |
| SDH   | Synchronous Digital Hierarchy          |
| SLED  | Superluminescent Light Emitting Diode  |
| SMF   | Single Mode Fiber                      |
| SNR   | Signal to Noise Ratio                  |
| SOA   | Semiconductor Optical Amplifier        |
| SONET | Synchronous Optical Network            |
| SPM   | Self-Phase Modulation                  |
| SRS   | Stimulated Raman Scattering            |
| TDM   | Time division Multiplexing             |
| TE    | Transverse Electrical Mode             |
| TM    | Transverse Magnetic Mode               |
| UNI   | Ultra-Fast Nonlinear Interferometer    |
| VCSEL | Vertical Cavity Surface Emitting Laser |
| WDM   | Wavelength Division Multiplexing       |
| WGR   | Waveguide Grating Router               |